REPUBLIC OF TURKEY

YILDIZ TECHNICAL UNIVERSITY

GRADUATE SCHOOL OF SCIENCE AND ENGINEERING

INVESTIGATION OF EFFECTIVE DRAINAGE METHODS IN SPORTS FIELD UNDER VARIOUS RAINFALL CONDITIONS

Erdal KESGİN

DOCTOR OF PHILOSOPHY THESIS

Department of Civil Engineering

Hydraulics Program

Supervisor

Prof. Dr. Hayrullah AĞAÇCIOĞLU

August, 2021

REPUBLIC OF TURKEY

YILDIZ TECHNICAL UNIVERSITY

GRADUATE SCHOOL OF SCIENCE AND ENGINEERING

INVESTIGATION OF EFFECTIVE DRAINAGE METHODS IN SPORTS FIELD UNDER VARIOUS RAINFALL CONDITIONS

A thesis submitted by Erdal KESGİN in partial fulfillment of the requirements for the degree of DOCTOR OF PHILOSOPHY is approved by the committee on 06.08.2021 in the Department of Civil Engineering, Hydraulics Program.

Prof. Dr. Hayrullah AĞAÇCIOĞLU

Yıldız Technical University

Supervisor

Approved By the Examining Committee

Prof. Dr. Hayrullah AĞAÇCIOĞLU, Supervisor
Yıldız Technical University ______________________

Prof. Dr. Yalçın YÜKSEL, Member
Yıldız Technical University ______________________

Prof. Dr. Mehmet ÖZGER, Member
İstanbul Technical University ______________________

Doç. Dr. Berna Ayat Aydoğan, Member
Yıldız Technical University ______________________

Doç. Dr. M. Cüneyd DEMİREL, Member
İstanbul Technical University ______________________

I hereby declare that I have obtained the required legal permissions during data collection and exploitation procedures, that I have made the in-text citations and cited the references properly, that I haven't falsified and/or fabricated research data and results of the study and that I have abided by the principles of the scientific research and ethics during my Thesis Study under the title of Investigation of Effective Drainage Methods in Sports Field Under Various Rainfall Conditions supervised by my supervisor, Prof. Dr. Hayrullah AĞAÇCIOĞLU. In the case of a discovery of a false statement, I am to acknowledge any legal consequence.

Erdal KESGİN

This study was supported by the Scientific and Technological Research Council of Turkey (TUBITAK) Grant No: 214M616

Dedicated to my family,

my beloved wife

and my baby boy, Alperen.

ACKNOWLEDGEMENTS

In the name of Allah, most gracious and most merciful. All praise and glory to Almighty Allah (SWT) who gave me courage, patience, and the ability to carry out this work. Peace and blessing of Allah be upon last Prophet Muhammad (PBUH).

A comprehensive research project like this is never the work of anyone alone, however, the support of many people, in which the contribution of them, in different ways, had made this possible. I would like to express my sincere gratitude to my advisor Prof. Dr. Hayrullah AĞAÇCIOĞLU. I appreciate his continuous support of my Ph.D. study and related research, patience, motivation, and immense practice knowledge.

Besides my advisor, I would like to thank the rest of my thesis committee: Prof. Dr. Yalçın YÜKSEL, Prof. Dr. Mehmet ÖZGER, Assoc. Dr. Berna AYAT AYDOĞAN and Assoc. Dr. Mehmet Cüneyd DEMİREL for their insightful comments, but also for the question, which incented me to widen my research from various perspectives.

I would like to thank Prof. Dr. Ahmet DOĞAN (may Allah rest in peace) who passed away two years ago. I appreciated him for his motivation and support in overcoming numerous obstacles and had been facing through my project, thesis, and my life since we met in 2013. He left us an enlightening legacy that I will always carry and benefit from through all my life.

I would like to thank the hydraulic division for helping me to conduct thesis experiments and providing any assistance requested. Special thanks go to numerous undergraduate students for their continued support in the TUBITAK project. I really appreciate them.

I acknowledge the people who mean a lot to me, my grandparents, for showing faith in me and giving me love to choose what I desired. I salute you all for the selfless love, care, pain, and sacrifice you did to shape my life. They have a significant place in my life. In addition, I express my thanks to my aunts especially Fatma Uçar and my uncles-in-law. I also thank to my cousin, who is like my sister, Rabia. I spent valuable time with her in my childhood.

I owe special thanks to father-in-law, Akif TAN, mother-in-law, Emine Dilek Tan and brother-in-law. They open to me their life, share valuable times and support in the last two years of my thesis journey. I am so grateful to them.

Last but not the least, I would also like to extend my deepest gratitude to my family: my parents Ali KESGİN, Rukiye KESGİN, and to my brothers Erdoğan and Emirhan KESGİN for supporting me spiritually throughout writing this thesis and my life in general. I owe everything to my family who encouraged and helped me at every stage of my personal and academic life.

I owe thanks to a very special person, my wife, İlayda for his continued and unfailing love, support, and understanding during my pursuit of a Ph.D. degree that made the completion of my thesis possible. You were always around at times I thought that it is impossible to continue, you helped me to keep things in harmony. I greatly value her contribution and deeply appreciate her belief in me. The words would never describe how grateful I am to my beloved wife. I consider myself the luckiest in the world to have such a lovely and caring family with my beloved wife and my baby boy, Alperen, standing beside me with their love and unconditional support.

Finally, I dedicate this work to my generous family, my beloved wife, and my baby boy Alperen.

Erdal KESGİN

TABLE OF CONTENTS

LIST OF SYMBOLS

C_uC	Coefficient of Uniformity
C_D	Drag Coefficient
α	Inverse of Air Entry (Bubbling Pressure)
KE	Kinetic Energy
cm	Mean of Measured Values
rm	Mean of Predicted Values
PC	Pearson Coefficient
l	Pore Connectivity
h	Pressure Head
θ_r	Residual Water Content
θ_s	Saturated Water Content
S	Sink Term
cd	Standard Deviation of Measured Values
rd	Standard Deviation of Predicted Values
n	Steepness of the Soil Water Retention Curve
K	Unsaturated Hydraulic Conductivity
θ	Volumetric Water Content

LIST OF ABBREVIATIONS

KGE	Kling and Gupta Efficiency
MD	Mole Drainage
NSE	Nash-Sutcliffe Efficiency
PC	Pearson Coefficient
PD	Pipe Drain
RS	Rainfall Simulator
SG	Sand Grooving
SD	Slit Slitting
SWRC	Soil Water Retention Curve
SWT	Suspended Water Table
USDA	United States Department of Agriculture

LIST OF FIGURES

LIST OF TABLES

ABSTRACT

Investigation of Effective Drainage Methods in Sports Field under Various Rainfall Conditions

Erdal KESGİN

Department of Civil Engineering

Doctor of Philosophy Thesis

Supervisor: Prof. Dr. Hayrullah AĞAÇCIOĞLU

The starting point of this study is to investigate different techniques and drainage mechanisms of sports fields which takes the attention of big crowds all over the world due to big sports organizations. These type of international sports organizations has social and economic impacts on countries hosting these events. Therefore, drainage of sports fields under various rainfall conditions is a very crucial engineering issue to be investigated. The first goal of the two main purposes of the thesis is to investigate the optimum thickness and particle size gradation of the drainage layer which is consisted of rootzone-sand- and gravel, the second goal is to determine the behaviors of different constant rainfall intensities and durations under which a sporting event can be performed comfortably without any ponding on the surface of the turf and without deteriorating turf quality required for sports events. This study has both experimental and modeling portions. An experimental setup (rainfall simulator and drainage tanks) was developed and calibrated to model the field conditions of sports fields under critical rainfall duration and intensity. Experimental rainfall hyetographs for different durations and return periods were also designed. 100 experiments were conducted to investigate hydrological descriptions of unsaturated flow (variable saturated flow) by using multiple packed sports field drainage layers (Pipe Drain (PD), Suspended Water Table (SWT), Sand Groove (SG), and Slit Drain (SD). The hydrograph parameters which are a time to start to drain, maximum outflow, time to reach maximum outflow, and infiltration rate were also evaluated for PD, SWT, SG, and SD. The hyetographs had more distinctive effects on the shape of the drainage outflow hydrographs for PD and SWT. The rainfall intensities were not separately caused to surface ponding for each drainage method in this study. For 90 mmh^{-1} and lower rainfall intensities, three drainage methods demonstrated similar drainage behaviors except for SD. The subsequent greater rainfall intensities were induced different maximum drain outflows for each drainage technique. The SWT was thought that it is the most drainable and applicable drainage technique in terms of hydrological perspectives. Therefore, for SWT, time-dependent water contents were also monitored using soil moisture sensors at different depths in the drainage layers. Soil water retention curve (SWRC) of each drainage layer obtained from calibration tests and empirical parameters were optimized with HYDRUS-3D model which solves 3-D Richards's equation using finite element method through saturated unsaturated media by using water contents and suction pressure results. Observed drain outflow hydrographs were compared with simulated drain outflow hydrographs by using statistical indices of Nash-Sutcliffe Efficiency (NSE) index, Kling and Gupta Efficiency (KGE) index, and determination coefficient (R^2). Experimental results and HYDRUS-3D simulations showed good compatibility with the values of NSE, KGE and R2 varied between 0.859-0.958, 0.594-0.972, and 0.868-0.975, respectively.

Keywords: Drainage, Sports field, HYDRUS, Rainfall simulator, Nash-Sutcliffe efficiency

ÖZET

Spor Alanlarında Etkili Drenaj Yöntemlerinin Farklı Yağış Koşullarında Araştırılması

Erdal KESGİN

İnşaat Mühendisliği Bölümü

Doktora Tezi

Danışman: Prof. Dr. Hayrullah AĞAÇCIOĞLU

Büyük kitlelerin ilgisini çeken, sosyal ve ekonomik anlamda uluslararası öneme sahip spor etkinliklerinin düzenlendiği çim sahaların her türlü yağış şiddetine karşı hızlı ve etkin bir biçimde drenajını sağlayacak tekniklerin araştırılması, ayrıca hangi yağış şiddeti ve süresinin etkinliğe engel olabileceğinin araştırılması bu tezin çıkış noktasıdır. Bu projenin başlıca hedefinden birincisi, spor yapmaya uygun bir çim tabaka ile drenaj boruları arasındaki tabakanın optimum kalınlığının ve buradaki kum-çakıl katmanlarının dane boyutlarının gradasyonunun belirlenmesi, ikincisi ise bu drenaj tabakasının hangi şiddet ve süreli yağışı etkin ve hızlı bir şekilde çim tabakadan alıp drenaj borularına ulaştırabileceğinin araştırılmasıdır. Bu konu, hem hidrolojik, hem de drenaj tabakasındaki katman sayısı ve dane boyutlarının sıralaması (gradasyonu) ve aynı zamanda çim tabakanın spor yapmaya en elverişli koşullarda korunması göz önünde bulundurularak araştırılmıştır. Tez çalışması hem deneysel hem de modelleme çalışması içermektedir. Çalışma kapsamında, spor sahalarının zeminlerini modellendiği ve kritik yağışları zaman-şiddet olarak ayarlayabileceğimiz yağmurlama sistemine ve drenaj tankına sahip bir deney düzeneği geliştirilmiş ve kalibre edilmiştir. Çalışma kapsamında, farklı süre ve tekerrürlere sahip tasarım hiyetografları oluşturulmuştur. Farklı doygunluğa sahip ya da doygun olmayan akımların hidrolojik açıdan değerlendirilmesi amacıyla farklı drenaj teknikleri (Basit Boru Drenajı (PD), Üç Katmanlı ya da Askıda Su Seviye Drenajı (SWT), Kum Oluklu Drenaj (SG) and Kum Yarmalı Drenaj (SD) üzerinde toplam 100 adet deney yapılmıştır. Bu drenaj deneyleri için çıkış hidrografları elde edilmiş, hidrograflara ait drenaj başladığı süre, maksimum debi, maksimum debi çıkış süresi ve sızma oranları gibi parametreler saptanmıştır. Hiyetograf türünün hidrografın şekli üzerinde etkisi PD ve SWT teknikleri üzerinde daha belirgin olduğu bulunmuştur. Deneyler sırasında herhangi bir deneyde göllenme oluşmasına izin verilmeden deneyler gerçekleştirilmiş, 90 mmh^{-1} ve daha düşük yağış şiddetlerinin SD dışındaki diğer teknikerlerde drenaj davranışının benzer olduğu bulunmuştur. Hidrolojik açıdan daha elverişli olduğu tespit edilen SWT drenaj tekniği için farklı drenaj tabaklarında su muhtevası ve metrik potansiyel ölçümleri yapılmıştır. Su-Zemin Karakteristik eğrileri farklı katmanlar için kalibrasyon deneyleri sırasında tespit edilmiş bu değerleri doygun olmayan ya da farklı doygunluğa sahip zeminlerde Richard denklemini sonlu farklar yardımıyla çözen HYDRUS yazılımı ile modelleme çalışması gerçekleştirilmiştir. Deney sonuçları ile HYDRUS simülasyon sonuçları hem çıkış hidrografları hem de su muhtevaları Nash-Sutcliffe verimi (NSE), Kling and Gupta verimi (KGE) ve determinasyon katsayısı kullanılarak (R^2) mukayese edilmiştir. Sonuçlar birbirleriyle uyumlu olup NSE, KGE and R^2 değerleri sırasıyla 0,859–0,958, 0,594–0,972 and 0,868–0,975 arasında bulunmuştur.

Keywords: Drenaj, Spor Sahası, HYDRUS, Yağmurlama Simülatörü, Nash-Sutcliffe verimi

---

YILDIZ TEKNİK ÜNİVERSİTESİ

FEN BİLİMLERİ ENSTİTÜSÜ

1
INTRODUCTION

1.1 Literature Review

The global warming has changed the regime of many hydrological events such as rainfall-runoff relationship, stormwater, and urban drainage in the last decades. One of the most affected issues is the drainage of the sports field. The sports field are significant places that bring thousands of people together as part of social and sportive activity. Many global sports organizations were canceled due to the insufficient drainage which was not drained fast enough from field surfaces and high intense rainfalls for a short time that interrupted the game in the field. As commonly known, these organizations attract the attention of thousands of people and bring them together as a part of social activity. Due to unexpected rainfall events there happens considerable economic losses and discomfort of people. The increasing number of cancellations showed that this problem should be investigated and can be evaluated as a hydrological problem considering drainage of the multi-layered soils in the sports field.

The drainage of the sports field is quite different from the land and urban drainage systems such that the quality of the rootzone has to be protected and drainage gutters cannot be placed on the sports field to capture the runoff. For many years, only a few researchers have focused on the drainage of the soil, however, there are no comprehensive studies that deeply evaluated the processes of sports field drainage. The main objective of this study is to develop a methodology for the mechanisms of sports field drainage that remove excess rainfall from the surface of the field as fast as possible, monitor the unsaturated flow characteristics through the drainage layers, and investigate the effects of intense rainfalls by considering design storms for different rainfall intensities both experimentally and numerically. A new RS-DT setup was developed to investigate the drainage in the multi-layered soils of the sports field, which can produce and measure the natural-like rainfall characteristics together with required measurement abilities for the drainage process.

This study was dedicated to evaluating the drainage of a sports field by considering unsaturated flow characteristics and simulated natural rainfall according to historical precipitation records. Therefore, within this scope, some sub-topics regarding this research were specified to investigate the literature such as rainfall simulator, sports field drainage, numerical modeling with HYDRUS.

1.1.1 Rainfall Simulator

To understand the drainage process, a rainfall simulator and measurement methods of rainfall toward obtaining natural rainfall characteristics are very crucial. It is the fact that natural rainfall is a stochastic event that its effects are grueling to estimate. The RSs are common and useful tools that allow for controlling these effects properly. They have been also used for many years to understand the logic of agricultural, environmental, and hydrological studies such as runoff, soil erosion, and soil crusting, nutrient and pollute transport, infiltration, and drainage of soils.

The primary purpose of the RS is to simulate the characteristics of natural rainfall. Its performance is characterized by several criteria that require drop diameter to natural rainfall (Bubenzer, 1979), impact velocity close to the terminal velocity of natural rainfall (Laws and Parsons, 1943), and spatial uniformity (Laws and Parsons, 1943). Two common types of RSs are classified according to how they produce raindrops: non-pressured RSs (drop former simulators) and pressured RSs such as spraying nozzles. Many researchers have studied with different rainfall simulators. Hignett et al. (1995) studied using a non-pressured rainfall simulator to evaluate the breakdown of soil aggregates (Figure 1.1). Their study described the laboratory rainfall simulator capable of producing rainfall of variable raindrop kinetic energy flux at the soil surface by varying raindrop size, drop height, and rainfall intensity. This simulator was designed to study the breakdown of soil aggregates during simulated rainfall under conditions of variable soil and rainfall factors. Hereby, minimum energy should be identified, below which many soils do not break down, irrespective of rain depth even at the very high rainfall intensity.

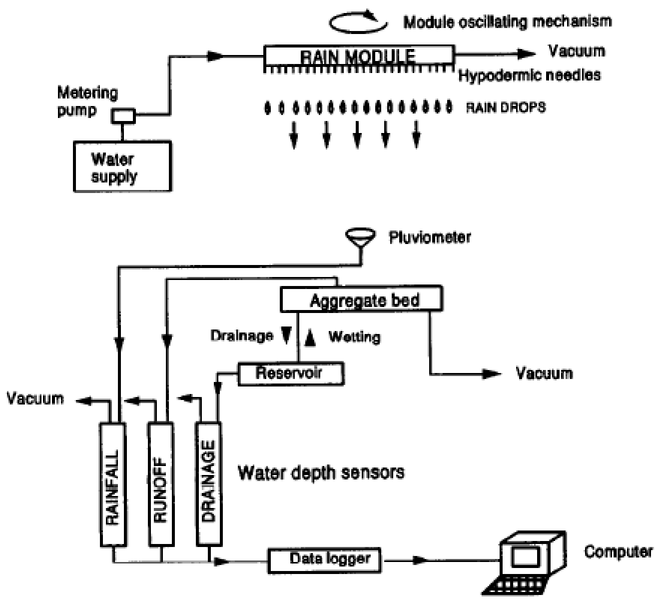

Figure 1.1 Laboratory Scale Non-Pressured Rainfall Simulator (Hignett et al., 1995)

Rainfall simulators applied in field erosion researches need to have a uniform distribution of drops over a large area (~1 m^2). Spinning disk and spray disk nozzle types achieve these requirements but suffer from the disadvantage that raindrop energy is constant and high irrespective of the intensity of application. Therefore the in such sprays, the nozzle flow, and drop size distribution remain constant and variation in intensity is achieved by intercepting the stream before it reaches the soil. The particular importance of this study was the control of rainfall energy flux density which could be varied by independently varying raindrop energy and rainfall intensity. The incorporation of electronic sensors in various parts of the simulator allowed detailed measurements of rainfall intensity, runoff, and drainage, producing insights into the effects of rain on surface sealing and soil compaction. During this study ponded water on the soil surface was removed by runoff, preventing interaction between water on the surface and rain. Depth of rainfall and runoff and drainage was measured by electronics sensors and data stored in a computer. Using the electronic measurement of high sensitivity, with computer monitoring has provided a level of chronological detail not previously possible in this work. The properties of rain that are most important in understanding soil structural stability, total energy, and energy flux density could be controlled in this designed rainfall simulator.

Humphry et al. (2002) stated that drop former RSs have not been preferred in laboratory tests due to the limited access to the water supply. Therefore, they generate a narrow range of drop diameters and small fall velocities. It can be inferred that they have numerous disadvantages compared to pressured RSs. However, Clarke and Walsh (2007) and Corona et al. (2013) investigated surface runoff, splash and slope wash assessment using a drop former simulator (Figure 1.2)

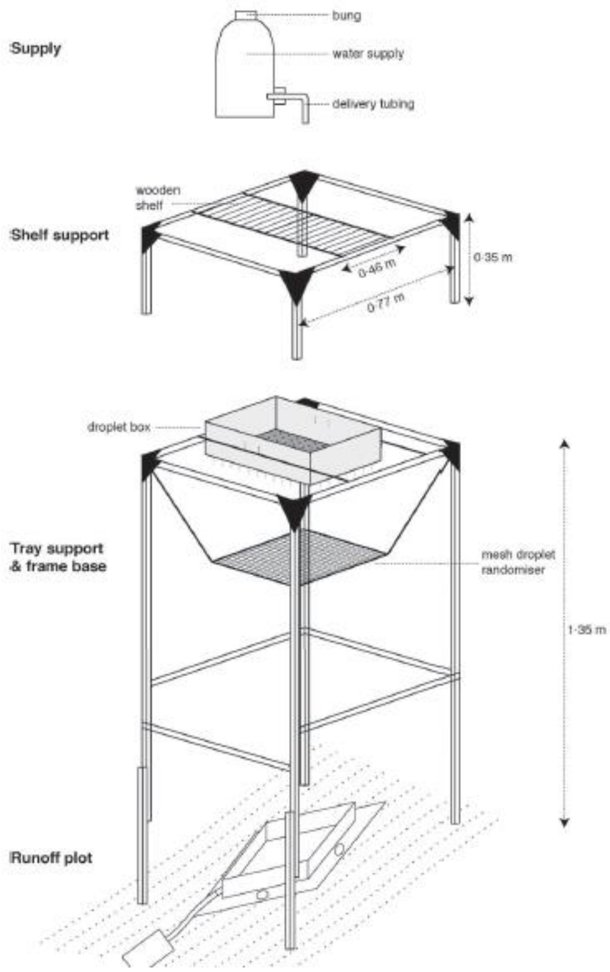

Figure 1.2 Design of Drop Former Rainfall Simulator (Clarke and Walsh, 2007)

Many investigators have used the pressured RS in their research, especially, those focused on runoff and erosion studies. They developed a laboratory-scale RS that is capable of producing rainfall with various raindrop kinetic energy at the soil surface by varying raindrop size, drop height, and rainfall intensity. It was also clearly demonstrated that pressured RSs can produce raindrops approaching terminal velocity without relying on gravity. Iserloh et al. (2013) compared the 13 fields RSs that were developed in Europe to standardize the rainfall characteristics such as rainfall intensity and raindrop distribution (Figure 1.3). They mentioned that identical measurement techniques enabled to comparison of simulated rainfall parameters for different RSs. They also evaluated to assess the erosion, infiltration, and runoff in field conditions. Similarly, Battany and Grismer (2000) developed a field RS that was used in hillside vineyard runoff and erosion studies. On the other hand, Clarke and Walsh (2007) stated the laboratory-scale RSs have less effacer effects on temperature, wind, and humidity. Aksoy et al. (2012) also emphasized the importance of a laboratory-scale RS that is used for rainfall-sediment transport processes.

Determining the drop diameter of simulated rainfall is a difficult task about which a few techniques were developed in the literature. Accurate raindrop size is also significant for the simulation of natural rainfall. Manual measurement techniques to determine the raindrop diameter have been used in literature for many years. These include (Kathiravelu et al., 2016) stain method (measurement of stains dyed absorbent paper), flour pellet method (measurement of flour pellets that are formed raindrops), and oil immersion method (determination of the raindrops in containing oil). Despite the availability of recent technological methods such as disdrometer and laser measurement techniques, manual methods are simpler,

Figure 1.3 The View of The Small Scale 13 Rainfall Simulators: a) Tubingen, b) Cordoba, c) Basel, d) Granada, e) Almeria, f) Malaga, g) Murda, h)Trier, i) Zaragoza, j) Valencia, k) Zaragoza-University, l) La Rioja, m) Wageningen (Iserloh et al. (2013).

cheaper but time-consuming. In this study, raindrop diameters were determined by using the flour pellet method which was first used by Bentley (1904) to determine the drop size distribution of rainfalls in Washington. Many researchers preferred this technique due to its practicality. They successfully simulated natural rainfall with the great accuracy of raindrop diameters. Aksoy et al. (2012), Clarke and Walsh (2007), and Perez-Latorre et al. (2010) were used the flour pellet method to determine the diameter of simulated rainfall raindrops for sediment transport, runoff studies, and field assessment of slope and splash, respectively. Laws and Parsons (1943) were also found raindrop diameters using this method and most of the design parameters of RSs are referred to in their study. Blanquies et al. (2003), Hudson (1963), Kohl (1974), and Asante (2011) were similarly measured drop sizes using different versions of the flour pellet method. In the literature, a summary of the research studies that used the flour pellet method to determine raindrop diameter is given in Table (Kathiravelu et al., 2016).

The study of Abudi et al. (2012) has the main objective of designing and constructing portable rain simulators that should be used in the field for simulating rainfalls that can induce soil crusting and thus lead to the generation of runoff and eventually to soil erosion. Rainfall simulators have a wide application in different studies such as soil, agricultural, and environmental studies. The advantage of using rain simulation is the rapid data collection under relatively uniform conditions. As presented by Hignett et al.(1995), the desirable feature for a rain simulator is an accurate reproduction of natural rainfall drop sizes and energies, nearly continuous, uniform application over an area of 1 m^2 or larger, the ability to apply rainfall of varying durations and intensities of interests, and portability and low cost. One limitation of the existing rain simulators is that they are not quite successful in applying an energy flux similar to the one characteristic of natural rainfall. The energy produced by these existing rain simulators is usually high in respect to the intensity of application and this high energy becomes a crucial disadvantage for runoff studies (Hignett et al., 1995). The main components of field rain simulators are: (1) a drop generator and its pedestal capable of homogeneously wetting a preferably large area and producing water distribution drops with a drop size distribution similar to that of natural rainfall; (2) a water feeding system and (3) a windshield surrounding the irrigated area.

Table 1.1 Summary of the studies used the flour pellet method (Kathiravelu et al., 2016).

Research Study and Location	Purpose of Use	Method used
Laws & Parsons (1943)	To measure drop sizes from natural storms	After sampling with raindrops, the formed pellets were dried in an oven. Pellets were sized with sieves and weighed. The size was calibrated by weighing dried pellets produced by drops of a known size.
Hudson (1963)	To measure drop sizes from natural storms	A tray (0.05 m^2) of flour was exposed to simulated rainfall for a period of 1 s. The flour wf s then dried for 24 h at ambient temperature (28-30 °C) and the pellets formed were passed through a series of sieves (4.75, 3.35, 2.36p 1.18 and 0.85 mm). The pellets were then dried for 24 h at 105 °C, weighed, and measured.
Kohl (1974)	To verify the nozzle produced drop sizes in the rainfall simulation studies	Circular pans 21 cm in diameter and 2 cm deep were filled with flour and made level with a straight edge. After exposure to raindrops, the flour was dried (24 h at 38 °C). An 18. 3 cm diameter sample was taken from the tice center of the pan to avoid splash effects. The pellets were sieved (U.S. series 5 to 50 mesh) and weighed.
Carter et al. (1974)	To study drop size distribution of natural rainfall	A circular pan (31 cm diameter) of flour (1.6 cm deep), was exposed in a rain for a short time. The pellets formed were first air- and later oven-dried and weighed. Raindrop diameter was estimated from the weight of the pellets.
Navas et al. (1990)	To verify the nozzle produced drop sizes in the rainfall simulation studies	A 25.4 cm diameter plate containing an uncompacted, layer of flour (2.54 cm thick) is exposed to rainfall for 1-4 s. The small flour balls are dried for 24 h at 105 °C and sieved (5000, 3000,1000, 630, 500 and 250 pm) the fractions are weighed. Calibration of drops is required.
Ogunye and Boussabaine (2002)	To verify the simulated drop sizes in the rainfall simulation studies	Exposure time is restricted to 1 s to minimize coalescence of the pellets in the flour. Large sample size is required to minimize the variability in counts of the rare large drops.
Arnaez et al. (2007)	To verify the nozzle produced drop sizes in the rainfall simulation studies.	Raindrops formed small pellets in the flour that were photographed and analyzed by a computer.
Herngren (2005) Egodawatta (2007) Miguntanna (2009)	To verify the nozzle produced drop sizes in the rainfall simulation studies.	A tray (diameter 240 mm) of compacted flour was exposed to simulated rainfall for a period of 2 s. Flour was dried for 12 h at 105 °C, and the pellets were sieved (4.75 mm; 3.35 mm; 2.36 mm; 1.18 mm; 0.6 mm; and 0.5 mm).

Table 1.1 Cont. (Kathiravelu et al., 2016).

Perez-Latorre **et al.** (2010)	To verify the nozzle produced drop sizes in the rainfall simulation studies.	A flour layer (1 cm depth) was placed over a surface of 50 cm x 50 cm and compacted using a ruler. The floured surface was covered to protect it from rainfall except when the cover was removed for 2 s during the simulation to collect drop samples. The diameter of pellets was measured using a caliber (+0.1 mm).
Asante (2011)	To verify the nozzle produced drop sizes in the rainfall simulation studies.	A thin layer of cassava flour and wheat flour were spread on separate trays and passed through a rain shower. The flour was dried and the pellets separated according to their size ranges using a nest of sieves. The size of raindrops was calculated from the size of pellets.
Parsakhoo **et al.** (2012)	To verify the nozzle produced drop sizes in the rainfall simulation studies.	The drop impact on flour was estimated using a ruler.

When dealing with runoff generation on natural soil, the wet area becomes an important parameter. The area of the irrigated plot should be no less than 1x1 m (Hignett et al. (1995). For this study, the 1 ½ H 30 nozzle was used. This nozzle is able to generate a 90° full cone of water drops with a D_{50} of 2.25 mm and with a uniform distribution (C_uC=0.85) when working under a constant flow rate of 7.7 m^3/h and pressure of 0.6 bar. This nozzle should be located above 2 m above the ground level for the generated drops to achieve their terminal velocity. The intensity is determined by the rotating disc mechanism that creates the pulsed flow, and the flow rate of the rain simulator is regulated by a pneumatic valve operated by an electric controller (Miller, 1987).

The rainfall intensity changes according to the duration that the valve is open and the time intervals between each spraying pulse. The required pressure of 0.6 bars was archived by connecting a pressure regulator to the nozzle inlet. Water was supplied by the tank which can provide enough water storage for the high flow rate nozzle. As result, the high accuracy portable rain simulator for a field that generates drops of D_{50}=1.5 mm, with a ground velocity that nearly matches the theoretical terminal velocity without the need for a relative high tower, was built. The energy flux of simulated rain is 76% of the energy flux expected for a natural rainfall of the same intensity.

In the literature, it was seen that meshes have been used in the RS beneath the spraying nozzle to arrange the simulated rainfall parameters. Carvalho et al. (2014) investigated the mesh effects on the rainfall simulation by controlling the intensity, drop size distribution, and fall velocity with the changing differences between mesh and nozzle over the 1 m^2 control plot as shown in Figure 1.4 Experimental Setup of Carvalho et al.'s Study (Carvalho et. al., 2014). They finally resulted that the meshes increased the rainfall intensity over the plot, fall velocity was not remarkably affected and the median diameter of simulated rainfall increased by the presence of meshes. It can also be mentioned that the meshes contributed to the spatial uniformity on the control plot due to the formations of bigger simulated raindrops.

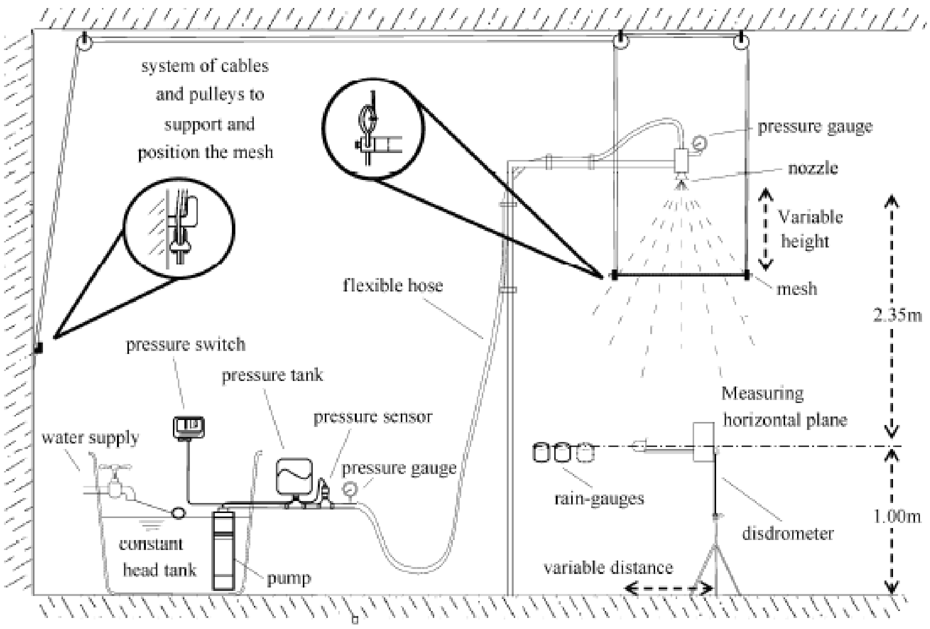

Figure 1.4 Experimental Setup of Carvalho et al.'s Study (Carvalho et. al., 2014)

Moreover, Carvalho et al. (2015) also stated to explore the usefulness of incorporating meshes underneath pressurized nozzles that intercept the drops sprayed out by the nozzles and change the simulated rain characteristics, namely by increasing the rainfall kinetic energy (Figure 1.5). Experimental field and laboratory work, relying on simulations of rain, has contributed much to the increased understanding of various hydrological and geomorphologic processes. The versatility of rainfall simulators enables them to be used in the laboratory and the field, providing controlled conditions of rainfall intensity and duration. However the capacity of reproducing natural rainfall events through simulations is limited, the simulated raindrops should desirably have the size and fall speed observed in nature because these are the key variable affecting the key kinetic energy of individual drops that particularly enhance soil detachment.

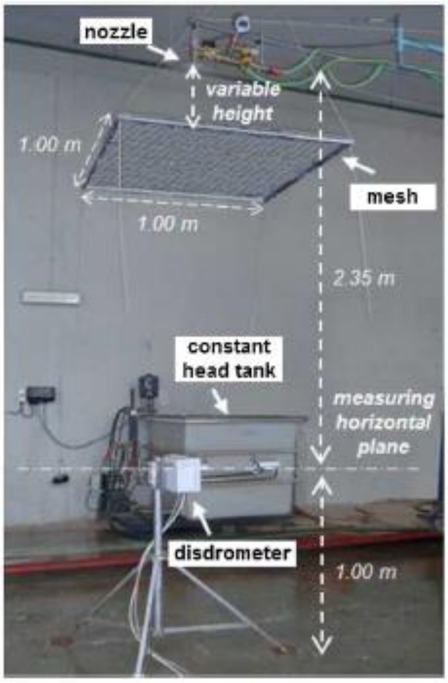

Figure 1.5 Schematic View of Laboratory Installation of Rainfall Mesh (Carvalho et al., 2015)

In literature, similar RSs were generally developed to investigate the mechanism of infiltration, runoff, sediment transport, erosion. Table summarized the rainfall characteristics of different pressured rainfalls by comparing the type of RS, simulated area, rainfall intensity, drop diameter of produced rainfall, the kinetic energy of raindrops, and uniformity of spatial distribution over the control plot and scope of the study.

Table 1.2 Comparison of rainfall characteristics for different rainfall simulators in the literature (Abudi et al., 2012 and Kesgin et al., 2018).

Study	Type of RS	Area (m^2)	Intensity ($mm\ h^{-1}$)	Drop Diameter (mm)	Kinetic Energy ($J\ mm^{-1}\ m^{-2}$)	Uniformity (%)	Scope of Study
Morin et al. (1967)	Single Nozzle	1.75	29-142	1.5-2.25	16-22	80-90	Design and operation of RS.
Meyer and Harmon (1978)	Single Nozzle	2.54	10-140	1.5-2.5	20-27	-	Erosion.
Miller (1987)	Three Nozzle	3	43-116	2.25-2.5	23.1	83	Design and operation of RS.
Cerda et al. (1997)	Single Nozzle	0.24	10-60	2.53	7.1	93	Design and operation of RS.
Borselli et al. (2001)	Full Cone Nozzle	0.6	67	2.25	16.63	97	Infiltration, runoff and erosion.
Hignett et al. (1995)	An array of 1600 Hypodermic needles	1	40-100	2.7, 5.1	1.6-19.9	-	Soil Drainage.
Assouline et al. (1997)	Single Nozzle	16	12, 20, 28	1.17, 1.21, 1.34	$\cong$ 13	85	-
Singh et al. (1999)	Rotating Perspex Cylinder with Capillary Holes	0.15	60, 100	5.17, 5.86	-	-	Infiltration, runoff, and erosion.
Abudi et al. (2012)	Single Nozzle	9	130	1.5	9.89	98	Runoff studies.
Aksoy et al. (2012)	4-5 Veejet Nozzles	8.84	45-105	2.19-3.13	21.1-32.6	82-89	Runoff-sediment transport.

1.1.2 Sports Fields Drainage

It was understood from the literature that RSs were generally used for erosion and runoff studies with different versions. The drainage process of the sports field which is intended to remove excess rainfall from the surface of the field as fast as possible is also an essential engineering problem that needs to be investigated carefully.

However, there are a limited number of studies that specifically focused on this issue. The main objective of this study is to develop an instrument of a setup at a laboratory scale to evaluate processes of the sports field drainage under various hydrological conditions. To achieve this goal, a new experimental setup was developed in creating natural rainfall by successfully measuring the intensity and uniformity with the suggested methodology. Furthermore, Adams (1986) stated that sports field drainage is different from agricultural drainage. It required that incident rainfalls were transmitted to drainage pipes for maintaining a proper and playable field surface. His study stated that complete profile reconstruction, which consists of rootzone for turfgrass, blinding layer (sandwich layer), and permeable bed with gravel, is the most comprehensive approach for high-quality sports field although it is one of the most expensive designs (Figure 1.6). He also focused on the content of rootzone mixture, grain sizes used in blinding, and gravel layers in terms of practical aspects of sports field drainage.

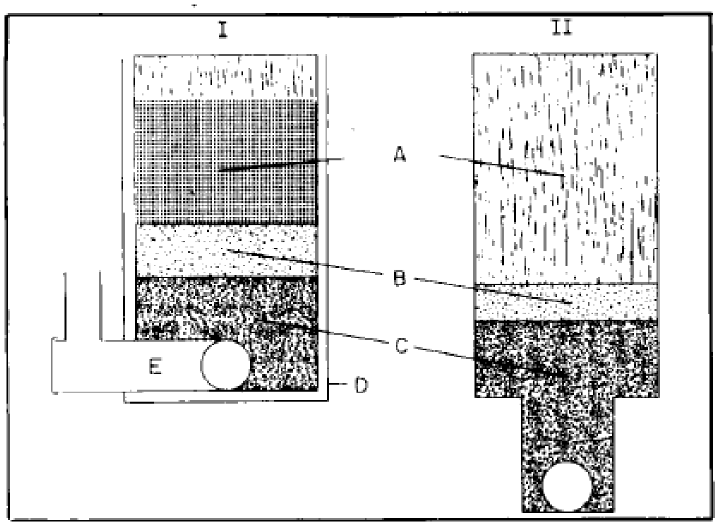

Figure 1.6 Constructions of Three-Layer Type. A: Rootzone; B: Blinding Layer; C: Permeable Bed; D: Polythene Liner; E: Drain Outlet with Water Table Control (Adams, 1986)

Therefore, the drainage of the sports field has not been comprehensively investigated in the literature and its design was based on traditional experience with considering indefinite science (Fleming et al., 2017). The hydraulic performance of the drainage of the sports field has not been determined sufficiently in terms of hydrological perspectives. Fleming et al. (2017) investigated the drainage behavior of the sports field using field observations and mathematical modeling by using Microsoft Excel. They reported that the field observations from the sports field were not reliable and predictable with comparing measured and estimated drain outflows. Moreover, their study also showed that porous field designs provided high attenuation of peak rainfall of drain outflow hydrograph with considering the design procedure of Conceptual Model for Sustainable Drainage System in SuDs shown in Figure 1.7 for storms varying periods between 2011 and 2014.

The study of Fleming et al. (2017) did not consider the unsaturated flow characteristic of drainage layers. In addition, their mathematical model was not sufficiently comprehensive to simulate the hydraulic behavior of drainage layers. In detail, their study findings were evaluated by dividing 3 parts into fieldwork, laboratory results, and mathematical modeling. As fieldwork,

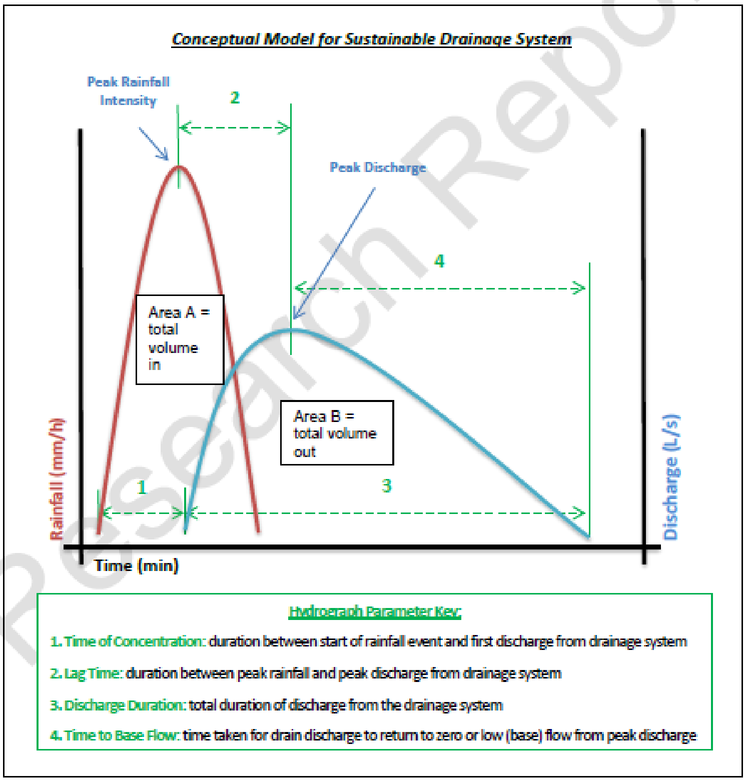

Figure 1.7 Conceptual Model for Sustainable Drainage System in SuDS (Fleming et al., 2017)

eight different in-service sports fields were monitored during the study for different periods between 2011 and 2014 in England. These fields involved both artificial and natural turf pitches. Figure 1.8 and Figure 1.9 showed the typical design view of the artificial and natural sports fields, respectively. They mentioned that collecting field data had many challenges for research due to uncontrolled and inconsistent conditions. They finally concluded that this study was not sufficient to monitor the drainage mechanism of the sports field in detail. Therefore, the field observations were not consistent and predictable. According to field findings, natural sports fields are more effective to remove excessive rainfall from field surfaces compared with artificial sports fields. In brief, Fleming et al. (2017) evaluated that the drainage of a sports field can be considered as a sustainable drainage instrument for integrated stormwater management.

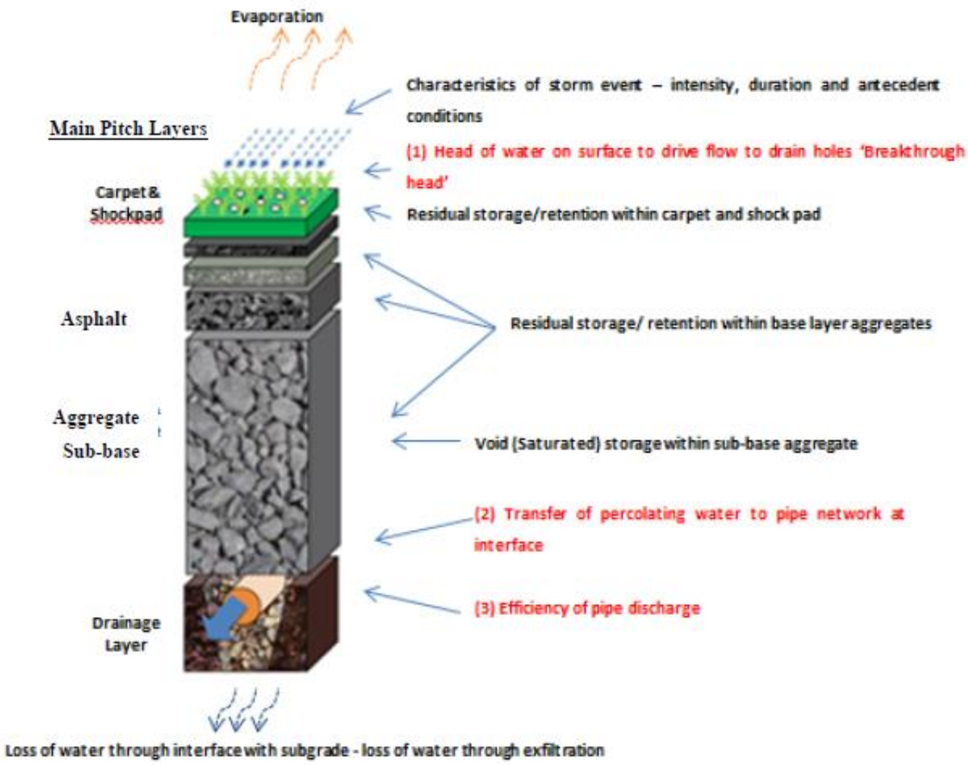

Figure 1.8 The Design of the Typical Artificial Sports Field Construction (Fleming et al., 2017)

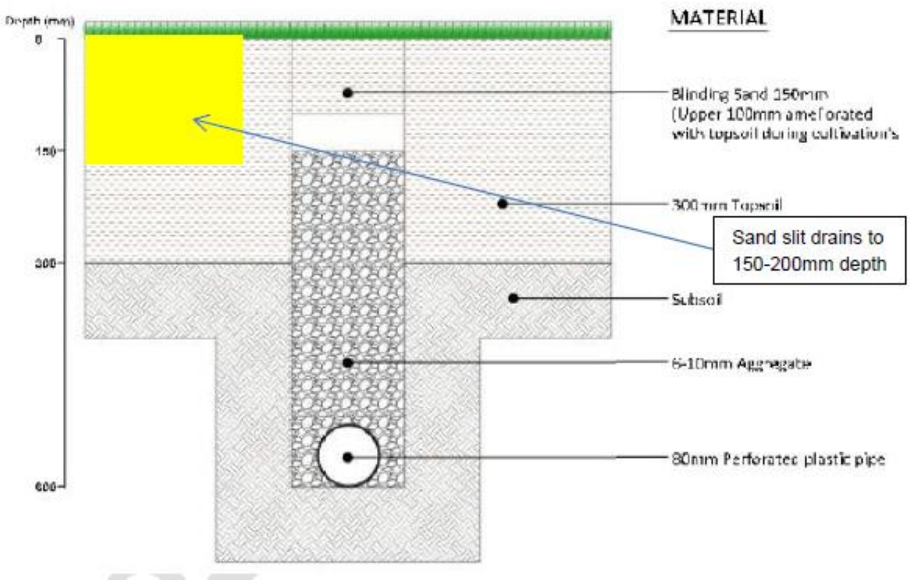

Figure 1.9 The Cross-Section of the Natural Turf Pitches Construction with Sand Slits (Fleming et al., 2017)

Similarly, Hudepohl et al. (2016) investigated hydrological modeling of synthetic turf fields. They aimed to understand the flow characteristics by considering different storm events in the synthetic turf drainage system and determine the rainfall-runoff process by developing a computer model. They used one of the most common cross-sections of the synthetic drainage layers. Moreover, the size of the main collector drainpipe was determined peak flow rates based on the rational method. They finally stated that their study was not sufficient to estimate the peak flows from a synthetic turf field, however, an overall hydrological process was characterized by governing runoff at these fields.

Focusing on the infiltration in layered soils by using RS, Zhao et al. (2014) investigated the processes of the rainfall-runoff and soil moisture dynamics in grasslands plots under simulated rainfall. They prepared soil bins that were packed with a 2.5cm fine sand layer at the bottom and cultivated a silty loam soil layer to a total depth of 50cm. They also measured the soil water characteristics such as soil moisture using the EC-5 sensor. It could be concluded that the soil moisture in the 20cm soil depth responded rapidly to rainfall and interflow into the soils occurred under continuous rainfall conditions. For runoff mechanism, the infiltration-excess overland flow was dominant when the experimental setup was exposed to high rainfall intensity, on the other hand, the saturation-excess flow would occur when the soil profile became saturated.

Sports field can be considered as a part of the urban drainage; however, there are some main differences that the sports field have independent drainage systems which are designed not to cause runoff and ponding water condition on the surface in terms of optimum design standards. Besides the differences, Sustainable Urban Drainage Systems (SuDS) design principle is to provide sufficient storage, drain outflow control, to prevent runoff as stated by Woods et al. (2015). There is no standard for runoff rate for the green field, but preserving the quality of turfgrass and creating playable field surfaces corresponding to FIFA (Federation Internationale de Football Association) criteria, no runoff - no ponding condition is more applicable and preferable for a sports field.

There are different drainage techniques in the sports field, one of them is there layer profile construction that is one of the most common methods mentioned by Adams (1986). On the other hand, James et al. (2007) investigated mole drainage as an alternative to sand slit drainage demonstrated as schematic view in Figure 1.10 in natural sports field on clays. They expressed that the main difference between agricultural and sports field drainage is the particular need to protect and maintain sports surfaces for the requirement of safe and enjoyable participation. They reported that mole drainage is an applicable alternative to sand slit drainage due to observing greater reduction for soil water content through the same soil depth in the mole drainage.

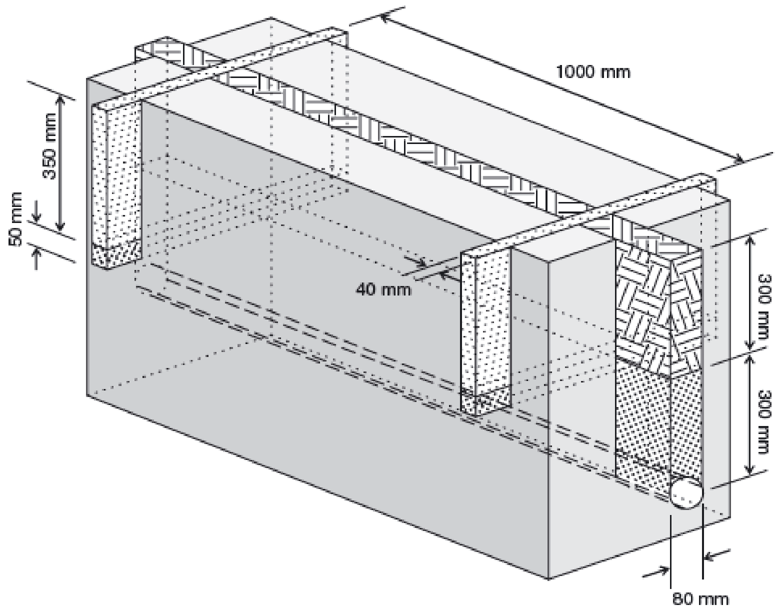

Figure 1.10 The Schematic View of the Sand Slit Drainage (James et al., 2007)

Taylor et al. (1994) had an important study regarding profile layering especially sand or gravel layer beneath the rootzone for golf greens. They focused on the retained water content through the rootzone for different sub-layer treatments shown in Figure 1.11. They emphasized that retained water in the rootzone was affected by soil mixture properties and the coarseness of the underlying layers. Therefore, they resulted that the performance of the drainage of the golf greens was not only dependent on the rootzone mixtures but also characteristics of the layers beneath the rootzone. They also expressed that the sandwich layer or blinding layer has a significant effect on water retention in rootzone mixtures although this layer has been only considered as a filter in a traditional behavior.

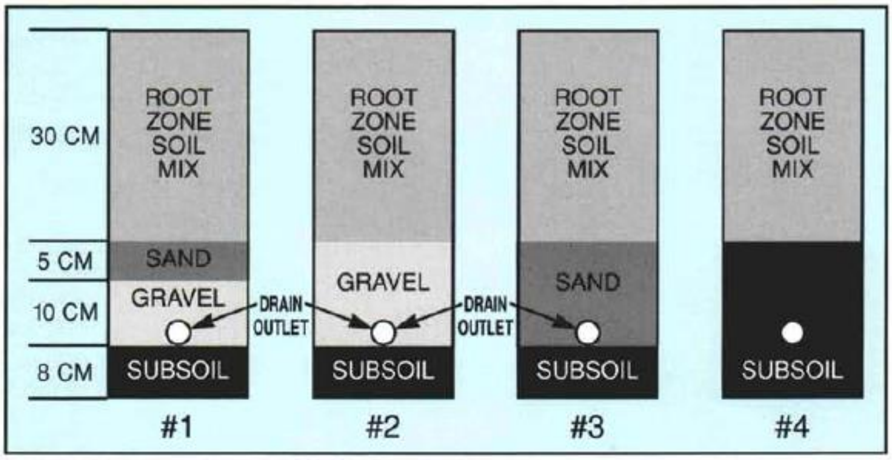

Figure 1.11 The Schematic View of the Sub-Layer Treatments (Taylor et al., 1994)

Therefore, Taylor et al. (1997) studied water retention in the upper layer of drainage profile (rootzone) in the layered soils by considering sub-rootzone layering effects (changing blinding layer and gravel layers). Their study showed the effect of the blinding layer on the water retention of the rootzone. Therefore, selecting rootzone material is very crucial for both the root growth of turfgrass and drainage. Especially, sand-dominated rootzone was used due to its resistance to compaction and healthy drainage. On the other hand, it has some disadvantages because of the little holding capacity and not enough for storing plant nutrients. A laboratory study at Michigan State University demonstrated that at least 90% sand or more (10% silt and clay mix) were acceptable in terms of drainage rate (Henderson et al., 2001). Considering firm footing, adequate resiliency, and resistance to tearing, it is not appropriate to select a 100% sand-dominated rootzone. Determining the optimum thickness of drainage layers plays an important role in terms of enough water holding capacity in the rootzone and draining excessive rainfall without a runoff on the field surface.

Prettyman et al. (2003) investigated profile layering, rootzone permeability on the soil water content in the putting green drainage. They mentioned that soil water content should assist in turf management on sand-dominated greens. The results of their study were mostly related to the presence of the gravel layer beneath the rootzone. It directly affected the lateral soil water content distribution compared with no gravel layer. Hereby, this layer allowed sufficient lateral flow and more uniform water contents.

1.1.3 Unsaturated Flow and Numerical Modelling

Determining the hydraulic behavior of materials used in multi-layered soils of the sports field is crucial to properly model the unsaturated flow. These soils generally have heterogeneities through the profile. Makrantonaki (1997) investigated water drainage in layered soils experimentally and numerically. Soil water content and pressure were measured in a vertical column and the results compared with simulations obtained from the results of the finite difference method by solving the Richards equation in her study.

Similarly, Alfnes et al. (2004) stated that textured layers increased the water capacity of soils and reduced percolation with considering waste contaminants. They investigated the mechanism of water flow and solute transport in the layered soils by conducting drainage experiments. Huang et al. (2011) also investigated the drainage processes in the multi-layered coarser soils. They evaluated the hydraulic performance of natural soils by using HYDRUS-1D through 20 different textured layers. They compared simulated and measured soil water content profiles and drained water volumes during infiltration and drainage phases. Their study demonstrated that a heterogeneous soil profile could store more water when compared to more homogeneous soils under the same drainage conditions.

It has considerably seen progress in the understanding of water flow in the unsaturated zone. HYDRUS model which is commonly used in the literature was used to simulate water flow in variably saturated porous media. In many scientific fields, the HYDRUS model was successfully applied by considering unsaturated flow characteristics with solving Richards' equation. For instance, Hilten et al. (2008) modeled stormwater-runoff relation from green roofs using HYDRUS-1D. They simulated soil moisture of packaged green roofs for a 24-hour storm to find peak flow, retention, and detention time for runoff. The validation of simulated runoff was carried out using collected data from green roofs. Their results demonstrated that the depth of rainfall based on corresponding design storms had significant effects on stormwater mitigation. Furthermore, green roofs reduced stormwater runoff distinctively for small storms that have smaller than 2.54 mm of rainfall depth. Moreover, Ebrahimian and Noory (2014) simulated subsurface drainage of paddy fields with HYDRUS-3D. They stated that the corresponding software was highly capable of simulating subsurface drainage of paddy fields. They also stated that the amount of cracking for topsoil in paddy fields considerably affected the drainage of the subsurface.

Turco et al. (2017) also investigated the unsaturated hydraulic behavior of permeable pavement with HYDRUS-2D. They compared measured and modeled hydrographs with the Nash-Sutcliffe efficiency (NSE) index and determination coefficient using sprinklers to create rainfalls. They did not give sufficient details about the simulated rainfall that is highly significant for the hydrological relation between the hyetograph and drain outflow hydrograph. Their experimental setup was shown in Figure 1.12. They tested the effectivity of HYDRUS-3D that was highly related to the description of hydraulic behavior of pavement system packed in the laboratory. In brief, the hydraulic behavior for laboratory-scale experimental setups (not native soil) that involved a different kind of stratified soils was accurately simulated if the experimental and numerical process or methodology was created precisely with an appropriate model like HYDRUS-3D.

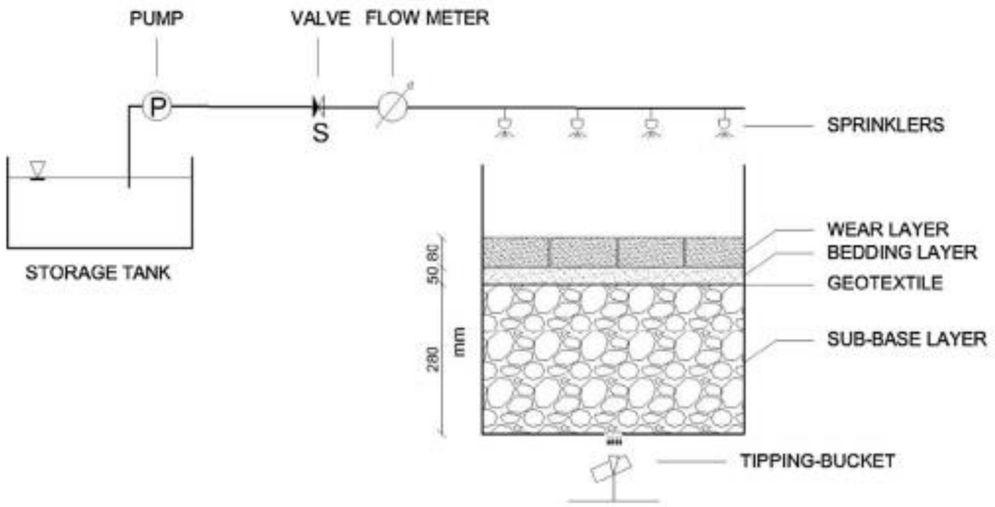

Figure 1.12 Schematic View of the Laboratory Setup of Pavement System (Turco et al., 2017)

1.1.4 Statistical Analysis and Hydrological Model

In the field of hydrology, parameters of the hydrological model are not accurately measurable, therefore it is a fact that this condition is deficient. The design of the drainage systems is directly related to the statistical probability of a rainfall storm occurring based on historical rainfall records and the exceeding of drainage capacity is highly possible in its design life (Fleming et al.,2017). Besides, hydrological model accuracy is generally performed by a few statistical indices in the literature. The coefficient of determination (R^2), Nash-Sutcliffe Efficiency index (NSE) proposed by Nash-Sutcliffe in 1970, Kling and Gupta Efficiency index (KGE) that was developed by Gupta et al. (2009) were widely used to practice for model accuracy. These descriptive statistics were estimated for the validation of the simulation capability of drain outflow results based on Eqn. (1) and Eqn. (2) as follows:

$$NSE = 1 - \frac{\sum^{n}(\hat{Y} - Y_i)^2}{\sum^{n}(Y_i - \bar{Y})^2} \tag{1.1}$$

where $\hat{Y}$ and Y_i are the predicted and measured values for the dependent variable Y, $\bar{Y}$ is mean of the measured values and n sample size.

$$KGE = 1 - \sqrt{(PC-1)^2 + (\frac{cd}{rd} - 1)^2 + (\frac{cm}{rm} - 1)^2} \tag{1.2}$$

where PC is the Pearson coefficient (R), cm and rm are the mean of the measured and predicted values, cd and rd are the standard deviation of measured and predicted values, respectively.

In the study, the hydrological analysis was performed by comparing drain outflow hydrographs corresponding to different rainfall hyetographs for no runoff conditions. Therefore, considering a conceptual model of drainage system that demonstrates the relationship between hyetograph and drainage hydrograph some key parameters describe the behavior of the drainage system; time of concentration (the time from the start of the rainfall to the point of the time of drain outflow starts) and lag time (the duration between peak rainfall intensity and peak drain outflow discharge). The drainage mechanism of the sports field was thoroughly evaluated by using a newly developed experimental setup that can create rainfall patterns for different return periods and durations. Drainage experiments were conducted by using different drainage layers under different hyetographs. Unsaturated flow parameters of the drainage layers were optimized by using HYDRUS-3D from water contents and suction pressures measured during the experiments and SWRC for each material were obtained. Measured and modeled drain outflow hydrographs were compared with statistical analysis using the NSE index, KGE index, and determination coefficient (R^2). Time-dependent water content profiles were obtained from each drainage experiment. Considering initial and maximum water content, the drain outflow hydrographs were evaluated considering peak discharge, time of concentration, and lag time.

1.2 Objective of the Thesis

The objective of this thesis is to give a deep investigation over the subject of sports field drainage to improve the understating of the drainage process of a sports field by considering unsaturated flow characteristics and hydrological modeling under different rainfall conditions. The study objectives include:

- To develop a methodology for the mechanisms of sports field drainage that remove excess rainfall from the surface of the field as fast as possible;
- To monitor the unsaturated flow characteristics through the drainage layer with investigating water content and suction pressure;
- To investigate the effects of intense rainfall by considering design storms for different rainfall intensities;
- To develop a new experimental setup which consists of a rainfall simulator which can produce and measure the natural-like rainfall characteristics together with required measurement abilities for drainage process and drainage tank where is packed the multi-layered soils of a sports field to investigate the drainage mechanism;

- To determine the appropriate rainfall discharge relation for the comprehensive methodology to create rainfall patterns using rainfall simulator;
- To simulate any type of hyetograph that represent possible storm events that are highly likely to happen based on historical rainfall records for a region;
- To evaluate crucial and critical rainfall intensities that allow high-quality sports organizations and an applicable standard for the thickness and gradation of drainage layers
- To evaluate and compare optimum drainage layers that can drain obtained rainfalls over different drainage construction methods of a sports field,
- To simulate the experimental results with HYDRUS-3D and to develop a methodology with rainfall-infiltration and drainage layer to link the meteorological forecasting to drainage conditions of sports fields which will be able to use as an early warning system to sports games for possible cancellations of games.
- To investigate key drainage mechanisms with experiments and models.

1.3 Hypothesis

Designing a methodology regarding sports field drainage processes due to unsaturated flow characteristics is a difficult task and it has not been comprehensively investigated in the literature. Its design was based on traditional experience with considering indefinite science (Fleming et al., 2017). The main objective of this study is to develop a methodology for the mechanisms of sports field drainage that remove excess rainfall from the surface of the field as fast as possible, monitor the unsaturated flow characteristics through the drainage layers, and investigate the effects of intense rainfalls by considering design storms for different rainfall intensities both experimentally and numerically. Therefore, a new RS-DT setup was developed to investigate the drainage in the multi-layered soils of a sports field, which have the ability to produce and measure the natural-like rainfall characteristics together with required measurement abilities for the drainage process.

2
SOIL DRAINAGE

2.1 Infiltration and Soil Drainage

Infiltration and drainage are hydrological key parameters in aspects of agriculture, irrigation, and civil engineering with considering soil-water relations. Indeed, soil infiltration and drainage are governed by the character of the soil moisture and suction pressure because of the pore system. The infiltration process can be defined that when the water enters into the soil, water movement starts with the presence of gravitational forces, it is considered as an infiltration. Moreover, Assouline (2013) defined infiltration as a complex hydrological consideration that depends on soil and rainfall characteristics and boundary conditions. In addition, the theoretical background of infiltration was comprehensively developed with the contributions of many researchers in the last decades (Assouline, 2013). On the other hand, the simple definition of drainage process means the removal of excess water from a corresponding place.

Water flows faster through coarse-textured soils such as sandy soils and pebbles in a saturated condition because of the positive head. Water is transmitted so quickly through the bigger pore sizes. Furthermore, first, the soil becomes from saturated condition to unsaturated condition due to the interrupting of the water source. In unsaturated circumstances, the movement of water is distinctively slower. Moreover, the water does not fill the larger pores and move along to larger pores. This has important effects on the rate of water movement. However, the flow rate will be greater due to the larger number of small pores in an unsaturated condition. For instance, silt loam soil has a greater amount of available water than sandy loam soil and silt loam soil is optimal for plant growth. Soils in nature are not homogeneous, especially urban soils. In addition, considering a soil that has a coarse-textured sandy layer over a finer textured soil layer, when the upper coarse layer is saturated, the flow rate is governed by the saturated rate of the finer textured layer. This is rapidly observed in the water flow. On the other hand, when the soil consists of the finer textured material over the coarse-textured material has a more dramatic and important effect. In this condition, upper fine-textured soil stores almost all of the water until it becomes nearly saturated, then the water movement starts to lower layer.

In brief, the sand or gravel layer below the fine-textured soils does not improve the drainage rate. These layers have distinctive effects on the critical condition which is the occurrence of a great amount of lateral drainage. In the case of the three layers, the rootzone of loamy material over sandy material, over a subsoil, similar conditions are effective for water movement. For both plant growth and acceptable drainage rate, the layering is highly significant in terms of determining water movement in both saturated and unsaturated conditions.

As commonly known, drainage is the removal of excess water from the surface and profile of the soil. It can be accomplished with both gravity and artificial ways. Therefore, drainage is one of the most significant tasks for managing a sports field. If a field does not have surface and sub-surface drainage systems, it is not possible to drain excess water from the field properly. A well-drained field surface enables safety/security and playability and allows turfgrass to access necessary nutrients, better air exchange, and improves turfgrass recovery potential.

2.2 Soil-Water Relationships

Water content and water potential are two main components to describe water status in soil. Water content refers to the fraction of the soil that is occupied by water and can be measured by mass or volume (Waller and Yitayew, 2016). Total water potential refers to the energy of the water in the soil and generally involves matric potential, gravitational potential due to elevation, and osmotic potential due to salinity.

2.2.1 Definitions

In this chapter, basic definitions regarding soil drainage that related to the soil-water characteristics were given. Some of them are saturation, field capacity, wilting point, water content, and matric potential. Figure 2.1 shows the relationship between these terms.

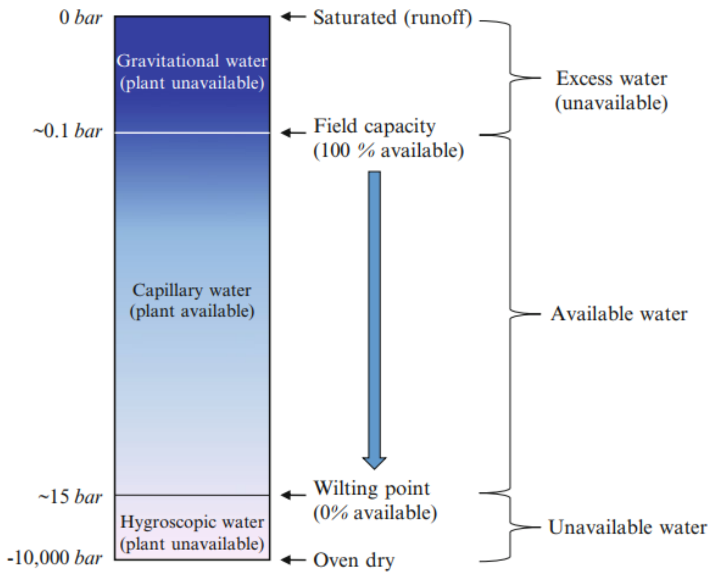

Figure 2.1 The Relationship between Basic Definitions of Soil-Water Interaction (McCarty et al., 2016)

2.2.1.1 Saturation

Saturation shows the amount of liquid that is accumulated in the soil layers. Moreover, saturated soil means that all pore space is filled with liquid. Saturated water content is almost the same as the porosity of the soil.

2.2.1.2 Field Capacity

Field capacity (water holding capacity) is the amount of water that remained in the soil after free drainage by gravity. It also means that larger pores of soil have already drained. This occurs very quickly in coarser soils (a few hours), less quickly in medium-textured soils (about a day), and slowly (several days) in finer soils (Waller and Yitayew, 2016). In other words, any water in excess of water holding capacity will drain because of gravity (McCarty et al., 2016).

2.2.1.3 Wilting Point

Wilting point is defined as the minimum amount of water in the soil that the plant needs not to wilt. It is also called a permanent wilting point. In other words, the permanent wilting point shows the limit that there is no available or accessible water for plants. The wilting point is defined as -15 atmospheres (Easton and Bock, 2016).

2.2.1.4 Water Content

Water content or moisture content is the quantity of water compromised in a soil (called soil moisture). It is also expressed as a ratio, which can range from ‘0’ (completely dry) to the value of the materials' porosity at saturation.

2.2.1.5 Matric Potential

Matric potential is called water potential that due to the force strived on the water by the soil. It also is the union of adsorptive and capillary forces. Water potential is a dynamic parameter that is fundamentally zero for a saturated soil, negative at water contents below saturation (Easton and Bock, 2016). It never takes a positive value.

2.2.2 Soil Composition and Texture

Soils have four main components: mineral solids, organic matter solids, water, and air. The solids are made of geological and organic minerals, made from plants or animals and living organisms. Either water or air occupies the vacant spaces between the solids called pores.

The sand, silt, and clay mineral solid fraction of the soil determine the soil structure in the special ratios. Sands are between 0.05 mm and 2.00 mm, the silt is between 0.002 mm and 0.050 mm and the clay fraction is made up of particles with a diameter of less than 0.002 mm (Figure 2.2). Particles larger than 2.0 mm are referred to as rock fragments and are not considered for soil structure determination, although they may have an impact on soil and soil water relations.

The textural class can be determined using a textured soil triangle (USDA-SCS, 1987) once the sand, silt, and clay fractions are known (Figure 2.2). Determining soil texture is important because the texture influences numerous soil characteristics: drainage, water retention capabilities, aeration, erosional susceptibility, cation change capabilities, capacity, and tilth of soil (Easton and Bock, 2016). Organic matter is generally seen as beneficial to soil because it provides water retention capacity, releases nutrients gradually for plant growth, and improves the structure of the soil.

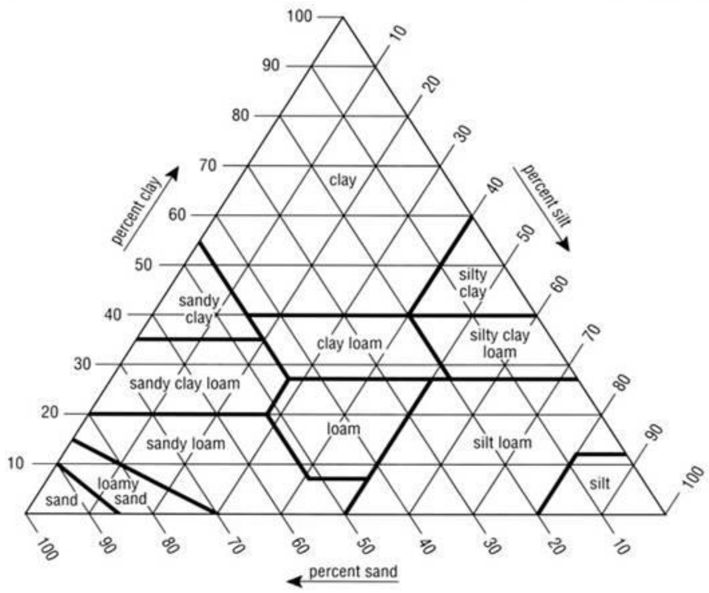

Figure 2.2 USDA Soil Texture Triangle (USDA-SCS, 1987)

2.2.3 Soil Structure

The form and organization of soil particles into aggregation units, also known as peds, is referred to as soil structure. Platypus, prismatic, columnar, blocky, single-grained, and granular soils are the six main structural types as shown in Figure 2.3. The rate at which water and air will pass through the soil, root penetration and the availability of nutrients to plants are all influenced by soil structure. The structure of the soil affects the rate of water and air throughout the soil, root permeation, and plant nutrient availability. Water percusses very quickly through the earth in single-grained soils such as sand, and water is very slow on massive soils such as dense clays.

Due to horizontally arranged storeys, the Platy structure hinders the downward movement of the water. In soils with a granular, prismatic, or blocky structure, more favorable water movement characteristics for crop production are generally found. Well-structured soils tend to be more desired for farming because structured soils can hold and convey water, gasses and support load-bearing activities like field traffic.

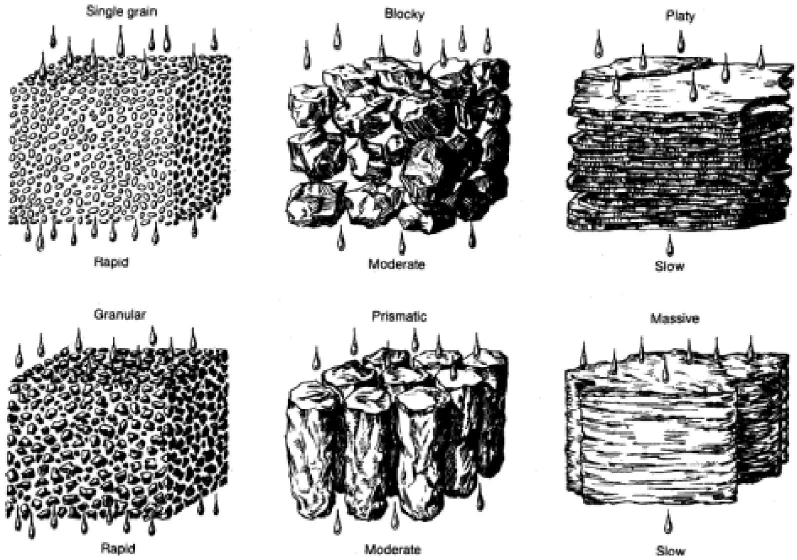

Figure 2.3 Main Soil Structural Classes with Water Movement (Adapted from USDA-SCS, 1991)

2.2.4 Soil Water Content

Soil water content is the amount of water held in the soil, which can be expressed in volumetric or gravimetric. The volumetric water content is the volume of water per unit volume for dry soil and is the most useful way to express a water content. In this study, water content is expressed volumetrically.

All soil water is accessible for plants to explain the water content of soils. Water that supports plant growth is known as plant water and represents the difference between field capacity and wilting point (Figure 2.4). Field capacity demonstrates the water left in the soil profile after 48 to 72 hours of free drainage. The field capacity is also considered to be one-third of the air tension (Easton and Bock, 2016), it is clear to state that water is weakly held in the soil and can easily be taken up by plants. Figure 2.4 also shows that although the field capacity of the available water is considered the maximum limit, this is not entirely accurate (Easton and Bock, 2016). After a saturation occasion, water that descends in the soil can be effectively used by growing plants. Since gravity flows are transient, however, this water is generally not taken into account in calculations to determine the water capacity of the earth but it can affect things like planning irrigation. Water drained freely by weight is referred to as gravitational water and, depending on environmental conditions, could be or could not be used by plants (Figure 2.4).

The gravitational, plant-available, and unavailable water contents as seen in Figure 2.4 can be very different depending on the type of the soil. For example, sands have relatively low plant water and a significant portion is gravitational water that flows through a macro pore and is, consequently, more sensitive to drought to crops grown on sandy soil. In contrast, clay soils are usually a bit tighter in plant water because of their increased aggravation, but also because the water is kept tight in the micro pores, so the plants are unable to access it. Moreover, Table 2.1 demonstrates the available water contents for different soil textures like sand, sandy loam, loam, silt loam, clay loam, silty clay, and clay.

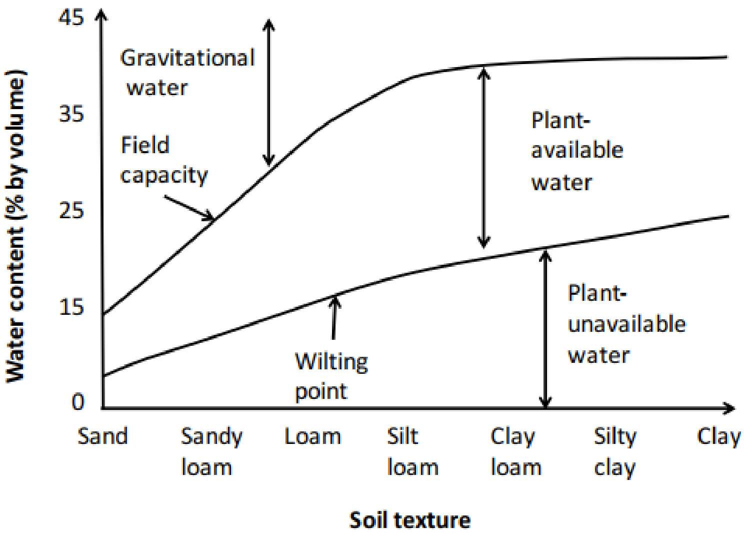

Figure 2.4 Water Contents for Different Soil Structures (Easton and Bock, 2016)

Table 2.1 Average available water contents for different soil textures (Easton and Bock, 2016)

Textural Class	Wilting Point	Field Capacity	Available Water
	(%) Moisture)		
Sand	5	12	7
Sandy Loam	9	21	12
Loam	16	36	20
Silt Loam	18	39	21
Clay Loam	24	39	15
Silty Clay	24	39	13
Clay	27	39	12

2.2.5 Soil-Water Retention Curve (SWRC)

A soil-water retention curve (SWRC) describes the amount of water that is stored in a soil (expressed as the water content in mass or volume) in the balance of a certain matric potential (Tuller or Or, 2005). SWRC is an important hydraulic property, relating to the size and connection between the pores and the soil structure and other components, including organic matter, which therefore has a strong influence. The SWRC has significant effects on the water management and prediction of the transport of solvents and contaminants into the environment to model water distribution and flows in partially saturated soils. In general, an SWRC is highly non-linear and difficult to accurately achieve.

Since the matric potential exceeds several orders of magnitude for the range of water, the various slopes of the ratios result from varying pores. Water potential is often expressed on a logarithmic scale in content commonly found in practical applications. Figure 2.5 shows representative SWRC curves for the soils of different textures, showing saturated water content and the different slopes of the relations arising from varying pores. Furthermore, in fine-textured soils, the matrix potential is generally higher than in coarse grounds because of larger surface area and smaller pore dimensions, and therefore clay soils have a higher plant unavailable level of water than sands. This effect is at the ground-water interface due to adhesive and cohesive forces (Easton and Bock, 2016).

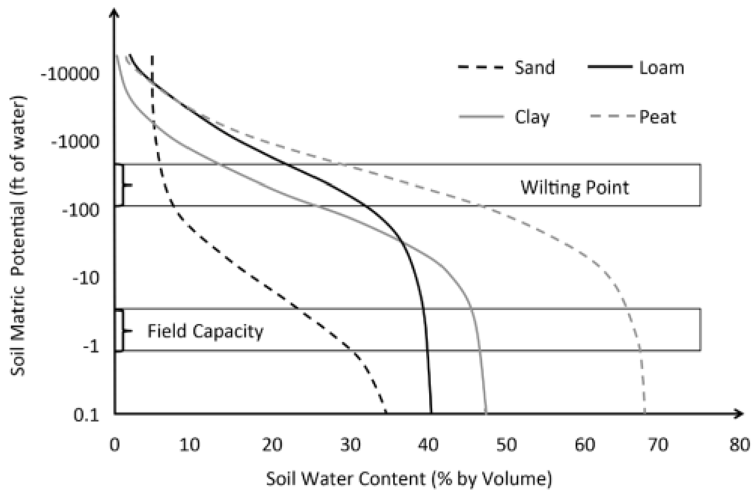

Figure 2.5 The SWRCs for Different Soils with Field Capacity and Wilting Point (Easton and Bock, 2016)

Figure 2.6 shows various zones on an SWRC which can be distinguished for air intake points, field capacity, or permanent wilting points by assigning values. These zones include:

- Soil saturation zone (perched water table): between zero tension and air entry point,
- Gravitational water zone: between the air entry point and field capacity, water drains via gravity before it can be used by plants,
- Plant available water zone: between the field capacity and the permanent wilting point, when the capillary strength is more than a gravity pull, but matrix absorption by plant root absorption can be overcome,
- Hygroscopic water zone: all water held at further tensions than a permanent wilting point, where the plants do not access water.

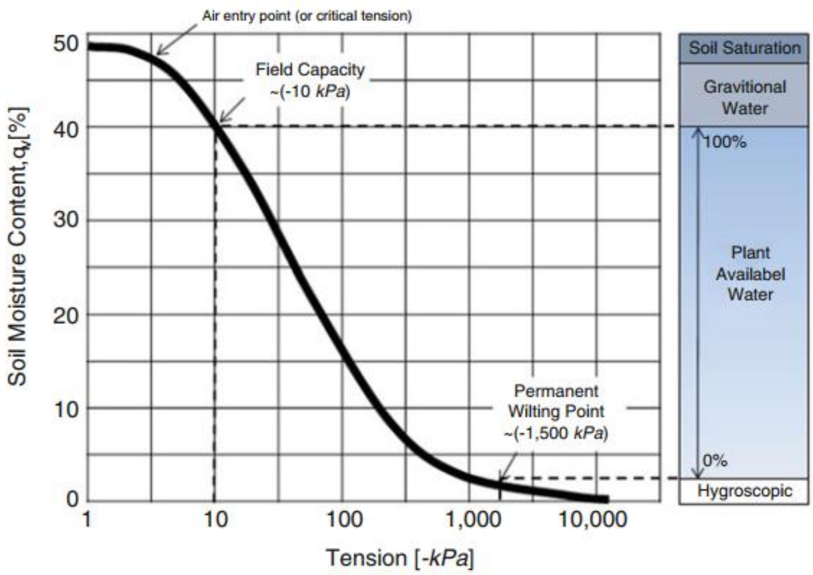

Figure 2.6 A SWRC for Different Water Zones (McCarty et al., 2016)

2.2.6 Soil-Drainage Classifications

Significant properties of soils that influence sports fields are drainage characteristics. Well-dried soils are the most productive, as long as the rainfall is not limited, while poorly drained soils reduce root growth and therefore lower the quality and playability of fields (Easton and Bock, 2016).

The five commonly used drainage classifications related to potential productivity are shown in Figure 2.7. Very poorly drained soils have a barrier to shallow root penetration between 0 and 45 cm, whereas well and medium-drained soils are not often restricted to depth, so that roots penetrate the soil fully and access available water, nutrients, and other resources. Soils with restricted drainage are often anaerobic (oxygen-depleted) and diminished (a chemical status favoring certain reactions). Soils with reduction are usually gray, often with accumulations of iron oxide colored with rust, which indicates a fluctuating water table.

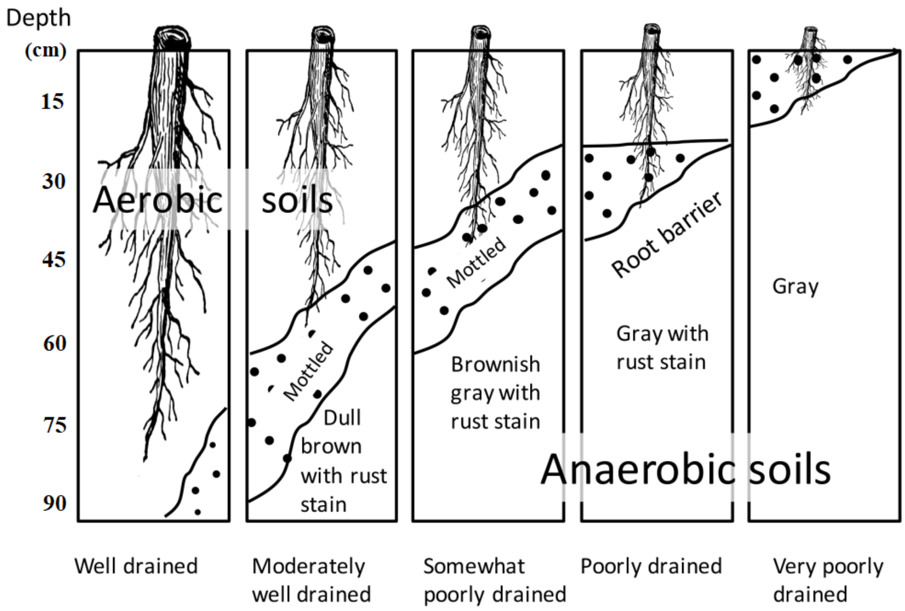

Figure 2.7 Five Frequently Used Soil Drainage Classifications According To Depth (Easton and Bock, 2016)

2.3 Types of Drainage for Turfgrass

There are two main drainage types for turfgrass plants: surface and subsurface drainage. These drainage types are very crucial to have proper, adequate drainage systems. Figure 2.8 shows the insufficient drainage of field surfaces that which is a very common problem.

Figure 2.8 Insufficient Surface Drainage of Football Fields and Golf Greens (McCarty et al., 2016).

2.3.1 Surface Drainage

Surface drainage is the removal of the excess water from the surface of the soil by removing low spots where water accumulates by land forming or by excavating ditches or a combination of them. In the surface drainage, the surfaces of the soil are shaped, sloped, and glued, as necessary to remove the pond and lead to the outlet of gravity (Figure 2.9). Diversion ditches, swales, and floodways. Floods are often used for diverting and excluding water from an area (McCarty et al., 2016). Moreover, land forming is mechanically changing the land surface to drain surface water by smoothing, grading, bedding or leveling. Ritzema (2015) expressed that there are two main components of surface drainage: forming of the surface by land shaping to improve or increase to flow of water through to drain outlets of the field and the design and production of open drainage structures for diversion of this water to the drainage collectors. He also expressed the different methods for surface drainage design as land grading, land planning by smoothing land surfaces, random field design, and parallel field design as given in Figure 2.10.

Figure 2.9 Surface Drainage Types: Sidelines Drain (Left), Surface Contouring (Right) (McCarty et al., 2016).

Nowadays, the design of modern golf courses and sports fields has a significant lack of construction of surface drainage components (McCarty et al., 2016). Sports fields were traditionally raised (crowned) in the center to deal with surface drainage. Soccer fields, for example, have almost entirely transitioned to "flat" surfaces in recent years, as numerous football fields have. Surface drainage also creates a hydraulic gradient by supporting potential energy.

The design of surface drainage aims to reduce or minimize water ponding due to rainfall or irrigation on the surface of the soil. Surface drainage also struggles to reduce the volume of water entering the soil profile. Therefore, the proper slope is a necessary component of sports fields design for proper surface drainage. In other words, slope and field crowns are two essential criteria to construct sports fields.

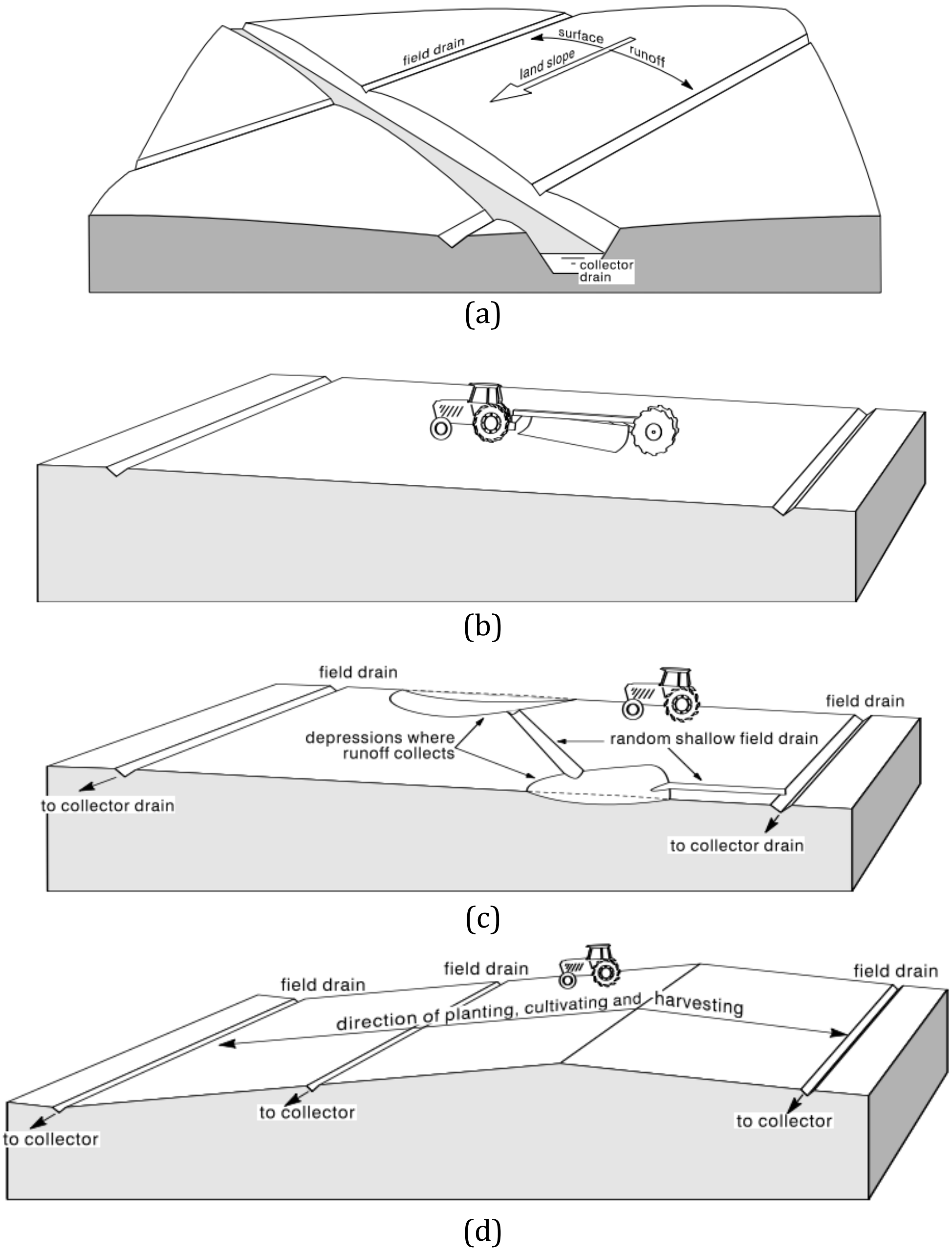

Figure 2.10 Different surface drainage systems: a) Land grading, b) Land planning by smoothing land surfaces, c) Random field design, d) Parallel field design (Ritzema, 2015).

2.3.2 Subsurface Drainage

Water movement through a soil profile is referred to as subsurface drainage involving the installation of subsurface drains to remove excess water, which can lead to unfavorable growing conditions. Capillarity holds water available to plants in the soil, while gravity channels excess water into drains. This lowers the groundwater level below the plant's rootzone. Some important parameters affect the water movement into the soils such as soil hydraulic conductivity, drain size, drain depth, drain spacing, etc. (McCarty et al., 2016).

Subsurface drainage systems also enable the removal of water from the soil by providing a path for "excess" or "drainable" water to exit the soil. Subsurface drainage is effective at removing excess water from the rootzone and lowering the water table during heavy rainfall events. When sports fields have proper surface and subsurface drainage, they are most effective together.

McCarty et al. (2016) also stated that soil modification to improve/increase hydraulic conductivity is the key tool for the successful subsurface drainage system. This includes a gradation of rootzone, sand, gravel layers, and depth of drainage layers.

2.4 Drainage of Sports Fields

Sports fields' drainage is a very important task to deal with common drainage problems. Evaporation, surface runoff, rootzone drainage, percolation, etc. are major water drainage/exits ways out of the rootzone profile, preferably, through an underground drainage network. The drainage of sports fields has different soil profiles, in the literature, there are three different soil profiles used in sports fields, which are native soils, modified soils, and sand-based soils (McCarty et al., 2016).

The fields that have native soils are designed to remove excess water from existing soils and depend mainly on surface drainage. The advantages of these kinds of soils are: (1) getting adequate nutrients and a high capacity for holding water, require less fertilizer and water; (2) maintaining stability, shearing strength, and traction; and (3) building less expensive as the soil is local. Costs depend on the amount of surface grading and the construction of drain tile (McCarty et al., 2016).

Modified soil profiles are native soil-based fields that are modified by topical addition and sand rotary. The performance is dependent on different sand and soil proportions and their relative distribution of particle size. The advantages of the modified soil fields are the construction and maintenance of soil fields are less expensive than the use of sand fields and have better drainage compared with native soil profiles (McCarty et al., 2016). They have some disadvantages with limited drainage like native soils, dependency on surface crowning, and requirement of irrigation and semi-aggressive fertilization (McCarty et al., 2016).

Sand-based soils depend on 80-100% sand rootzone with 0-20% native soils or other modifications. These fields of sand are flat, not highly crowned, and have high rates of infiltration. Internal drainage should be designed to quickly remove large quantities of water. It has the best drainage compared with native and modified soils. The key parameter does design is that the sand particle size is selected correctly. These fields have optimal internal drainage, a minimum crown has required a minimum of soil compaction is achieved when the sand properly has a higher resistance to the soil compaction than silty or argillaceous grounds (McCarty et al., 2016).

2.4.1 Football Fields

High-quality football fields for numerous purposes require optimal drainage so that play can begin on time or not delay. The existing rootzone is replaced by adequate sand mixed with organic and/or loamy soil for this purpose. There should be a set of parallel drainage tile lines spaced between 3 and 6 m across the field length. As the rootzone falls shallower, the closer the drain lines. An initial infiltration rate of 15 to 41 cm/h should be established for the modified roots (McCarty et al., 2016). The center field crown can be reduced to about 1 to 25 cm if an amended sand profile is used. The field should have a minimum life expectancy of 20 years with proper maintenance. This design enables high quality and perfect drainage conditions for football fields.

A wide variety of alternative sports field designs and costs are available. For instance, suction pumps can be linked to drainage outlets to improve the removal of water. While these systems have succeeded, most fields using suction pumps seldom have a life expectancy of over five years. Other designs regulate drainage by elevating or lowering the water table of the field. The construction of these concepts is costly and agronomic problems with shallow turf rooting and the invasion of surface algae. Considering rootzone depth, some fields use 25 cm of sand instead of 30 cm. This reduces the cost of rootzone material by about 17 percent. The field will probably gain 5 cm of depth during the first five years if routine topdressing is performed. A faster rate of drainage is advisable and a closer connection between subsurface drains. In addition, instead of 30 cm or 25 cm, 15 cm of sand rootzone were used. High drainage sands should therefore be used together with a distance of 2.6 m for this design to succeed (McCarty et al., 2016).

Fields, which require frequent resodding, also introduce different types of soil, which reduce the efficacy of these and other systems in general. The new field managers will also amplify this by using a different material of top dressing than the soil used to build the field. These real-life conditions can pose major problems and should be closely considered during the design phase.

If an alternative design is used, the expectation of field performance should be limited (McCarty et al., 2016). These fields are not draining quickly, but absorb small rain showers and offer improved conditions for growth rather than modification. However, during heavy rainfall they should not be drained rapidly, normally require further aeration and shorter life expectancies than sand-based rootzone facilities.

2.4.2 Soccer Fields

Soccer fields are designed similarly to football fields according to sand-based rootzone and optimum drainage conditions. On the other hand, a 15 cm to 30 cm crown can be planned and it should be increased for native soils. Furthermore, soccer fields have lower surface slope due to the greater width of the field and higher crowns (McCarty et al., 2016).

2.4.3 Baseball and Softball Fields

A great amount of water is removed from field surfaces with runoff in the baseball and softball fields. Therefore, the slopes of the fields are especially determined and designed. Most of the fields have different combinations of sand, clay, and silt for rootzone. Especially, %60 sand, %20 silt, and %20 clay combination is preferred and used (McCarty et al., 2016).

2.5 Different Drainage Methods for Sports Fields

In recent years, sports fields have evolved rapidly into a more significant position in terms of hosting both social and sports activities. Due to the deficient drainage, numerous sports organizations have been canceled or postponed resulting in huge economic losses for the industry. Kesgin et al. (2020) mentioned that the drainage of sports fields has distinctive differences when compared to the land and urban drainage systems considering the quality of the rootzone and the lack of runoff capturing systems. In many sports, such as football, the playing surface is in contact with the open air and is highly affected by environmental factors (temperatures, precipitation, etc.) affecting the conditions and even playability of the game, especially during the wet months (Dixon et al., 2015). In order to increase the participation, many studies have been conducted on the need to ensure the safety of the game surface against injuries, to provide an even surface and sufficiently soil strength where the player can demonstrate his functionality, and to improve the game features such as ball rolling and bouncing (James et al. 2007a; McAuliffe, 2011; James et al. 2007b). Therefore, since football is one of the most common sports in the world, it is a very important economic income source and prestige area with its high participation incidence. Considering the sports market worldwide ticket, media, and marketing incomes were 64 billion dollars in 2009, while football decisively surpassed other sports by about 43% with 28 billion dollars annually.

One of the most important conditions for sports fields, which is indisputable in terms of social and economic importance, is to have satisfactory drainage capacity and to establish an internal drainage system that will allow the game to continue without ceasing. Due to the lack of a clear and sufficient specification, an experience-based design is often prepared in the construction of sports fields, and as a result, irreversible or very costly results can occur (Fleming et al., 2016). For this reason, one of the most crucial issues when designing this engineering structure is to work with a talented and experienced consultant (Sport England, 2011). It is obvious that drainage is the most important parameter affecting the playing field of a sport in which participation, interest, economic income, and prestige are very intensive, should be examined carefully in terms of engineering and hydrology. To examine the precipitation trends due to global warming and to know the precipitation characteristics of the region during the design phase is a determining factor for the design of the drainage system to be installed and for the selection of materials to be used in the design (SAPCA, 2009). Chou and Lan (2012) and Liu et al. (2009) stated that there is an increase in rainfall incidence and intensity due to global warming and that there is a similar situation in extreme values. As a result of extreme rainfall conditions and wear on the field surface, the water infiltration rate will decrease significantly, resulting in an unfavorable playing surface that is slippery and puddled (Adams, 1986; Taylor et al., 1993). In conditions where the surface of the field is unfavorable, the risk of injury or the dysfunctionality of the players to adequately demonstrate their abilities affects the results. As a result of the installation of an effective drainage system, surface strength is maintained significantly and as a result, water on the field, infiltration rate, and effects on game and player functionality is minimized. However, it should be noted that additional maintenance costs that may arise due to the establishment of a hydrologically useful internal drainage system, field improvement and development features such as irrigation and fertilization in summer, covering with sand should be taken into consideration in the early stages of the design (SAPCA, 2009).

In the literature, the general emphasis in examining the drainage systems of sports fields is related to the kind of material to be used, the percentage of mix, and the amount of materials (Taylor et al., 1997; Taylor and Blake, 1979; Taylor et al., 1993; Baker, 1989). In addition, there are studies to express the association between precipitation conditions and drainage efficiency (Kesgin et al., 2020; Fleming et al., 2016). The general belief was that the rainfall hyetograph had a significant effect on the amount of water discharged and that a very small proportion of the rainfall had been drained. The main objective of this study was to experimentally investigate the different drainage techniques as the PD, SWT, SG, and SD from a hydrological perspective, commonly used in most sports areas to allow optimal field conditions in extreme rainfall conditions. Hereby, it is aimed to provide a hydrological comparison and an evaluation opportunity in deciding the system to be made by taking into account the rainfall conditions in the region before the field was built.

It is often difficult to re-functionalize the negativities (drainage problems, turf wear, surface imbalance, etc.) that may occur in the absence of a careful and detailed study before the construction of sports fields (Sport England, 2011). This is because football fields are actively used for various age groups and organizations for a very large part of the year, and it requires both time and intensive maintenance costs to make the pitch functional again after the improvement process. The most important problem that will have a negative impact on the playing surface and prevent the game from being played is the wearing of the grass and ponding of water that will occur due to the inability to remove the rainfall from the surface swiftly enough. In the 1960s, the United States Golf Association (USGA) proposed a cross-section of the sports field. In the section, at the bottom are gravel, which is a large porous material with a high permeability property, and sand and rootzone (sand+soil) are placed on it respectively. Recent studies have been conducted to study the drainage of sports fields both in terms of the properties and components of ground material, and rarely in terms of their hydrological aspects (Ceretti et al., 2003; James et al., 2007; Kowalik and Rajda, 2014; Kesgin et al., 2020). It was mainly intended to establish a connecting path between the surface and lower drainage outlets using high hydraulic conductivity and porous materials in a stratified form to remove rainfall waters from the area surface (Ward, 1983). If the natural soil does not have high drainage capacity, which in general the native soils do not ensure adequate drainage characteristics due to high clay content, this soil is excavated and replaced by a mixture of soil with high sand content. Taylor and Blake (1979) stated that the mixture of the rootzone (sand+soil+peat) must contain more than 90% sand in weight to achieve a satisfactory infiltration rate. Baker (1989) examined the infiltration rate of sports fields with 16 different sand and sand-soil mixed root layers and stated that the increase in the percentage of sand significantly increased the infiltration rate. Therefore, Baker (1989) and Magni et al. (2014) supported the need to construct sports fields with high sand content. The increase in the amount of sand positively affects not only the infiltration rate but also the surface aeration and the development of the grass plant.

Especially for pitches in local areas that are used by low age groups, it is often not economical to fill the pitch with material with high sand content. In addition, due to the high drainage of systems containing excess sand, the amount of moisture required for grass roots is not kept in the soil (Sport England, 2011). Several drainage techniques have been developed which have both advantages and disadvantages compared to each other in order to drain the surface water in a high amount and in addition not to reduce the amount of moisture in the root area too much. It is clear that there is a lack of academic work and information in the hydrological examination of these drainage designs. Constructing a sports field drainage system without evaluating the data such as the climatic conditions of the area where the field will be built, the amount and frequency of precipitation, and the maximum amount of precipitation that may occur in certain periods will result in excessive or incomplete designs. It is necessary to set up an internal drainage system to take away water that leaks from the surface into the soil and moves to the lower layers. The two major elements are indicators of the quality of the internal drainage system. The removal efficiency of water, longevity of the system, and these effects are associated with the number of drainage pipes, the correct slope to allow water movement, the characteristics of the drain pipes used, and the type of soil used in the field (Dixon et al., 2015). In brief, Pipe Drain (PD), Suspended Water Table (SWT), Sand Groove (SG), and Slit Drain (SD) drainage techniques that were recommended for high-quality sports field by Sport England (2011) were evaluated in this chapter of the presented study. The technical details of these methods were also given in below.

2.5.1 Three-Layer Construction (Suspended Water Table, SWT)

When installing a drainage system on sports grounds, the most important point is to quickly remove water from the surface regardless of rain intensity and duration. Therefore, it is necessary to have top soil with a high infiltration rate and to install an internal drainage system to remove water from the area through pipes. SWT is one of the most suitable systems to accomplish these tasks and is therefore preferred as the drainage system of the sports fields with the highest importance (Sport England, 2011). The reason it is highly efficient in terms of drainage is that it has a layer of sand and a layer of rootzone containing a high amount of sand. However, it should be noted that in high-efficiency drainage systems, the moisture of the rootzone required for the growth and protection of the grass will be reduced, as it removes large amounts of water. Therefore, it is essential to establish an improved irrigation system along with the SWT. System installation is usually a 15 cm high gravel layer at the bottom, then a 5-15 cm sand layer comes over the gravel bed, and at the top part, it can be described as the root layer region with high sand content (Figure 2.11). Kesgin et al. (2020) in his experimental study examined the effect of the thickness of the blinding layer and the rootzone layer on the drainage output, it was stated that when the rainfall intensity is low, there was no effect of different depth combinations, but in high-intensity rainfall, larger amounts of water were drained in the experimental mechanisms where there was no blinding layer.

Baker (1989) compared 16 different sand-soil ratios for SWT systems. The results indicated that coarse sand could lead to problems in terms of surface stability, as well as that the sand content in the rootzone should be more than 90% to prevent wearing and ponding on the pitch surface. Alway and McDole (1917) observed water contents after irrigation between soils placed on coarse material and unlayered soil. As a result, they realized that water was more retained in the layered system. Miller (1973) stated that the factors affecting water retention in stratified systems are the depth of the underlying coarse layer, its characteristics, and the desorption property of the soil, and he also demonstrated that the amount of water held on it increased as the diameter of the material used in the sub-layer increased. Taylor et al. (1993) also established 4 different experimental mechanisms: gravel+sand+rootzone, gravel+rootzone, sand+rootzone, subsoil+rootzone, and examined the effect of sub-layer on water retention in the rootzone. The results confirmed Miller (1973) and stated that the highest amount of water was retained in the gravel + root-zone system. The water, which was held in the rootzone region, forms a water table at the bottom rather than uniformly spreading (Taylor et al., 1993). It has been observed that, under the same precipitation hyetograph, only by increasing the diameter of the sand in the blind layer and comparing the output hydrographs, the peak flow increased with the increase in the material diameter, but there was no significant difference in the peak flow output time (Kesgin et al., 202018). While the positive aspects are the drainage system which provides the maximum amount of water output and provides a playing surface for 4-6 hours per week, the need for an advanced irrigation system, the material with high sand content, and the intensive maintenance requirements can be considered as the negative aspects.

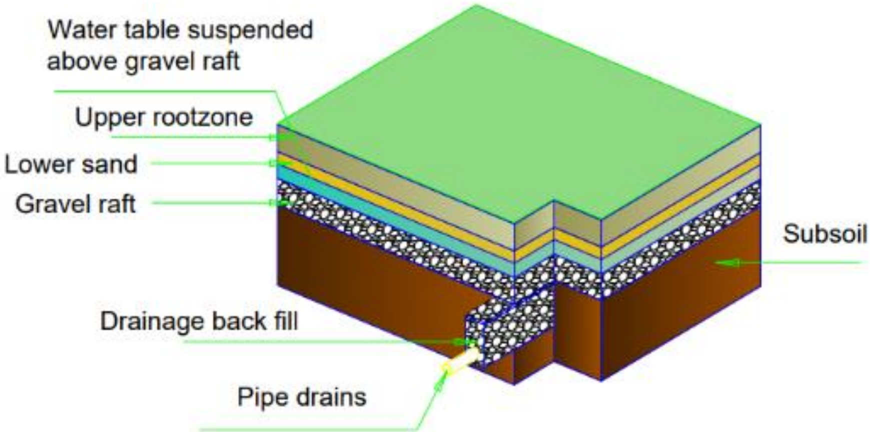

Figure 2.11 The Details of the SWT (Sport England, 2011)

2.5.2 Pipe Drained System (PD)

The PD is an internal drainage system that was widely used in the past, however, it is not preferable for high-quality football pitches due to its slow drainage feature and effective operation in areas with high sand content. To create an effective drainage system, ditches are filled up to 20 cm below the surface by single-size, angular gravel material, which is a large porous material (Figure 2.12). The top layer has a sand-dominated rootzone, but a 5 cm high blinding layer must be placed over the trenches filled with gravel to prevent the topsoil from leaking into the gravel layer and drainage pipes (Sport England, 2011). In general, the advantage of this system is that it is less costly. After the installation, it allows to increase drainage capacity and forms the basis of other systems. However, it is insufficient in pitches with a high amount of materials with low permeability such as clay and silt due to low infiltration rates in extreme rainfall situations. Canaway (1994) conducted a field experimental study, which included the comparison of drainage systems to evaluate the factors affecting the performance quality of turf pitch. Drainage types gave similar results in the processes prior to the wearing of the grass surface, but with the wear of the grass, there was much ponding in the PD.

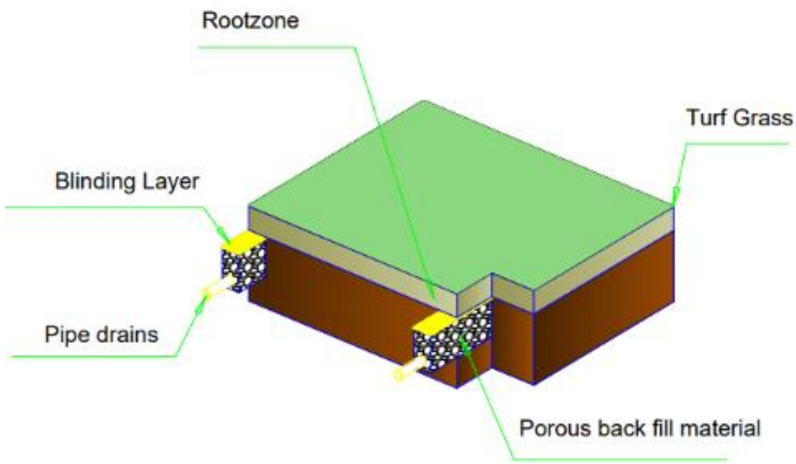

Figure 2.12 Details of the PD (Sport England, 2011)

2.5.3 Sand Slitting (SD)

The SD, just like the SG, consists of series of narrow, spaced crevices filled with gravel and sand installed and this allows water to pass quickly between the field surface and the underlying drainage layer. Generally, the slits prepared with 5 cm width and 25-30 cm height are respectively filled to the surface with gravel and sand as shown in Figure 2.13 (Sport England, 2011). SAPCA (2010) stated that during the installation, the slit should be filled with 5-8 mm gravel until there is still at least a 7.5 cm gap between slit and surface and this gap should be closed with sand to connect the slit with the surface. On the other hand, (James et al., 2007a) says that slits should be filled with 35 cm coarse sand on the 5 cm gravel. In order to prevent clogging of the system and to increase hydraulic conductivity, an improvement is made with medium-fine sand and a 2-3 cm sand layer on the field surface. In addition, as a result of the weakness and tendency of the field to shrink during very long dry periods, the excavated slits may expand and the fillings may collapse and this may create an uneven playing surface. To avoid this situation, the field surface should be covered with sand at least once a year, or the ground should not be deprived of water for a long time by establishing a regular irrigation system (SAPCA, 2010). Canaway (1994) stated in his study that the SD is more effective than the pipe internal drainage system (local field conditions, low sand content), but it will lose its efficiency when the surface is worn and slits are closed. In order to overcome these problems, the surface of the field should be covered with a 2.5 cm sand layer. It was also stated that covering it with a sand layer may provide a good playing surface. Ceretti et al. (2003) expressed as a result of these experimental studies that this system gave good results in terms of leakage rate and drainage and, it would be suitable for use in the sports field. The field surface conditions are inefficient in the presence of local soils (containing high levels of clay and organic material) in terms of infiltration rate, drainage rate, and amount. However, it is costly to remove all local soil and replace it with a root layer mixture with a high amount of sand. Therefore, creating a fast path to rainwater with SD is a smart and economical solution (James et al., 2007a).

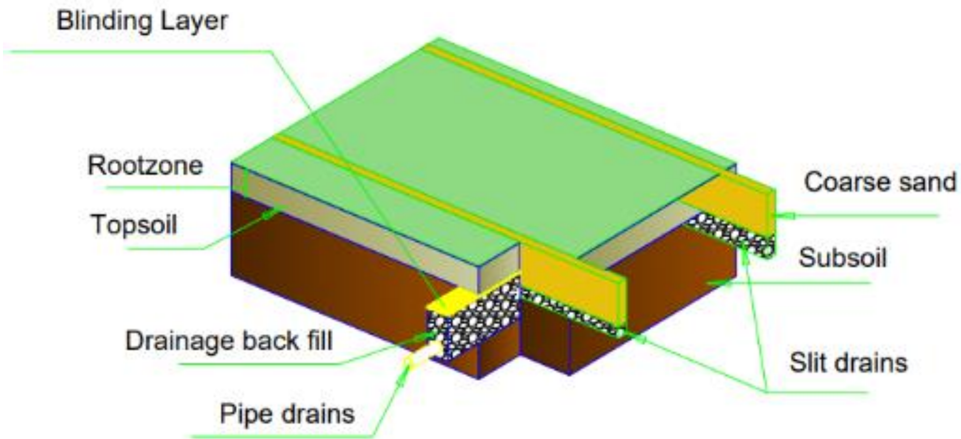

Figure 2.13 The Details of the SD (Sport England, 2011)

2.5.4 Sand Grooving (SG)

It is known that the PD drainage system is not sufficient for heavy rains in sports fields where the topsoil has low permeability. Due to economic constraints, in most cases, it is not possible to fill the site with sand material instead of undisturbed soil. For this reason, channels are dug from the soil surface and a connection is established between the surface and the drainage layer by filling this area with highly permeable sand (Adams, 1986; Sports Turf Institute, 2011). Although there are no clear installation dimensions, in general, 260 mm intervals, 20-50 mm wide, 150-200 mm deep channels are created from the surface (Figure 2.14). The benefits of this system include a high hydraulic conductivity drainage path, economic gain from the material, 3-6 hours of usage time per week, and a quick installation (Sport England, 2011). Top dressings are applied to increase the hydraulic conductivity on the field surface and to prevent the slits from being capping. The most important drawback of this type of slit system is that when it is installed on clay soils, settlement occurs due to the shrinkage of the soil in the summer, and therefore an uneven playing surface is formed. Reducing the width of the grooves systems and applying top dressing gives satisfactory results (James et al., 2007a).

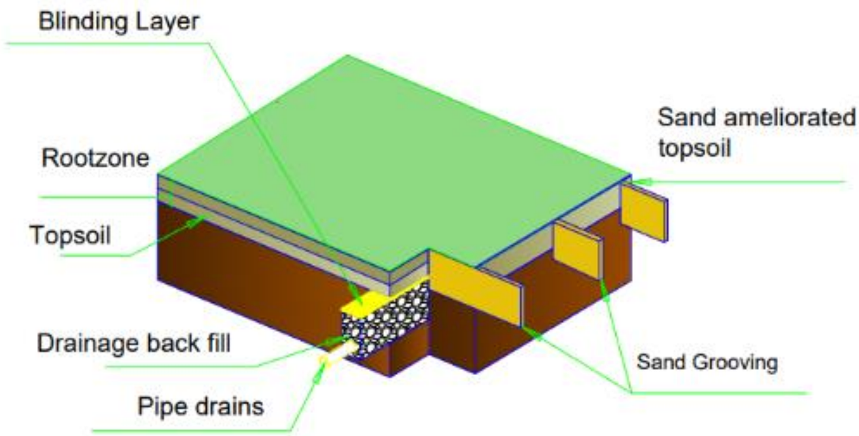

Figure 2.14 The Details of the SG (Sport England, 2011)

2.5.5 Mole Drainage (MD)

Mole Drainage (MD) is only appropriate for soils, which consist of more than 30% clay (Figure 2.15). The MD is also a very cost-effective solution to surface drainage. It comprises drains installed at 5 - 10 m distance with mole drains installed at about 1 m distance. The MD has approximately 3-5 years lifespan and it must be renewed. It is a vital point that important shrinkage problems have occurred for some clay soils; therefore, it has to take precautions regarding that potential problem. After mole drainage installation, it is most likely to occur during the first summer (Sport England, 2011). Moreover, clay stability, clay plasticity, mole channel depth, mole plow size are the most significant parameters for successful mole drainage installation.

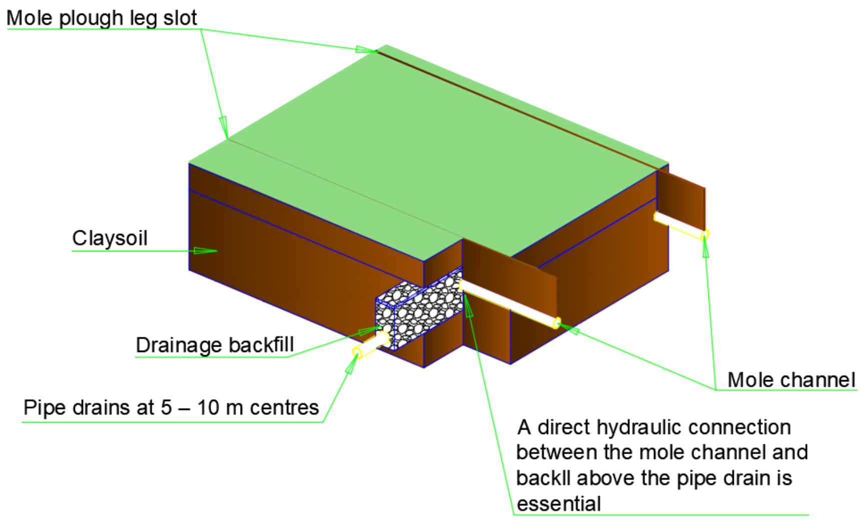

Figure 2.15 The Details of the MD (Sport England, 2011)

2.6 Components of the Three-Layer Construction

2.6.1 Rootzone

Suitable application and construction of the rootzone layer are some of the significant elements in every field construction but it is often the least considered. Selecting inaccurate rootzones causes a delay or cancel events and organizations and it becomes insecure for participants or supporters. Therefore, the appropriate selection of rootzones not only ensures the desired drain but also retains sufficient moisture and nutrients to ensure normal agro-growth (McCarty et al. (2016). In the literature, there are two types of rootzones: Native soils rootzones and sand-based rootzones.

Native soil is a suitable choice for lower-profile sports fields with limited budgets. They have higher water and nutrient holding capacities. In other words, they enable a better growing layer for turfgrass. Sand-based rootzones have numerous advantages in that they high water permeability and compaction resistance. For different and variable weather conditions, they can be preferred and used successfully. One of some disadvantages is poor surface stability, poor water holding capacity, and high maintenance costs when comparing native soils. In the literature, there are numerous studies about selecting rootzones. Taylor et al. (1997)

expressed that selecting rootzone material is very crucial for both the root growth of turfgrass and drainage. Especially, a sand-dominated rootzone is used due to its resistance to compaction and healthy drainage. On the other hand, it has some disadvantages because of the little holding capacity and not enough for storing plant nutrients. A laboratory study by Henderson et al. (2001) demonstrated that sand-dominated rootzones containing 90% sand or more (10% silt and clay mix or less) were appropriate in terms of acceptable drainage rates for sports fields. Considering firm footing, adequate resiliency, and resistance to tearing, it is not appropriate to select 100% sand-dominated rootzones.

2.6.2 Blinding Layer

The blinding layer is sometimes called as choker layer, intermediate layer, or sandwich layer. In the literature, there are no exact values regarding gradation and depth of blinding layer and some researches give a wide range (McCarty et al., 2016). Moreover, it is also seen as an optional layer. Its thickness also takes values between 5 and 10 cm; for instance, Adams (1986) recommended a 5 cm blinding layer in his research, and McCarty et al. (2016) suggested a range of 5-15 cm according to gravel and rootzone conditions. Besides, it prevents particle migration from rootzone to gravel bed. The comprehensive differences between the rootzone and gravel layer cause the perched water table or capillary break. These textural differences simply involve the gradation and depth of these layers. McCarty et al. (2016) defined this condition that water does not move to gravel bed with gravity before rootzone becomes saturated (sponge effect).

2.6.3 Gravel Bed

The gravel layer has an important role in the drainage of sports fields and it is the most uncertain part in terms of the technical perspective of sports field drainage. It is laid on the subgrade. Gravel layer can be selected between 5 cm and 15 cm, according to USGA (United States Golf Association) green section specifications (USGA Green Section Staff, 1993) and McCarty et al. (2016) also recommended a range of 5-15 cm and he said that 10 cm is suitable. In brief, according to traditional experience and a few research, this layer can be selected between 5-15 cm for the drainage of the fields.

3
SIMULATION OF NATURAL RAINFALL

A rainfall simulator (RS) and measurement methods of rainfall toward obtaining natural rainfall characteristics are very crucial for the field of hydrology. It is a widely known tool that is used to simulate natural rainfall and produce natural-like rainfall with considering characteristics of corresponding rainfall. Therefore, natural rainfall is a stochastic, unpredictable, and random event that its effects are grueling to estimate. The RSs are common and useful devices that allow for controlling these effects properly. They have been also used for many years to understand the logic of agricultural, environmental, and hydrological studies such as runoff, soil erosion, and soil crusting, nutrient and pollute transport, infiltration, and drainage of soils. The original aim of an RS is to make accurate simulation and the performance of an RS is characterized by several criteria to simulate natural rainfall successfully. Simulated rainfall requires reproducible rainfall patterns of duration and intensity (Moore et al., 1983), drop diameter close to natural rainfall (Bubenzer, 1979), fall velocity of raindrops near to terminal velocity of natural rainfall (Laws and Parsons, 1943), uniform spatial rainfall over the control plot (Laws and Parsons, 1943) and kinetic energy that is the function of raindrop size and fall velocity.

Moreover, two common types of RSs are classified according to how they produce raindrops: non-pressured RSs (drop former simulators) and pressured RSs such as spraying nozzles. Humphry et al. (2002) stated that drop former RSs have not been preferred in laboratory tests due to the limited access to the water supply. Also, they generate a narrow range of drop diameters and small fall velocities. It can be inferred that they have numerous disadvantages compared to pressured RSs. On the other hand, although drop formers RSs are not sufficiently useful for field and laboratory studies, Corona et al. (2013), Clarke and Walsh (2007) investigated surface runoff, splash, and slope wash assessment using a drop former simulator.

Hignett et al. (1995) also studied using a non-pressured rainfall simulator to evaluate the breakdown of soil aggregates.

3.1 Non-Pressured RS (Drop Formers)

Numerous simulators are worked with the principle of drops forming and dropping from the tubes or needles linked to a water supply (Figure 1.1). The size of a raindrop is directly related to the size of the tubes or hypodermic needles that are manufactured from metal, glass. Although there are some advantages such as constant fall velocity and raindrop size, uniform rainfall distribution over the test plot with low pressure, many disadvantages are clear that unless the device is located at a very high elevation (10-12 m), the drops fall over the test plot with small velocities much lower than the terminal velocity. Kinetic energy values are also very low due to the small impact velocities. Moreover, drop former simulators are not useful and successful for field studies because of the challenge of placing the 10-12 m height.

3.2 Pressured RS (Spraying Nozzles)

Pressured RS works with pressure spraying nozzles that are able to achieve bigger falling velocities to the terminal velocity. The velocity is dependent on the pressure that can be arranged with a pump and engine and increases to the test plot. Many types of spraying nozzle are commercially available and they are used for many purposes connected to RSs (Figure 3.1). On the other hand, a significant difficulty is that spraying nozzle increases the larger diameter of the raindrop by combining raindrops with high pressures. For the pressured RS, there are a few requirements to enable for producing simulated rainfall that is listed below. The RSs can be evaluated as a successful tool to create natural-like rainfall whether these requirements are provided or not. In this study, a pressured RS was designed and used to simulate natural rainfall and to determine the characteristic of rainfall such as rainfall intensity, raindrop diameter, and spatial distribution of rainfall over the control plot, fall velocity, and kinetic energy. The details of these criteria about how to determine were evaluated below. Therefore, the calculations regarding the RS were detailed in the chapter on Experimental Setup.

Figure 3.1 The Sketch of the Pressured RS (Spraying nozzle).

3.2.1 Rainfall Intensity

Reproducible rainfall patterns of significant duration and intensity are crucial criteria for successfully simulated rainfall (Moore et al., 1983). The RS in this study can produce a wide range of rainfall intensities according to a single nozzle and nozzle system (double nozzle). For the range of a single nozzle, rainfall intensities were determined between 26 and 266.6 mmh^{-1}, nozzle system was produced rainfall between 2 and 266.6 mmh^{-1}.

3.2.2 Raindrop Diameter

Raindrop size is also a crucial parameter to assess the quality of a new RS. In this study, 30cm diameter circular pans were filled with 2 cm depth of undisturbed wheat flour. They were exposed to different simulated rainfall for just a few seconds. Then, flour pellets easily formed when the raindrops fall into wheat flour pans (Figure 3.2). The flour was dried for 24 hours at 105 ^{o}C. Then, the flour pellets that were formed by raindrops for each rainfall, were sieved and weighted (Fig. 3b). The pellets were passed through different sieve such as 5.6, 4.76, 4.0, 2.38, 2.0, 1.6, 1.4, 1.0, 0.6 and 0.5 mm.

(a) (b)

Figure 3.2 a) A Circular Pan Filled Wheat Flour B) Flour Pellets after Sieve Analysis (Kesgin et al., 2018)

3.2.3 Spatial Distribution of Rainfall

Rainfall spatial uniformity is one of the most important criteria for the performance of the RS. The most commonly used technique to determine the uniformity coefficient (C_uC, %) is defined by Christiansen (1942) as follows in Eqn. (3.1) :

$$C_uC=\left(1-\frac{\sum_{i=1}^{N}\left|x_i-\bar{x}\right|}{N\bar{x}}\right).100 \tag{3.1}$$

where x_i is the rainfall depth at location *i*, $\bar{x}$ is the average rainfall depth and *N* is the number of points in which rain gauges are located on the drainage tank to collect rainfall. When C_uC is greater than 80%, the rainfall can be accepted as a uniform rainfall (Moazed et al., 2010). Luk et al. (1993) expressed that, for larger plots, rainfall can be accepted as uniform if C_uC is greater than 70%.

Figure 3.3 shows the plan view of the locations of 42 rain gauges on the 1.5mx1.3m surface area of the tank. Uniformity tests were conducted to determine the spatial uniformity of simulated rainfall for 20 minutes for each rainfall intensity. The amount of water exposed to different rainfalls was collected in rain gauges. The average uniformity coefficients, the minimum, and maximum rainfall intensities, and statistical parameters such as standard deviation and coefficient of variation of measured rainfalls were calculated.

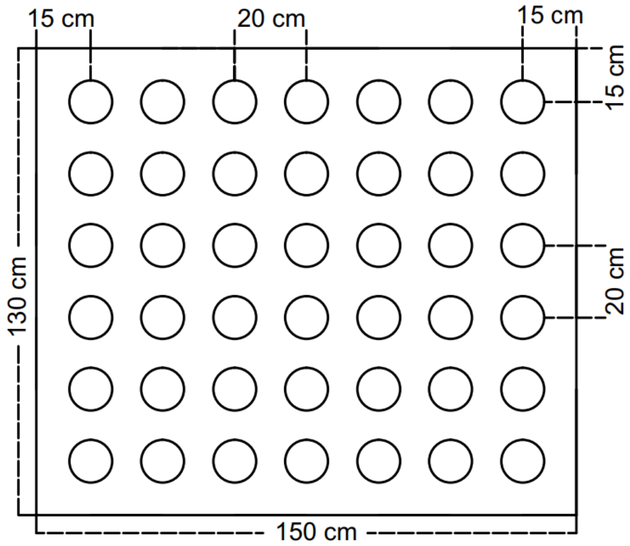

Figure 3.3 Locations of 42 Rain Gauges on the DT.

3.2.4 Raindrop Fall Velocity

Raindrop falling velocity is also a significant parameter for designing a rainfall simulator. Meyer and McCune (1958) stated that raindrops have terminal velocity in natural rainfall when they reach the soil surface. Therefore, a successful simulator must produce raindrops that have adequate size and velocity to simulate natural rainfall (Blanquies et al., 2003 and Cerda, 1997). The velocity of raindrops was not measured in this study, the however analytical analysis was used that was proposed by Aksoy et al. (2012). Generally, neglecting the air buoyancy, two forces acted on the raindrop, gravitational force and drag force (Abudi et al., 2012). According to Aksoy et al. (2012), the velocity in any fall distance is called an impact velocity calculated using Eqn. (3.2) as follows:

$$v(x) = \sqrt{\frac{g - e^{-2ax}(g - av_o^2)}{a}} \tag{3.2}$$

in which g is gravitational acceleration, x is downward vertical distance, v_o is the spraying (initial) velocity and a is given as:

$$a = 0.903525\frac{C_D}{D} \tag{3.3}$$

where C_D is drag coefficient that can be determined by Reynolds number, D is the drop diameter in mm. The terminal velocity of raindrops can be determined by Eqn. (3.4):

$$v_T = 3.2951\sqrt{\frac{D}{C_D}} \tag{3.4}$$

The impact velocities obtained by Eqn. (3.2) were first calculated at the distance between the mesh and surface of the drainage tank.

3.2.5 Kinetic energy

Drop size distribution, impact velocity and reproducible rainfall pattern are directly related to simulating kinetic energy (*KE*) of natural rainfalls (Blanquies et al., 2003). *KE* of rainfall is the sum of the energy for the individual drops. It is also a function of the size and fall velocity and is often used as a desirable parameter for an RS because it is known that kinetic energy is closely related to the ability of rainfall to cause surface degradation. Aksoy et al. (2012) stated that kinetic energy can be calculated by using drop size distribution, fall height, impact, and terminal velocities due to lack of direct measurements. It was determined by using drop size distributions and impact velocities for each sieve size class. It was also obtained using Eqn. (3.5) mentioned by Gilley and Finkner (1985):

$$KE\ (J\ m^{-2}\ mm^{-1}) = \frac{1}{2}mv^2\ (kg\ m^2\ s^{-2}) \tag{3.5}$$

where *m* is the mass of a raindrop, *v* is the impact velocity. Therefore, determining KE was reported with logarithmic relation by Van Dick et al. (2002) as:

$$KE\ (J\ m^{-2}mm^{-1}) = 11.9 + 8.73\log R \tag{3.6}$$

where *R* is the rainfall intensity in mmh^{-1}.

3.3 Nozzle Types

In this study, two different nozzle conditions which are single nozzle and nozzle system (double nozzle) were used. Nozzles with the name LNN and GG-W were manufactured by Spraying Systems (Figure 3.4). Their dimensions and weights are shown in Table 3.1. GG-W nozzle has a solid cone-shaped spray pattern with a round impact area. Therefore, it is able to spray wide angles between 100^{o}-120^{o}. On the other hand, the LNN nozzle is finely atomized and it is able to spray hollow cone (fine spray) without compressed air. It also has very small drops with a wider angle of 153^{o}.

Table 3.1 Dimensions and weights of nozzles.

View of Nozzle	Nozzle Type	Inlet Conn. (in.)	L (mm)	Hex. (in.)	Net Weight (kg)
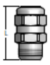	GG-W	1/4	39.7	11/16	0.04
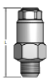	LNN-W	1/4	53.1	13/16	0.09

Figure 3.4 The Views for the LNN and GG-W Nozzles

Two nozzle system comprises of the combination of the LNN and GG-W nozzles linked to each other with the solenoid vanes and monometer at the junction point (Figure 3.5). They can be worked together within the identified time intervals. In the present study, a single nozzle was used in the first group of the tests, and the nozzle system was preferred for the other experiments. Details of the experiments will be given in Chapter 5.

Figure 3.5 Two Nozzle System with the LNN and GG-W Nozzles

4
NUMERICAL MODELLING AND VARIABLY SATURATED WATER FLOW

4.1 Numerical Modelling (HYDRUS)

This section is about the numerical modeling. The HYDRUS is one of the advanced models, which is applied in soil and water system for simulation of water flow, moisture distribution, and solutes transport in variably saturated media. This software has been developed at California University, solves Richard's equation, and appears to be a versatile modeling system with a well-designed graphical user interface (GUI) under the Microsoft Windows operating system. HYDRUS uses the finite-element (FE) method to simulate one-, two- or three-dimensional movement of water, heat, and multiple solutes in unsaturated, partially saturated, or fully saturated porous media. Two main variants of HYDRUS can be found: (1) HYDRUS-1D that has existed as a Windows-based code since 1998 (the latest version 4.0 was released in 2007); and (2) HYDRUS- 2D/3D that is a combination of HYDRUS-2D (1999 to 2007) and HYDRUS-3D (2006 to 2007). HYDRUS model would be a good choice for any researchers or environmental engineers interested in subsurface flow, transport, and remediation where variably saturated conditions must be considered. In this study, numerical modeling was conducted with HYDRUS-3D. HYDRUS model (Simunek et al., 2016) was used to simulate drainage of soil in the multi-layers of the sports fields. It is commonly used in the literature to simulate water flow in variably saturated porous media.

4.1.1 Model Theory

4.1.1.1 Governing Equation

The governing equation is given by the following form of Richard's equation (Eqn. 4.1):

$$\frac{\partial \theta}{\partial t} = \frac{\partial}{\partial x_i}\left[K\left(K_{ij}^{A}\frac{\partial h}{\partial x_j} + K_{iz}^{A}\right)\right] - S \qquad (4.1)$$

where θ is the volumetric water content $\left[L^3L^{-3}\right]$, h is the pressure head $[L]$, x_i $(i=1,2)$ are the spatial coordinates $[L]$, t is time $[T]$, K_{ij}^A are components of a dimensionless anisotropy tensor K^A, K is the unsaturated hydraulic conductivity function $\left[L\,T^{-1}\right]$, S is the sink term $\left[T^{-1}\right]$ that was assumed to be zero in this study.

HYDRUS-3D model uses the soil hydraulic functions proposed by van Genuchen (1980) who used the statistical pore-size distribution model of Muallem (1976). They described the soil water retention curve function $\theta(h)$, and the unsaturated hydraulic conductivity function, $K(h)$, respectively:

$$\theta(h)=\begin{cases}\theta_r+\dfrac{\theta_s-\theta_r}{\left[1+|\alpha h|^n\right]^m} & h<0\\ \theta_s & h\geq 0\end{cases} \tag{4.2}$$

$$K(h)=K_sS_e^l\left[1-(1-S_e^{1/m})^m\right]^2 \tag{4.3}$$

$$S_e=\frac{\theta-\theta_r}{\theta_s-\theta_r} \tag{4.4}$$

$$m=1\text{-}1/n \qquad\qquad n>1 \tag{4.5}$$

where θ_r and θ_s denotes the residual and saturated water content $\left[L^3L^{-3}\right]$, respectively, S_e is the effective water content $\left[L^3L^{-3}\right]$, K_s is the saturated hydraulic conductivity $\left[L\,T^{-1}\right]$, α $\left[L^{-1}\right]$, n, m are the parameters of the van Genuchen model. These empirical parameters are dependent on soil types that are considered to affect the shape of hydraulic functions. Muallem (1976) determined l the pore connectivity that was to be about 0.5 for an average for many soils. The pore size distribution index (n)is the steepness of the soil water retention curve and α is the inverse of air entry (bubbling pressure) that takes greater values for coarser soils (gravel and coarser sand).

4.1.1.2 Model Implementation

The details of the main processing and calculation steps were given below.

The main processing menu is:

- Geometric Data
- Time Data
- Information about Results Print
- Numerical solution Conditions
- Soil Hydraulic Properties

Calculation steps are as follows:

- Solving governing equation (Richard equation) using finite element method.
- Calculation of absorption and moisture values in a successive iteration based on specified time steps.
- Comparison of absorption and moisture values between two successful iterations as compared with solving accuracy (tolerance) given to the model.
- Provided that, Δh or $\Delta\theta$ is larger than the given accuracy, calculations are done at the next time step.

This software starts calculations by performing a model with an initial time step and then compares the obtained values in iteration to the given accuracy, eventually, arranges and modified values according to the maximum and minimum time steps specified in the software. The output data of the model include simulation time, number of iteration in each time step, total cumulative of the number of iterations, flows variations in the upstream border, total cumulative input flow in upstream, total cumulative water absorption by root, total cumulative output flow in downstream, matrix potential in upstream, downstream and by root. HYDRUS model is used in field and laboratory works, to simulate water flow, soil hydraulic properties, solute, and CO_2 transport.

4.1.2 Pre-Processing

The sections below demonstrated the pre-processing tasks done in the HYDRUS model.

4.1.2.1 Main Processes

In main processes, the name of the heading that appears in the output files is provided, and specify the scope of the project. In this study, the water flow and root water uptake were simulated together as shown in Figure 4.1.

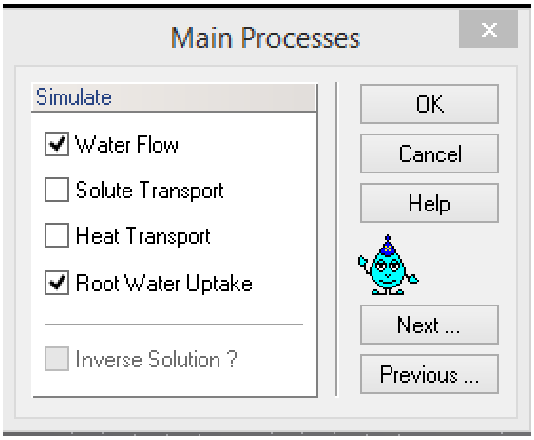

Figure 4.1 Main Processes of This Study.

4.1.2.2 Geometry Information

Geometry Type

In this study, a 3-D tank with different layers containing different materials was modeled while layering fine sand, coarse sand, and rootzone as seen in Figure 4.2.

Length units

The length unit was selected and used cm' in the model due to the inputs and outputs of the model are in cm (Figure 4.3). The size of the drainage tank size was also inserted into the model as shown in Figure 4.3.

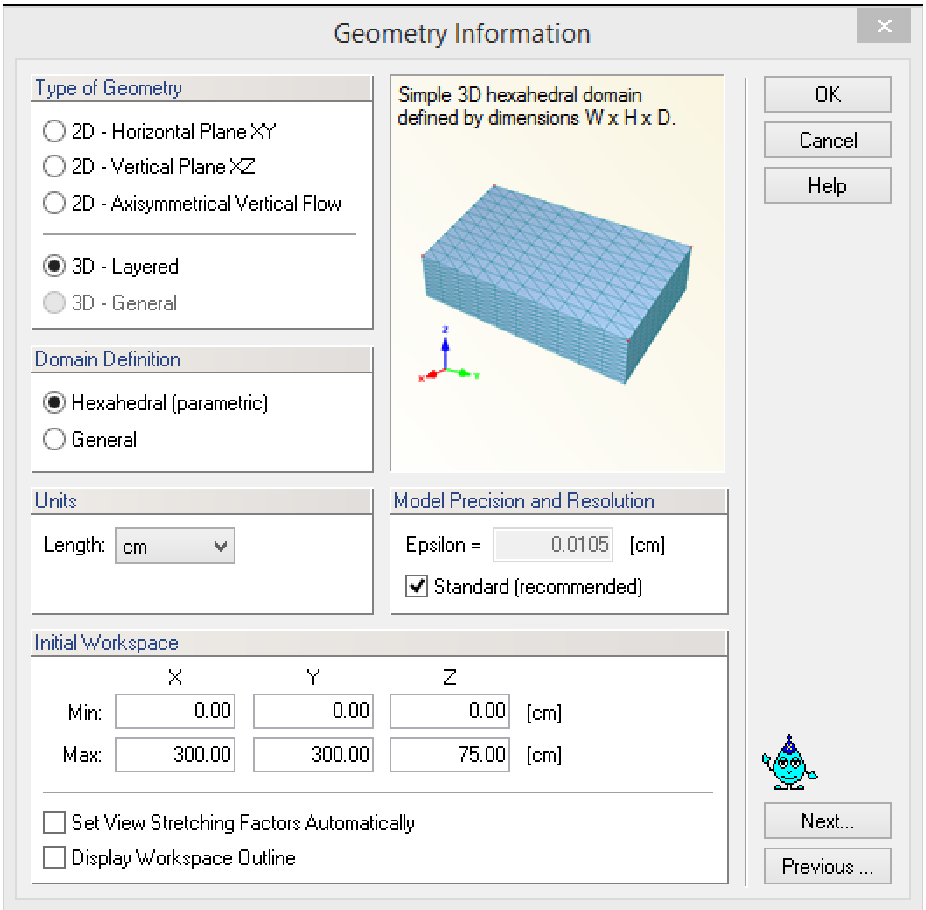

Figure 4.2 Geometry Information of the Model

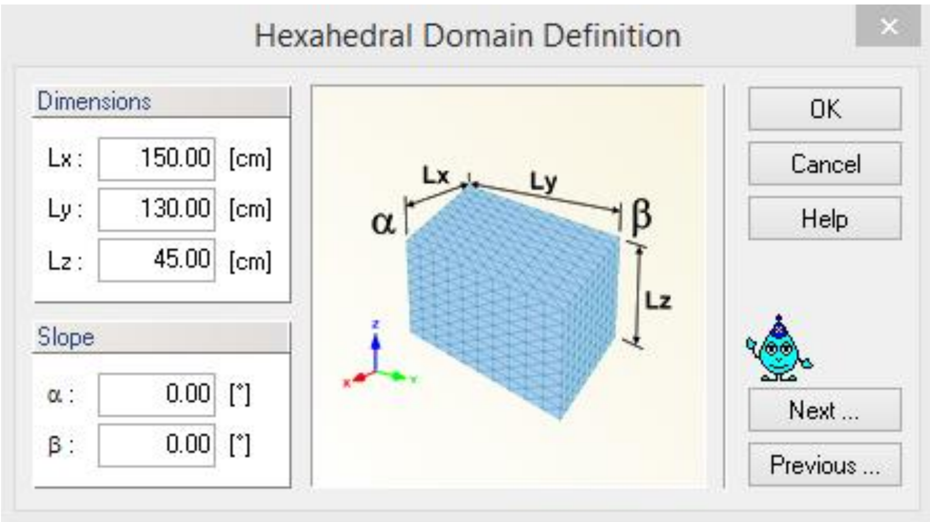

Figure 4.3 Geometry of the Model

4.1.2.3 Time Information

Figure 4.4 shows the time information such as the time units, time discretization, and boundary conditions. The minutes as time units were selected and the initial time was set to 0 minutes whereas the final time is 2880 minutes (2 days). Different time steps also were provided such as initial time step, minimum time step, and maximum step. The initial time step relates to the numerical solution, which is a self-adjusting time marching scheme. This is the initial time step that HYDRUS adopts at the beginning of the solution and whenever boundary conditions change significantly. As the iterative numerical solution finds it more difficult to converge, the time step is automatically reduced. However, a limit is introduced on how small the time step is allowed to become. This limit is the minimum time step. It is recommended by HYDRUS technical report that allowing the minimum time step to be on the order of 1 s (Simunek et al., 2006 and 2012). On the other hand, if the solution is converging fast, the time step is increased. The maximum time step is a limit on how large the time step can become.

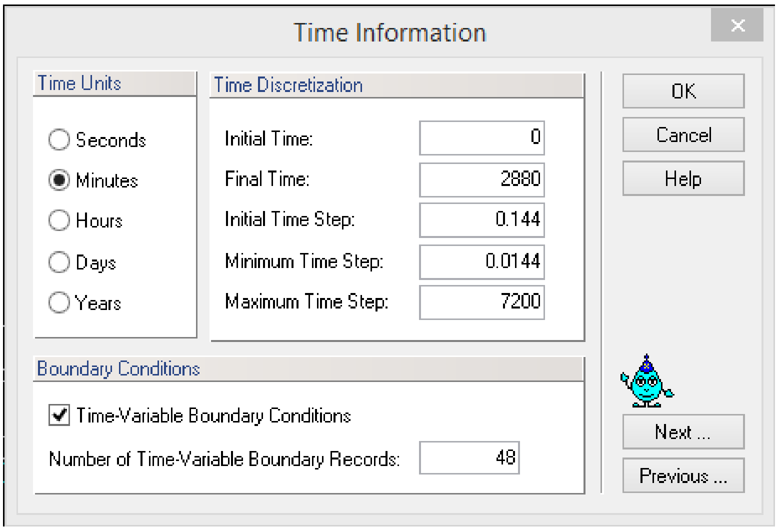

Figure 4.4 Time Information of the Model

Time-Variable Boundary Condition was also selected as it allows including atmospheric data such as precipitation and evaporation, plant transpiration, and timing variable boundary conditions such as pressure heads and/or fluxes; the relevant data is input as a time-series. Once this option is selected, the box 'Number of Time-Variable Boundary Records' will be activated and prompt the user to enter an integer ≥1 for our case the number of records of the time-variable boundary was set to 48.

4.1.2.4 Print (Output) Information

Figure 4.5 was given for the details of output information which include time level, screen output, and print times.

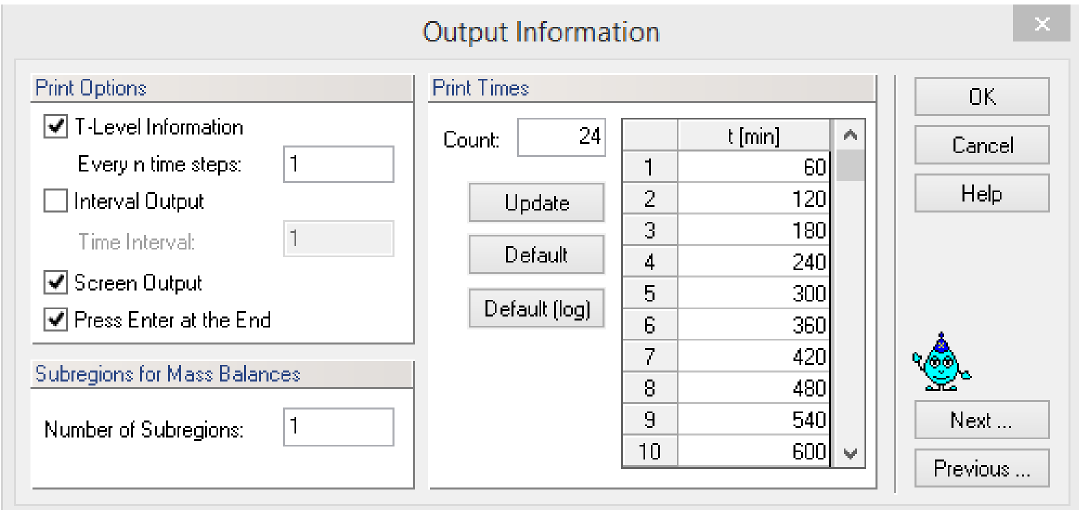

Figure 4.5 Output information of the Model

Time Level Information: If this option is checked, then detailed results of fluxes, pressure heads, and other variables are printed at each time step.

Screen Output: This option decides whether or not results are dynamically shown on the computer screen during a simulation. It is recommended to always use this option, especially for new projects so as to monitor their progress. It is, however, recommended to uncheck this option for "inverse solution".

Print times: These are prescribed times at which detailed run information is printed to the output files, such as fluxes, pressure heads, water contents, and concentrations. The number of Print Times: Specify the number of print times for the case we have used 24.

4.1.2.5 Iteration Criteria

Figure 4.6 states the details about the iteration that has been used for modeling this project. Due to the nonlinear nature of the Richards equation, an iterative process must be used at each new time step. This iterative process continues until a satisfactory degree of convergence is obtained, i.e., until the change in pressure head (or water content) at all nodes between two successive iterations becomes less than a small value (i.e., the absolute pressure head (or water content) tolerance).

Maximum Number of Iterations: The maximum number of iterations allowed during any time step. If the maximum number of iteration is reached without reaching a solution, the time step is divided by 3, and the computation at the current time level restarted.

Water Content Tolerance: Absolute water content tolerance for nodes in the unsaturated part of the flow region. This parameter represents the maximum allowed absolute change in the value of the water content between two successive iterations during a particular time step.

Pressure Head Tolerance: Absolute pressure head tolerance for nodes in the saturated part of the flow region [L]. This parameter represents the maximum allowed absolute change in the value of the pressure head between two successive iterations during a particular time step.

Initial water flow conditions can either be described in terms of volumetric water contents or pressure heads; they describe the state of the system prior to the simulation. The initial conditions themselves are later set in “Boundary Conditions Editor/Initial Conditions”. There are two options, pressure-head or water content. It is the “Initial Condition” option here under “Iteration Criteria” that will decide whether the initial soil conditions to be entered later are to be interpreted as water contents or pressure heads.

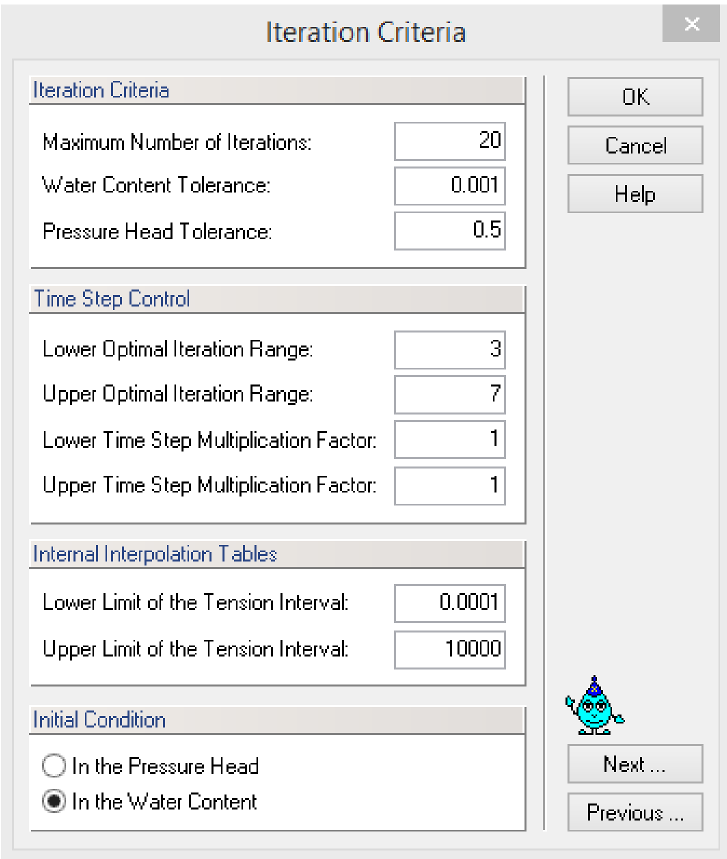

Figure 4.6 Iteration criteria of the Model

4.1.2.6 Soil Hydraulic Model

HYDRUS Model allows users to select three types of models to describe the soil hydraulic properties: van Genuchten (1980), Brooks and Corey (1964), and modified van Genuchten type equations (Vogel and Cislerova, 1988) (Figure 4.7). Those models describe the water retention parameters of the soil as well as the hydraulic conductivity function, often referred to also as the constitutive relationships. They relate water content and hydraulic conductivity to the pressure head. The van Genuchten was applied to this model.

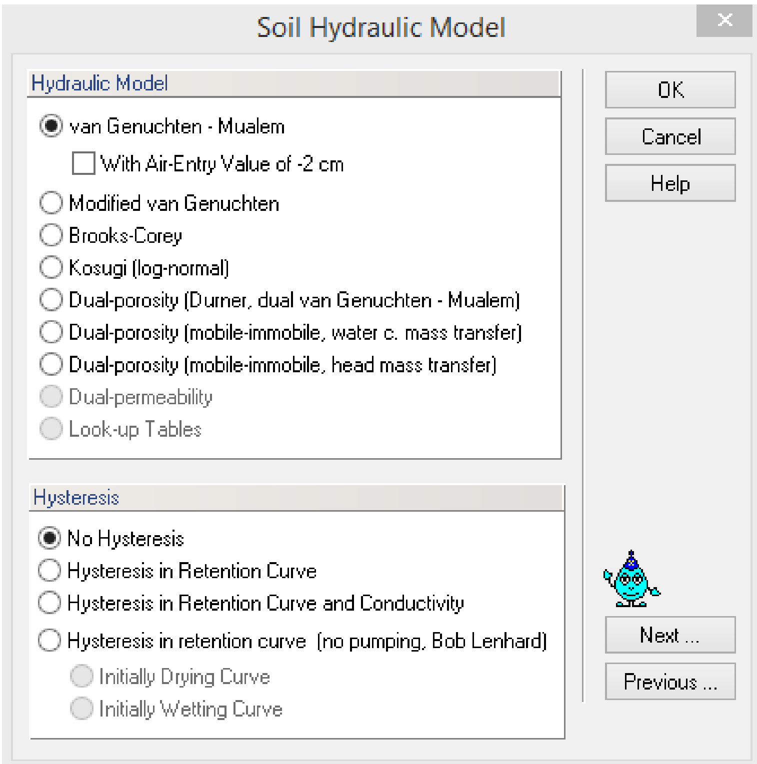

Figure 4.7 Soil Hydraulic Model of the Presented Study

4.1.2.7 Water Flow Parameters

The example of an experiment for water flow parameters was given in Table 4.1.

Table 4.1 Materials properties for water flow

Material	**Q_r (cm³/cm³)**	**Q_s(cm³/cm³)**	**α [cm⁻¹]**	**n [-]**	**K_s (cm/min)**	**l**
Rootzone	0.078	0.43	0.036	1.56	0.0173333	0.5
Blinding Layer	0.057	0.41	0.124	2.28	0.435	0.5
Gravel Bed	0.045	0.43	0.145	2.68	0.852	0.5

Where:

Q_r: Residual water content,

Q_s: Saturated moisture,

K_s: Saturated hydraulic conductivity, l: pore-connectivity parameter,

α and n are empirical values of the equation which affect the shape of hydraulic functions.

4.1.2.8 Root Water Uptake Model

In this study, the root water uptake (plant transpiration) was modeled. The water uptake reduction model defines the manner in which transpiration is reduced below the potential rate when the soil is no longer capable of supplying the amount of water demanded by the plant under the prevailing weather conditions. There are two alternative reduction models: one by the Feddes et al. (1978), further referred to as the Feddes model, and one by van Genuchten (1987), further referred to as the S-shaped model. The model needs to determine the sink volume, which represents the volume of water removed per unit time from a unit volume of soil due to plant water uptake. For this purpose, in this project, the Feddes model (Figure 4.8) was selected to reduce the potential root water uptake to the actual water uptake rate.

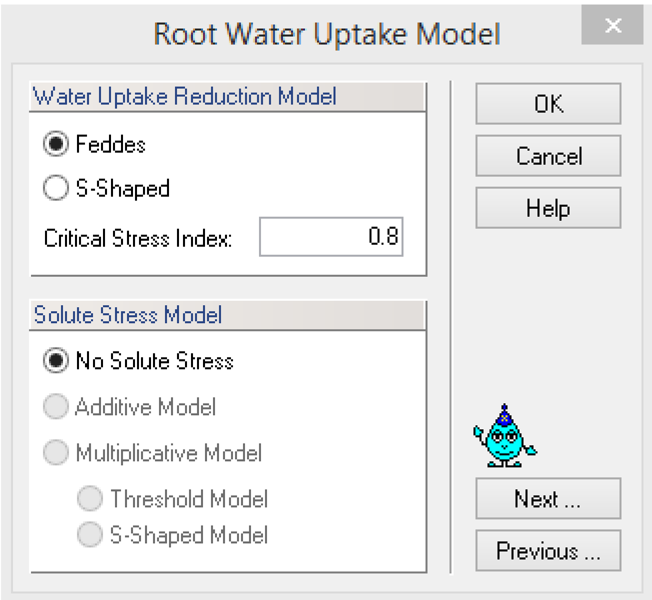

Figure 4.8 Root Water Uptake Model for the Model

Figure 4.9 also shows different Feddes' Model Parameters. The Feddes model assigns plant transpiration rates according to the soil's pressure head.

P0: Value of the pressure head below which roots start to extract water from the soil.

POpt: Value of the pressure head below which roots extract water at the maximum possible rate (potential transpiration).

P2H: Value of the limiting pressure head below which roots no longer extract water at the maximum rate (assuming a potential transpiration rate of r2H).

P2L: As above, but for a potential transpiration rate of r2L.

P3: Value of the pressure head below which root water uptake ceases (usually taken at the wilting point). A database of suggested values for different plants is provided based on studies by Wesseling (1991), Taylor, and Ashcroft (1972).

r2H: Potential transpiration rate (L/T) (currently set at 0.5 cm/day).

r2L: Potential transpiration rate (L/T) (currently set at 0.1 cm/day).

The above 2 input parameters permit one to make the variable P2 a function of the potential transpiration rate (P2 presumably decreases at higher transpiration rates). HYDRUS currently implements a linear interpolation scheme for this purpose.

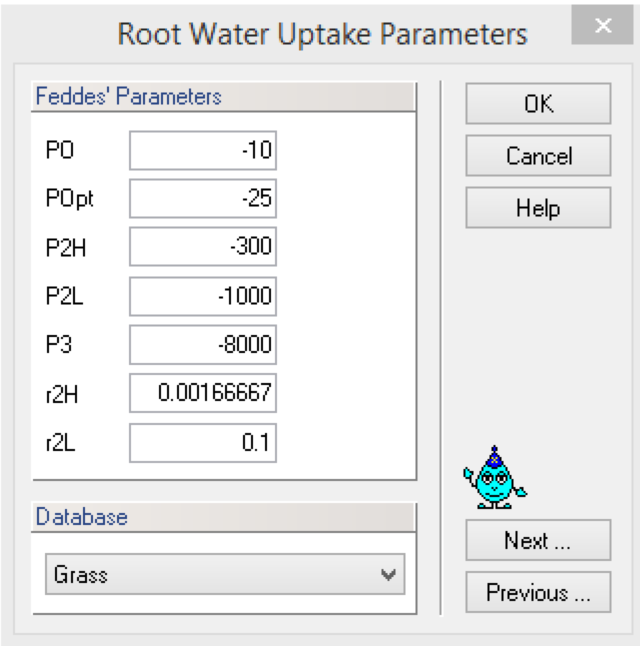

Figure 4.9 Root Water Uptake Parameters for the Project

4.1.2.9 Time Variable Boundary Conditions

In this window, the user is prompted to enter boundary conditions that vary with simulation time (Figure 4.10). These conditions are dynamic (variable) through the simulation but static (constant) through a defined period of time. That is, the modeling discretizes the total simulation time into portions with different boundary values. The number of rows (48 here) in this window depends on the number of "Time Variable Boundary Records" specified earlier in the "Time Information" window. Note that the last "Time" is equal to the "Final Time" specified in the "Time Information" window.

Time: Time for which a data record is provided (T)

Precip: Precipitation or rainfall rate (L/T)

Evap: Potential evaporation rate (L/T)

Trans: Potential transpiration rate (L/T)

hCritA: Absolute value of the minimum allowed suction at the soil surface (L).

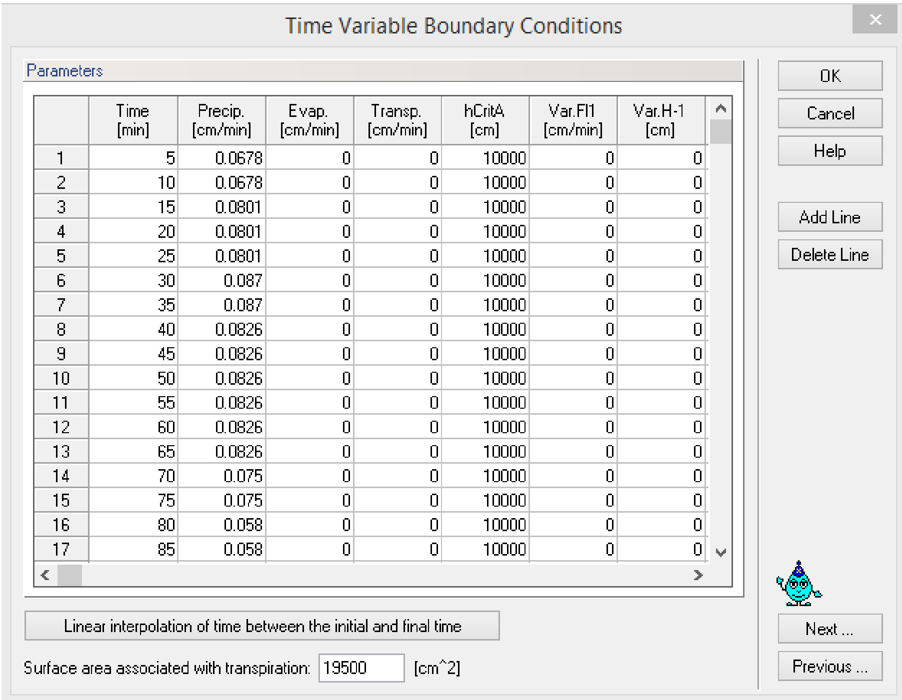

	Time [min]	Precip. [cm/min]	Evap. [cm/min]	Transp. [cm/min]	hCritA [cm]	Var.Fl1 [cm/min]	Var.H-1 [cm]
1	5	0.0678	0	0	10000	0	0
2	10	0.0678	0	0	10000	0	0
3	15	0.0801	0	0	10000	0	0
4	20	0.0801	0	0	10000	0	0
5	25	0.0801	0	0	10000	0	0
6	30	0.087	0	0	10000	0	0
7	35	0.087	0	0	10000	0	0
8	40	0.0826	0	0	10000	0	0
9	45	0.0826	0	0	10000	0	0
10	50	0.0826	0	0	10000	0	0
11	55	0.0826	0	0	10000	0	0
12	60	0.0826	0	0	10000	0	0
13	65	0.0826	0	0	10000	0	0
14	70	0.075	0	0	10000	0	0
15	75	0.075	0	0	10000	0	0
16	80	0.058	0	0	10000	0	0
17	85	0.058	0	0	10000	0	0

Figure 4.10 Time Variable Boundary Conditions

4.1.2.10 Geometry and Finite Element Mesh Editor

The finite element mesh is constructed by dividing the flow for three-dimensional problems into tetrahedral, hexahedral, and/or triangular prismatic elements whose shapes are defined by the coordinates of the nodes that form the element corners. The program automatically subdivides hexahedral and triangular prisms into tetrahedral, which are then treated as sub-elements. Two different ways are possible to subdivide the hexahedral into tetrahedral, whereas six different possibilities exist for subdividing the triangular prisms into tetrahedral. Figure 4.11 shows the geometry and the mesh generation of the project.

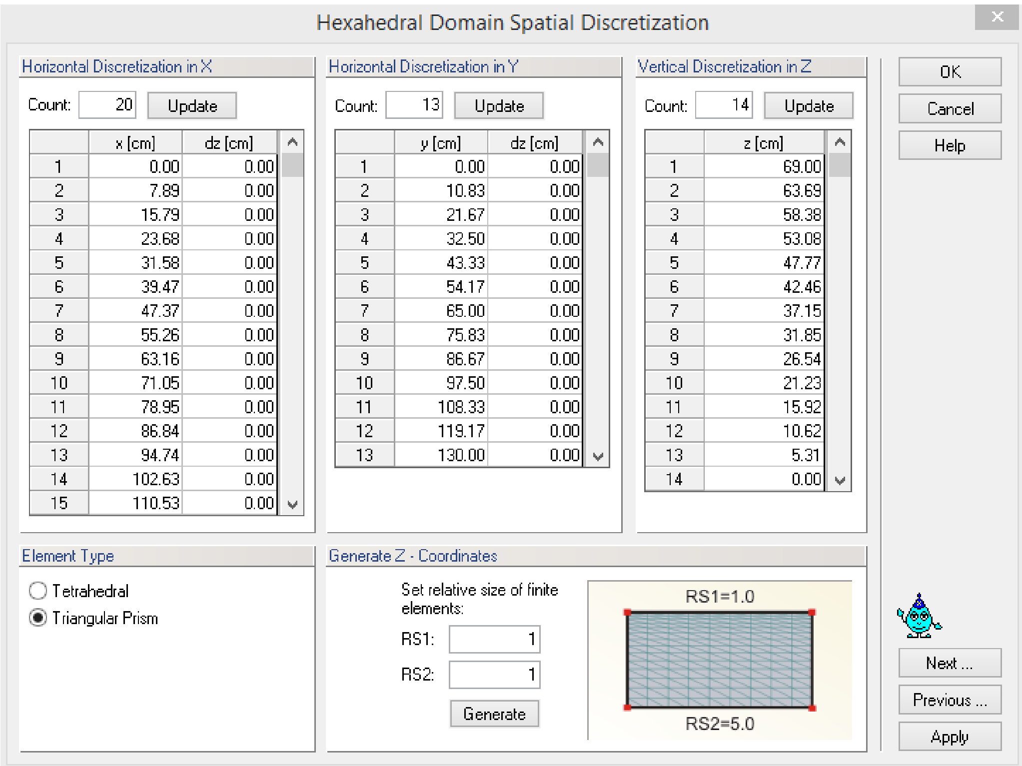

Figure 4.11 Geometry and Finite Element Mesh of the Model

4.1.2.11 Boundary Conditions

Specifying appropriate boundary conditions (BCs) is one of the most critical tasks when constructing a numerical model. A water flow BC is a known value of the flux, head, or gradient along the outer boundary of the finite element mesh (it means the external boundary of the selected flow domain; it is the interface between the soil and the outside world). Solving the governing equations for saturated/unsaturated flow, which means finding the new head at each node in the finite element mesh in a time-marching scheme, requires knowledge of those BCs. Otherwise, the problem becomes mathematically indeterminate.

In HYDRUS, boundary conditions are categorized as follows:

• ***System-dependent:*** or dynamic BCs, meaning that they can change during the simulation (i.e., they depend on the solution at the end of each time step). They may depend on saturation conditions (as in a seepage face or a drain), or on soil properties and/or climate conditions (as at soil/atmosphere interfaces).

• ***System-independent:*** This type of BC is entirely known as a priori, is implemented by the user, and is independent of the simulation results.

System-independent water flows BCs include:

- A known head (as in Constant Pressure and Variable Pressure)
- A known flux (as in No Flux, Constant Flux, Variable Flux, and Deep Drainage)
- A known gradient (as in Free Drainage)

Figure 4.12 shows the boundary conditions for the presented study. The soil surface boundary condition involved actual precipitation and potential transpiration rates for a grass cover. Model boundary condition upstream was considered as the atmospheric boundary where the intensity of rainfall was defined and downstream is considered as free drainage. There is no flux at the side of the considered profile soil.

Atmospheric Boundary Condition: this boundary condition lets us incorporate climatic conditions like rainfall (precipitation) and evaporation, or transpiration (root uptake) by plants. The latter is only activated if root water uptake is checked in 'Main Processes'.

Free Drainage: These Boundary Conditions specify a unit gradient along the lower boundary (outflow, drainage) of the finite element mesh. It is applicable in cases where the water table is located far below the domain of interest. This BC assumes a unit total vertical hydraulic gradient, that is, gravity flow with no pressure head gradient. This boundary condition should never be used along the sides of the transport domain. It should be used only at the bottom of the domain.

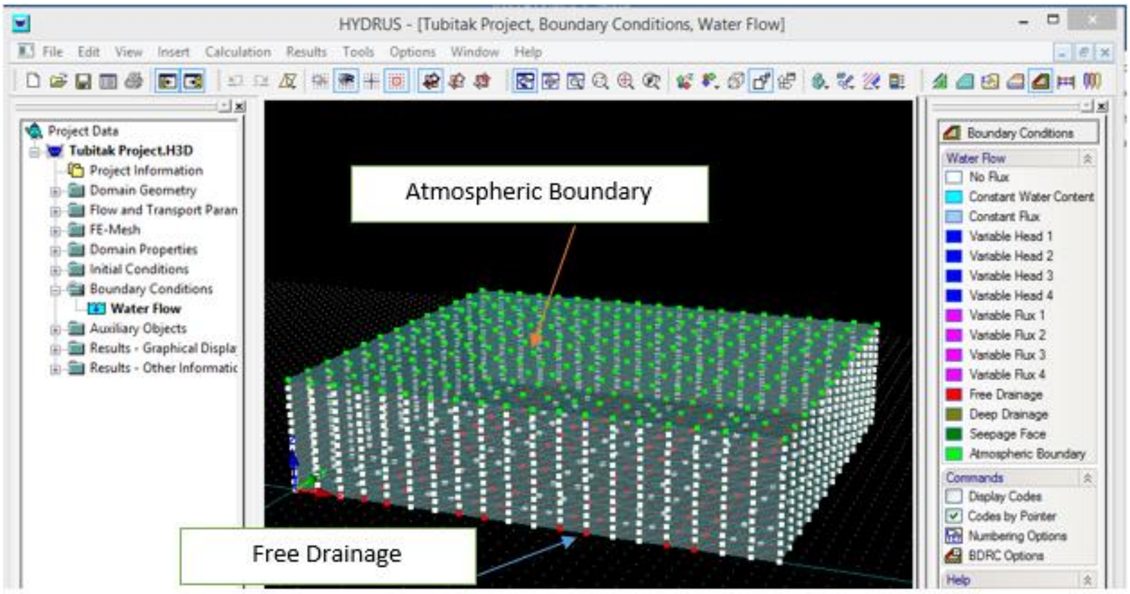

Figure 4.12 Boundary Conditions for the Model

4.1.3 Post-Processing

The results presented in this section are provided after modeling water flow in different types of layered soil profiles and rainfalls. Therefore, in this study, 5 observation nodes were used through soil profiles (Figure 4.13).

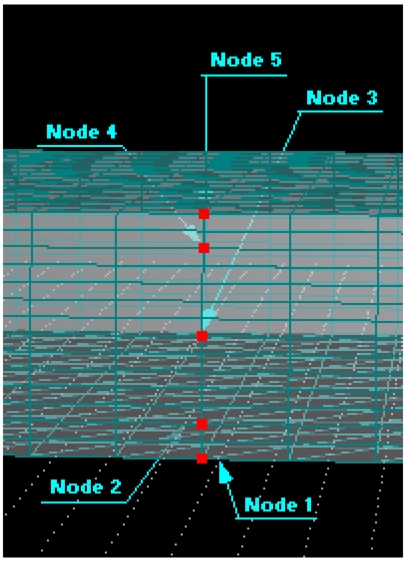

Figure 4.13 Observation Nodes

Therefore, an example experiment results were shown to evaluate the post-processing outputs according to observations points as abbreviated 'N'. Figure 4.14 shows the variation of water content and pressure heads at different observation nodes within the observed time. It can be inferred from Figure 4.14 that the soil was not totally dry, the initial condition for water content at the beginning of simulation was set to 0.15. It can be seen clearly that Node 5, located at the top surface (top layer) reaches the maximum water content of 0.43 during the first minutes of simulation. As time increase, the infiltration reaches different layers of soil, and the water content changes according to the position of nodes. The nodes, which are located in upper layers, are early saturated as the water passing through them. The pressure head for different observation points was increased from the dry state up to almost zero (saturation). As the time increase, the water flows down in the tank, the water content decreases in considered points, and the pressure decreases too as the soil becomes dry.

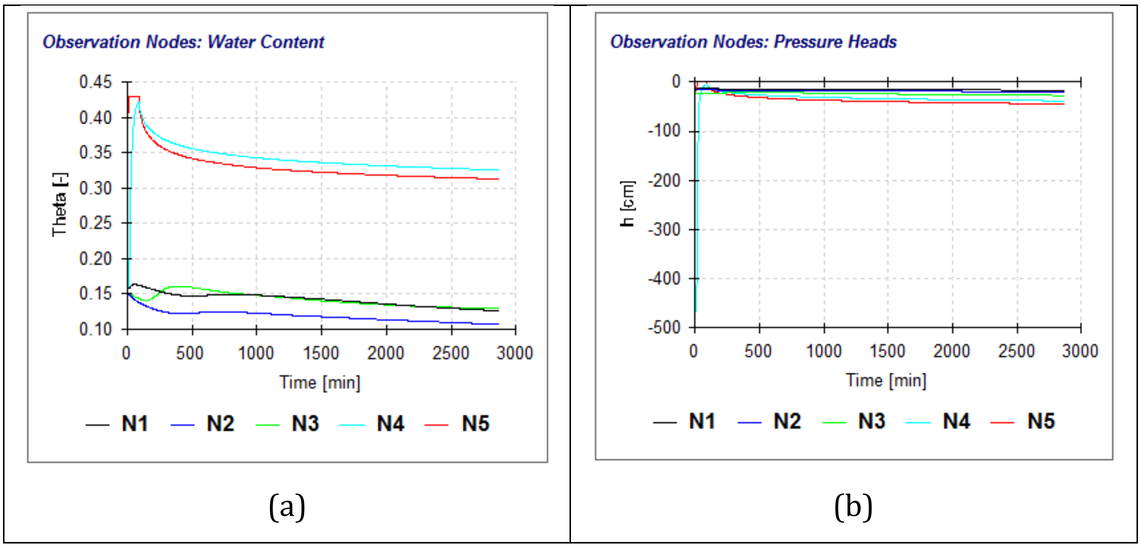

Figure 4.14 Basic Results According To Observation Points A) Water Content, B) Pressure Head

In brief, the HYDRUS-3D numerical model was used in a few set-up experiments. These are explained and demonstrated in the section of 'Experimental and Numerical Results'. Moreover, the comparison of the numerical results from the HYDRUS and experimental results was conducted in detail regarding water content and drain outflow hydrograph.

4.2 Variably Saturated and Unsaturated Flow

The variably saturated flow is a special form of Richards' equation for unsaturated flow with considering elastic storage arguments for defining specific storability that is necessary for saturated flow modeling. In this section, unsaturated flow and its characteristics were discussed.

Water under the ground surface occurs in two main zones, the unsaturated (vadose) zone and the saturated zone. In the unsaturated zone, the spaces between particle grains fill with both air and water. Although a substantial, amount of water can be present in the unsaturated zone, this water is not accessible and available for pumping by wells due to capillarity that forces hold water so strictly. On the other hand, the spaces are entirely filled with water in the saturated zone (Figure 4.15).

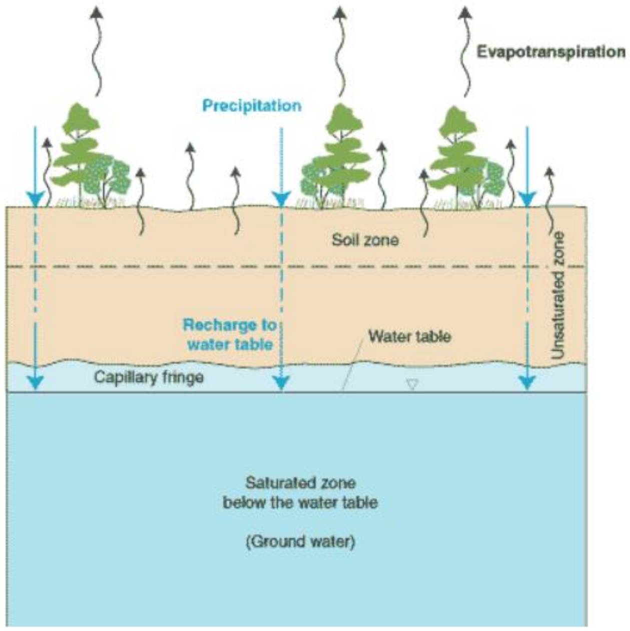

Figure 4.15 Schematic View of the Water Zones beneath the Ground Surface (USGS, 2013)

The approximate upper surface of the saturated zone is called the water table. Water is also referred to as ground water in the saturated area below the water table. The transition zone, the capillary fringe, is between the unsaturated area and the water table. In this region, the voids are saturated or nearly saturated by capillary forces with water (Figure 4.15).

The water table is the surface where the water in a saturated porous medium is at atmospheric pressure. Below the water table, pressure is greater than atmospheric pressure. Contrary, in capillary fringe, pressure is less than atmospheric pressure. The soil water zone is the highest zone in which water is obtained by plant activity or soil evaporation.

Therefore, Todd and Mays (2005) showed subdivisions of the vadose zone as soil water zone, intermediate vadose zone, and capillary zone (capillary fringe) (Figure 4.16).

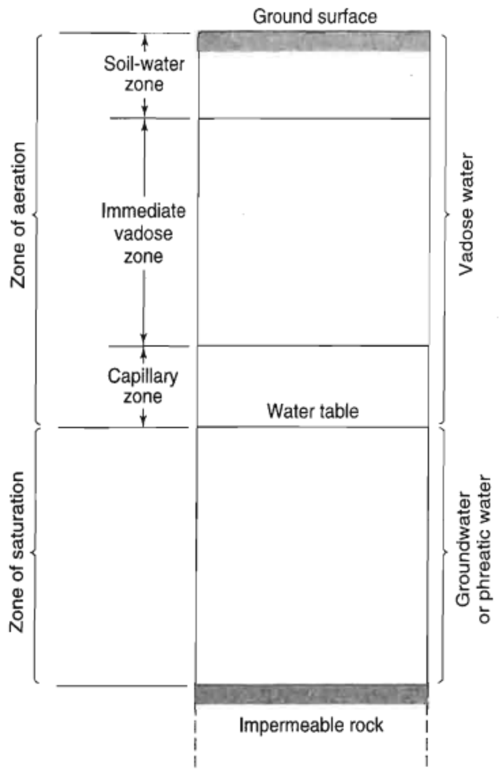

Figure 4.16 Water Zones (Todd and Mays, 2005)

There are some fundamentals properties of unsaturated flow, which are the matric potential, water content, and unsaturated hydraulic conductivity. Water is held in an unsaturated medium by some forces whose effect is expressed in terms of the water pressure that is referred to as the matric pressure or matric potential (increasing from the interaction of water with the rigid boundary). In other words, it is the pressure of the water in a pore of the medium relative to the pressure of the air. When a media is unsaturated, the water has lower pressure than the air; therefore, the matric pressure is negative.

Greater water content occurs with greater matric pressure. In other words, zero matric potential is allied with high (saturated or almost saturated) water content. While matric pressure increases the water content increases, however, the relationship is nonlinear and hysteretic. The relation between matric pressure and water content called a soil water retention curve (explained in previous chapters), is a characteristic of a porous media that is dependent on the nature of its pores. This relationship affects the motion of water and other substances in an unsaturated medium and controls the work of a plant for the extraction of water from the land. (USGS, 2013).

The hydraulic conductivity is the second significant characteristic that is critical to water movement in unsaturated flow. It is highly sensitive and nonlinear that alters with the water content. The flow rate of water is equal to the hydraulic conductivity times the driving force that this relation is known as Darcy's law. When applied to unsaturated conditions, Edgar Buckingham has often been referred to as the Darcy-Buckingham Law, which developed concepts of matrix potential and hydraulic conductivity that are crucial in implementing Darcy’s law in unsaturated media. (USGS, 2013). Darcy’s law is valid for steady flow.

The comprehensive cases of unsteady flow in an unsaturated porous medium is a highly dynamic characteristic and may be evaluated with a combination of Darcy's law and the continuity or conservation law for water (USGS, 2013). Richards' equation combines both of these laws in one formula. Although Darcy's law requires measured or estimated hydraulic conductivity over the appropriate range of soil moisture, Richards’ equation needs to determine the soil water retention curve in addition to hydraulic conductivity.

5
EXPERIMENTAL STUDY

5.1 Design of the Experimental Setup

As part of this study, an experimental setup to evaluate the process of sports field drainage under various rainfall intensities was developed that has the ability to measure natural-like rainfall characteristics and resulting drainage flow characteristics as shown in Figure 5.1 and Figure 5.2. The major components are the RS which consists of downward-oriented spraying nozzles fixed on a 5.5mx3.5m main frame; rainfall mesh located 1m beneath the nozzle, and drainage tank (DT) which includes two identical 1.5mx1.3m compartments. Each compartment has a 70 cm depth that is appropriate to simulate multi-layers 1 to 1 scale for the sports field drainage process. The experimental setup has a 100 lt water tank that stores and supplies water to the system with 2 cm diameter galvanized pipes for the production of simulated rainfall (Figure 5.2 and Figure 5.4). PLC (programmable logic controller) panel in the front of the apparatus controls the experimental setup by generating pulse signals with different precise periods (Figure 5.2, Figure 5.3, and Figure 5.4). It essentially controls a motor and pump system which is able to apply pressures ranging from 0-65 bar that produces rainfall with a wide range of rainfall intensities.

There is an orifice meter located between the pump and water tank as seen in Figure 5.2. The pumping flow rates were determined with pressure differences between pressure transmitters that are placed at the inlet and outlet of the orifice meter. Pressures measured by these transmitters are recorded by the PLC. The RS uses full jet nozzles made up of brass, mild and stainless steel that sprays as a full cone with the spraying wide angle. They were mounted at the edge of nozzle pipes that are fixed on the main frame (Figure 5.2). Nozzles are able to produce simulated rainfall with various intensities. The wire mesh is located 1m below the nozzle and 2.4 m above the ground surface of the DT in order to achieve terminal velocity for rainfall drops having zero initial velocity after they hit the mesh.

However, Carvalho et al. (2014) mentioned that most of the simulated raindrops reached the ground surface without hitting the mesh. Moreover, there are two grooves on the setup: the upper one is located around the mesh with the same elevation, the lower is located around the surface of DT (Figure 5.2). These grooves collect excess rainwater which goes out of the mesh and hits the curtains then seeps to the grooves because of water jet spraying out at an angle. Excess water collected by grooves is also measured during the experiments. Each DT with the dimensions of 1.5mx1.3mx0.7m has four perforated drainage pipes at the bottom of the tank which is located at 30 cm distance intervals. The 7 cm diameter drainage pipes convey drain water to gutters at the front and back of the experimental setup (Figure 5.1 and Figure 5.5). The drain water that was transmitted with gutters is then measured in the collectors.

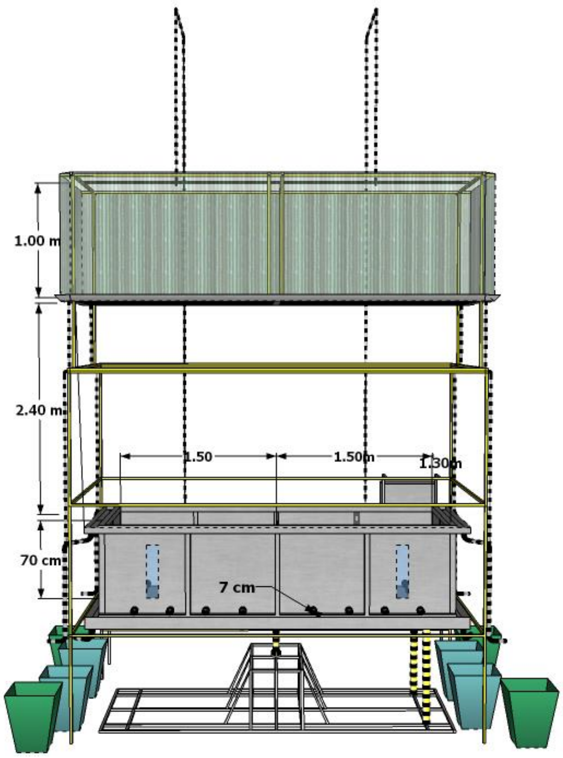

Figure 5.1 Schematic Front View of the Experimental Setup

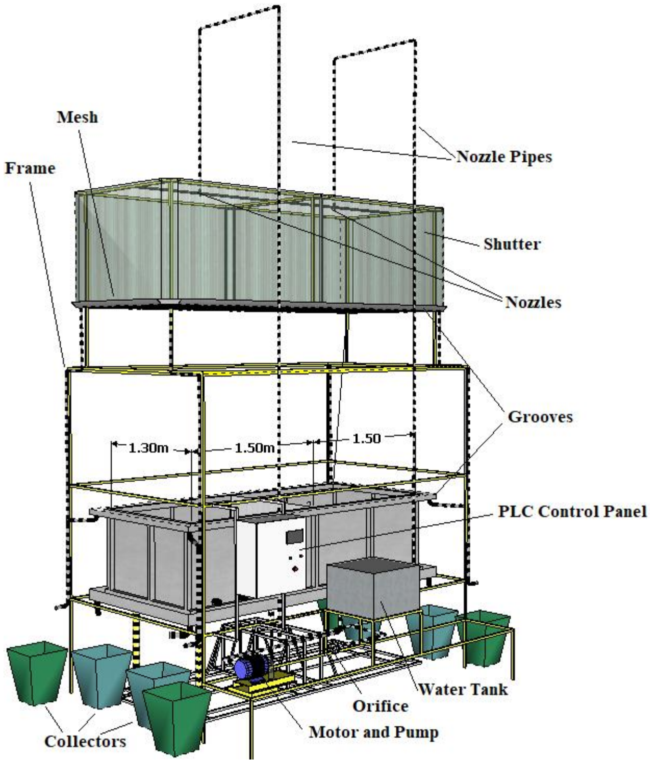

Figure 5.2 Schematic Rear View of the Experimental Setup.

Figure 5.3 Side View of the Experimental Setup

Figure 5.4 Details of PLC Control Panel, Motor, Pump, and Orifice Meter

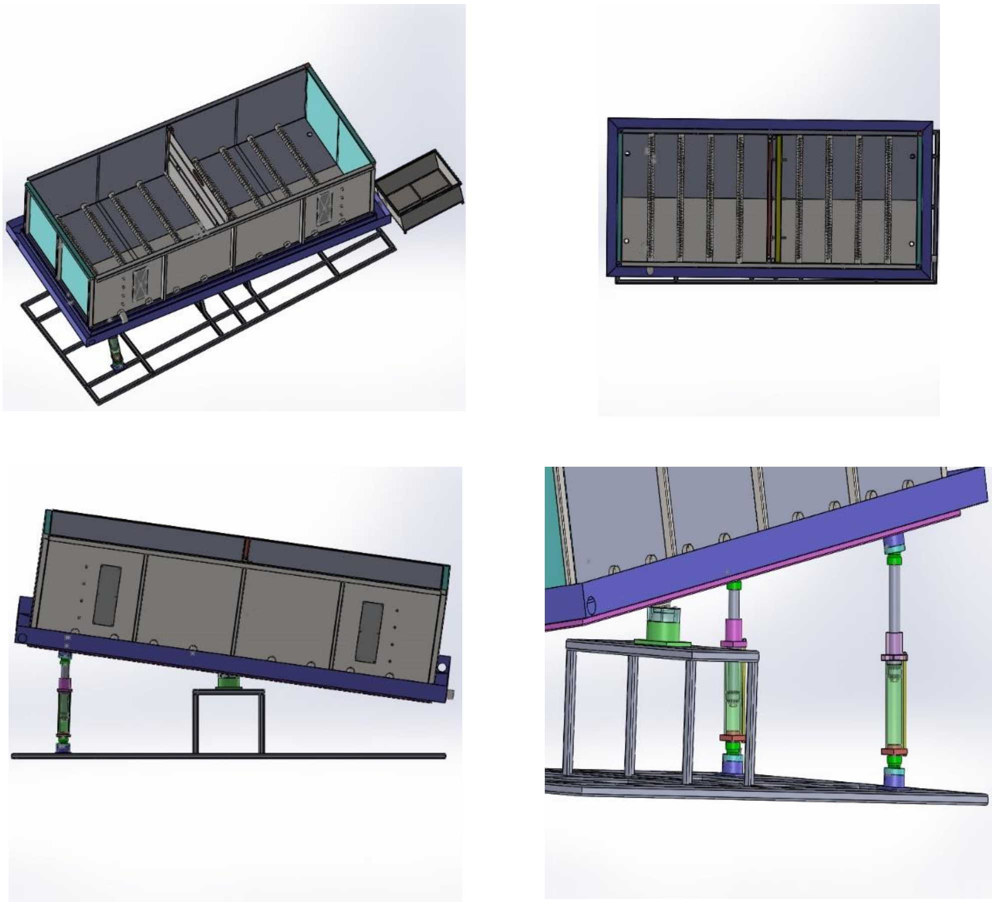

Figure 5.5 The Details of Drainage Tank (DT) and Pneumatic System

5.2 Material Properties

Properties of materials used in experiments were given in Table 5.1. In the presented study, five different materials were used with changing values of mean diameter between 0.5 mm-6 mm as shown in Figure 5.6. The layer of rootzone was constituted as sand dominated with 0.5 mm sand (M1). Mean diameters (D_{50}) were found from analyzing the Grain size distribution curve (Figure 5.7). Therefore, uniformity coefficient (C_u) and coefficient of gradation (C_c) were defined as $\frac{D_{60}}{D_{10}}$ and $\frac{D_{30}^2}{D_{60} x D_{10}}$, respectively. D_{10}, D_{30} and D_{60} are the effective particle sizes found from the grain size distribution curve.

This study, C_u was less than 4 and C_c took values between 1 and 3 for all materials that they considered to be uniformly graded. Bulk density, specific gravity, porosity, and field capacity were determined from laboratory experiments at Yildiz Technical University. Some views of the experiments were given in Figure 5.8.

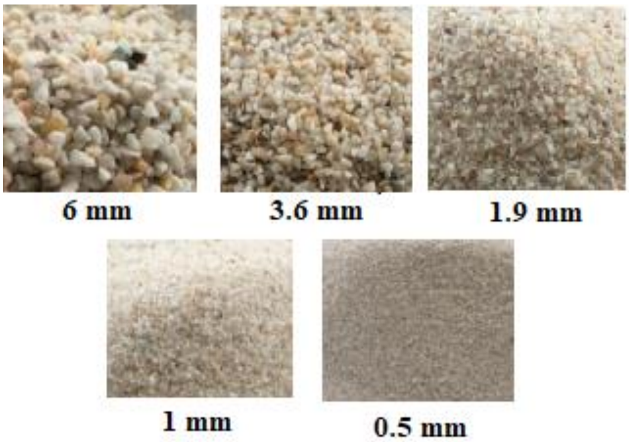

Figure 5.6 Material Views Used In This Study

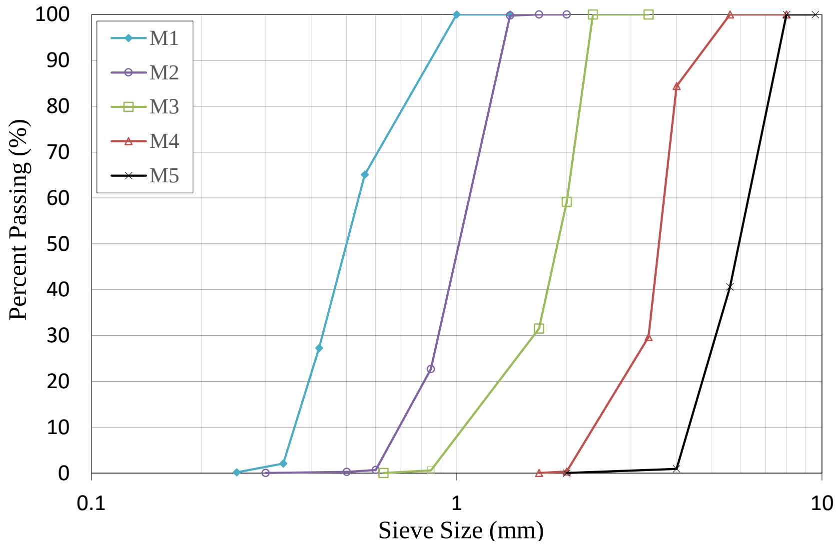

Figure 5.7 Grain Size Distribution Curves for Different Materials

Figure 5.8 The Views of the Experiments for Bulk Density and Specific Gravity.

Soil Water Retention Curve (SWRC) was also measured from calibration experiments for each material separately. Figure 5.9 indicated these curves in detail. The SWRC is a basic description of the amount of water retained in the soil. It is a significant hydraulic characteristic of soils that is directly based on the size, connectedness of pore spaces. Therefore, it is strongly affected by soil texture and structure, and by other constituents such as organic matter (Tuller and Or, 2005).

Moreover, Figure 5.10 showed the typical soil-water characteristic curves for different soil textures. It is a fact that M5, M4, M3, and M2 materials are the coarser materials (from coarse sand to pebble) and representative SWRCs were very close to each other as given in Figure 5.9. The turquois curve belonged to the finest material (M1) used in this study with a mean diameter of 0.5 mm that rootzone consisted of this material. Generally, typical characteristic curves for different soil textures was almost overlapped with the SWRCs obtained from calibration experiments in this study. In the following chapters, the SWRCs obtained from measurements were optimized with a numerical model of HYDRUS-3D used for the simulation of drainage processes in the presented study.

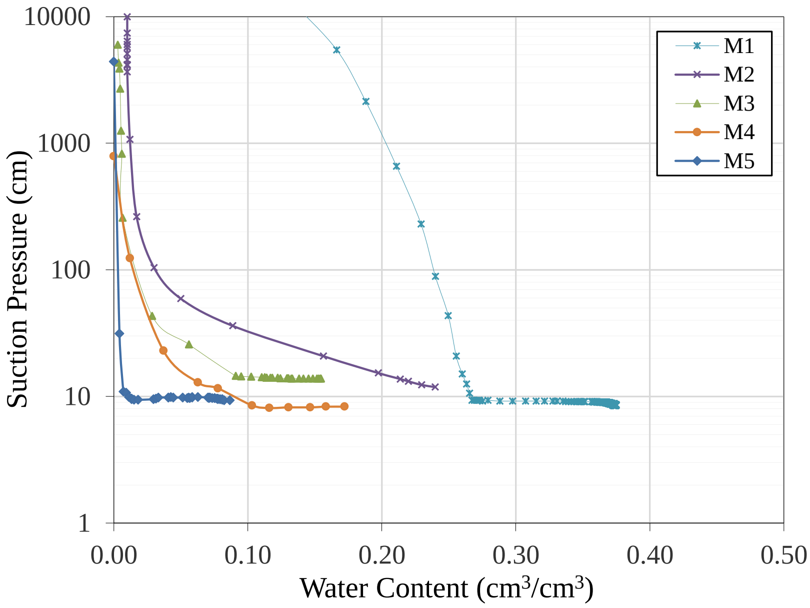

Figure 5.9 The SWRCs for Different Soils Used in This Study

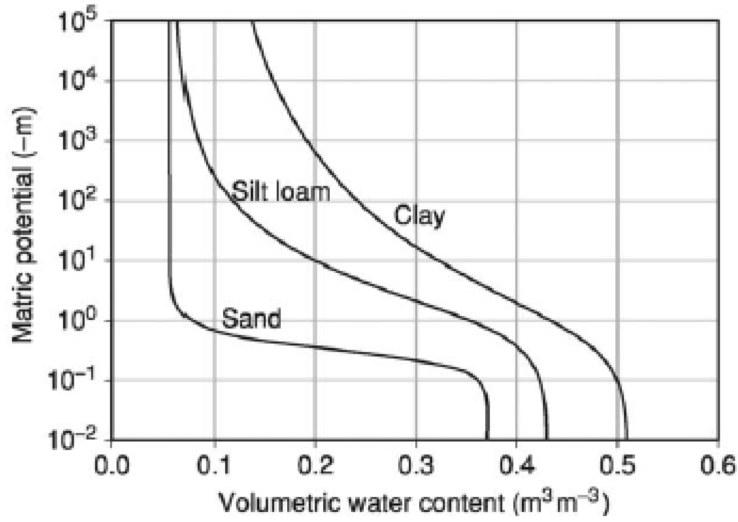

Figure 5.10 Typical SWRCs for the Different Soil Samples

Table 5.1 Analysis results of mixture content used for rootzones

Parameter	Unit	The result of the analysis
pH	-	5.58
EC (conductivity)	μmhos/cm	581.0
Salt ratio	(%)	0.021
Water content	(%)	57.42
Moisture	(%)	21.84
Organic matter	(%)	4.81
Lime	(%)	0.627
Fine Sand ratio	(%)	52.04
Clay ratio	(%)	20.60
Silt ratio	(%)	27.36

In this study, 90% sand (d_{50}=0.5 mm) dominated rootzone was used. Therefore, 10% of the rootzone consisted of organic mixture that was procured by Tree and Landscape Inc. of İstanbul Metropolitan Municipality. The sample of the mixture was analyzed in the laboratories of Istanbul Tree and Landscape Inc. The analysis result regarding this organic mixture was given in Table 5.1 where was detailed with electrical conductivity, pH, salt ratio, water content, moisture, organic matter, lime, fine sand ratio, clay and silt ratio.

Before determining the ratio of the mixture for the rootzone used in this study, three different rootzone with different ratios of mixtures were investigated. The unsaturated and saturated hydraulic conductivities of the rootzones were first determined as demonstrated in Figure 5.11.

Figure 5.12 also showed the mini disc infiltrometer that was manufactured by Decagon Devices was used to determine unsaturated hydraulic conductivities for different water content for each rootzones. Therefore, while Figure 5.13 indicated the change of unsaturated hydraulic conductivities of the increasing value of water content, Table 5.2 showed the saturated hydraulic conductivities that were determine by permeameter as shown in Figure 5.14 for each rootzones.

Figure 5.11 Determining Unsaturated Hydraulic Conductivities for Different Rootzones

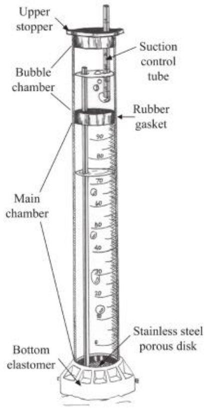

Figure 5.12 Mini Disc Infiltrometer

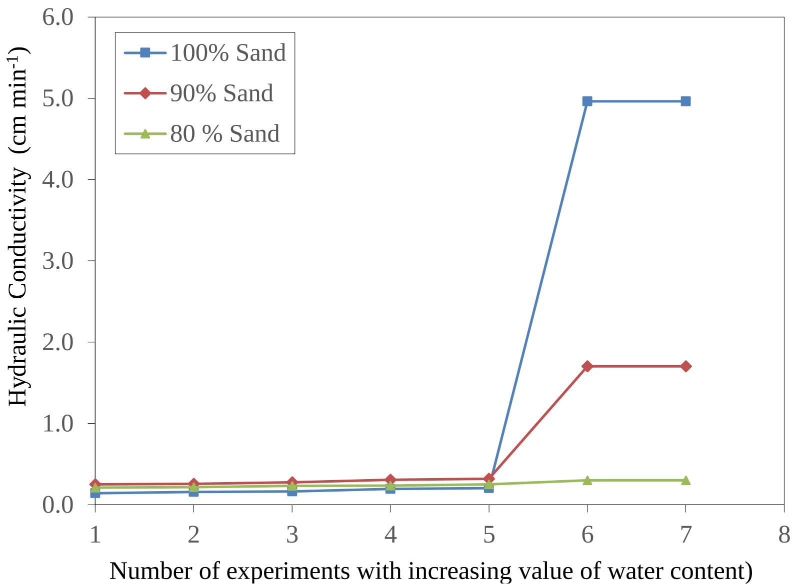

Figure 5.13 Change of the Hydraulic Conductivity for Different Water Contents in Different Rootzones

Table 5.2 Saturated hydraulic conductivities of different rootzones

Type of Rootzone	Saturated Hydraulic Conductivity K_s (cm min^{-1})
100% Sand + 0% Mixture	4.96
90% Sand +10% Mixture	1.74
80% Sand + 20% Mixture	0.32

Figure 5.14 The Photo of Great Scale Permeameter Used in This Study

Moreover, the turf grass for the sports field as demonstrated in Figure 5.15 is basically different from the grass used for landscape in terms of firm footing, adequate resiliency, and resistance to tearing. The details for this grass were given in previous Chapters. The sports field turf grass used in this study was specially grown by Istanbul Tree and Landscape Inc. in Edirne. Numerous experiments were conducted with this turf grass obtained from Istanbul Tree and Landscape.

Figure 5.15 Turf grass for sports field in this study

Table 5.3 summarized all hydraulic properties of materials used in the presented study. All results were compatible with the literature. Moreover, saturated hydraulic conductivity was measured by a permeameter that was appropriate for coarser material sizes. Saturated water content was arranged as porosity value in the HYDRUS-3D model for each material. Also, residual water content was highly difficult to determine for coarser materials and it took values very close to zero in the literature.

Table 5.3 Hydraulic properties of materials

Material	Rootzone (90% sand)	Turf grass	M1	M2	M3	M4	M5
Mean Diameter, D_{50} (mm)	0.48	-	0.50	1.00	1.90	3.60	6.00
Uniformity Coefficient, C_u	1.42	-	1.47	1.57	1.90	1.38	1.40
Coefficient of Gradation, C_c	1.03	-	1.05	1.13	1.54	1.19	0.96
Specific Gravity (g cm^{-3})	2.65	-	2.65	2.72	2.66	2.65	2.65
Bulk Density (g cm^{-3})	1.45	-	1.45	1.46	1.56	1.58	1.62
Porosity	0.425	-	0.418	0.410	0.400	0.394	0.391
Field Capacity, %	27.95	-	27.50	25.78	10.12	5.45	4.20
Saturated Hydraulic Conductivity, K_s (cm min^{-1})	1.74	0.125	4.96	15.6	29.4	56.3	64.2
θ_r (cm^3 cm^3)	0.025	-	0.023	0.020	0.006	0.006	0.006
θ_s (cm^3 cm^3)	0.42	-	0.410	0.40	0.40	0.39	0.39
α (cm^{-1})	0.086	-	0.086	0.145	0.151	0.158	0.165
n (-)	1.16	-	1.16	1.99	2.7	3.2	4.00
l (-)	0.5	-	0.5	0.5	0.5	0.5	0.5

5.3 Hydrological Analysis and Design Hyetographs

In the hydrological design, the time distribution of flowrates and precipitation were not generally considered, instead, peak values of flowrates or rainfall intensity are only used, for instance, rational method. Design methods have been developed with only time-dependent flow analysis that allows more predictable design hyetograph to obtain design hydrographs (Chow et al., 1988) in the last decades. In this study, a design hyetograph was determined by using the records of the meteorological station that is located nearby a sports field in Istanbul, Turkey. Essentially, design precipitation hyetographs were determined from Intensity-Duration-Frequency (IDF) relationships of that meteorological station (Sarıyer) as seen in Figure 5.16.

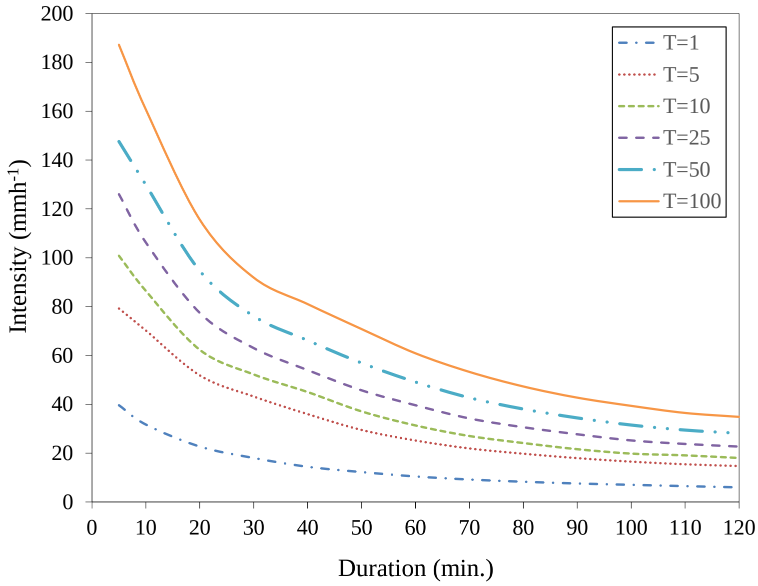

Figure 5.16 IDF curves for different return periods in Sarıyer Meteorological Station in Istanbul, Turkey

Chow et al. (1988) mentioned that there are basically two ways to obtain design hyetographs from IDF curves in the literature: Alternating block method (AB Method) and Instantaneous Intensity Method (II Method). Experimental hyetographs were developed by using the AB method in the present study due to it is simpler and easier to apply to compare to the II method. The design hyetograph produced by the AB method specifies the precipitation depth occurring in *n* time intervals of duration Δt over a total duration $T_d = n\Delta t$. After selecting the return period, the intensities were read from the IDF curve for each duration. Corresponding precipitation depths were found and the amount of precipitation was added for each additional time by taking differences between precipitation depths. Finally, Chow et al. (1998) stated that these blocks were reorganized into time sequence with the maximum intensity occurring at the center and the other blocks arranged in descending order alternately to the right and left of the central block to obtain a design hyetograph. The experimental design hyetograph was determined based on 100 year-return periods (*T*) rainfall intensities in this study. According to the selected time interval, rainfall intensities were determined from the IDF curve (Figure 5.16). The design hyetograph was obtained by considering the minimum and maximum rainfall intensity that is capable of producing by RS in this study. Actually, two groups of design hyetographs were determined, (1) single nozzle hyetographs that were created considering minimum rainfall intensity of 26 mmh^{-1}, (2) nozzle system (two nozzles) that were obtained with a wider range of rainfall intensities ($2mmh^{-1}$-$266.6mmh^{-1}$). The findings of experimental hyetographs were given in below.

5.3.1 Hyetographs for Single Nozzle

The hyetographs based on a single nozzle (GG-W nozzle) were used for the first part of the experiments. The reason for using a single nozzle is to prevent creating the intersection zones that highly affect the rainfall intensities due to the uniformity of rainfall over the control plot when the multiple nozzles were worked. Therefore, the single nozzle was started to use for the first group of experiments that were detailed in the Experimental Methodology section, and a nozzle system was tried to develop to create a wider range of rainfall intensities. Within this scope, the first original hyetographs were created using IDF curves as given in Figure 5.16 according to different return periods and time intervals. Second, a new type of hyetographs named with Experimental Applicable Equivalent Hyetograph (EAEH) was obtained because of becoming the rainfall intensities more capable for the appropriate nozzle. These hyetographs were given in detail from Figure 17 to Figure 20 for different return periods and time intervals. The reason for creating the EAEH was the lack of producing smaller rainfall intensities that are less than about 25-26 mmh^{-1}. Actually, in the literature there were no research studies involves smaller rainfall intensities, contrarily, numerous studies were focused on great rainfall intensities, especially erosion studies. Therefore, initial tests were also demonstrated that small rainfall intensities did not significantly affect the drainage of the sports field, they have only had effects on initial water content with reaching field capacity of soils used in the field. In brief, there was sufficient research that used rainfall intensities less than 25-26 mmh^{-1} and such kinds of rainfall intensities had relatively less important effects on the drainage. Due to these reasons, the EAEHs was created to apply for drainage experiments. For instance, Figure 5.17 showed the hyetographs for 10 minute time intervals and 100 year return period. For the simplest notation, the hyetograph obtained from the IDF curve directly is called original (Figure 17a) and the hyetograph obtained from the original one was named with the EAEH (Figure 17a'). Both hyetographs have the same maximum rainfall intensity of 160.7 mmh^{-1}. In the original hyetograph, the first 30-minute rainfall intensities with 6.1, 7.6, and 11.3 mmh^{-1} were converted to intensity of 37.5 mmh^{-1} for the first 20 minutes without altering total rainfall depth. In other words, the first three blocks in the original hyetograph were turned into the first 2 blocks in the EAEH. For the next step, the 4th block and 5th blocks in the original hyetograph with the intensities of 29.9 and 48.5 mmh^{-1} were changed as the rainfall intensity of 78.5 mmh^{-1} in the EAEH to protect the integrity of the AB method (with the increasing blocks to the maximum rainfall intensity). Similarly, the other parts of the original hyetograph were altered and finally, a new hyetograph was created with 60 minutes total duration. Furthermore, this EAEH was named with 10 minute time interval, 60 minutes total duration, and 100 year return period.

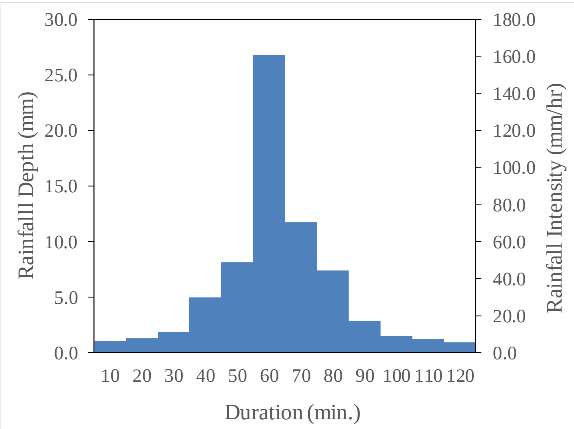

(a)

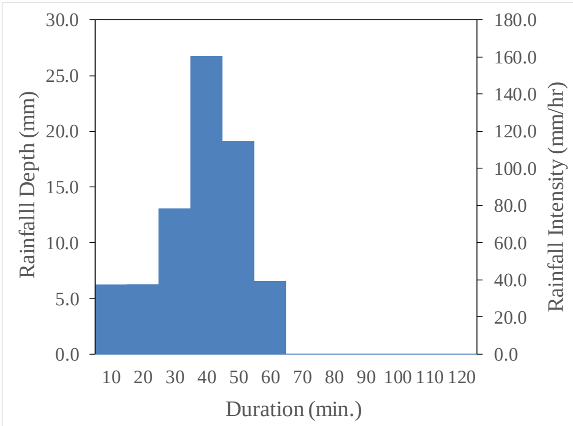

(a')

Figure 5.17 The Hyetographs with 10 Minute Time Interval for 100 Year Return Period; A) Original, A') EAEH (Set-9)

Following the same methodology, similar hyetographs were obtained for different time intervals and return periods. Figure 5.18 showed the original hyetographs and the EAEHs for the 20-minute time interval. While Figure 5.18a and 5.18a' showed the original hyetograph and the EAEH for 25 year return period, Figure 5.18b and 5.18b' demonstrated the hyetographs for the return period of 50 years, respectively. Similarly, the experimental hyetographs for 100 year return period were also given in Figure 5.18c and 5.18c', respectively.

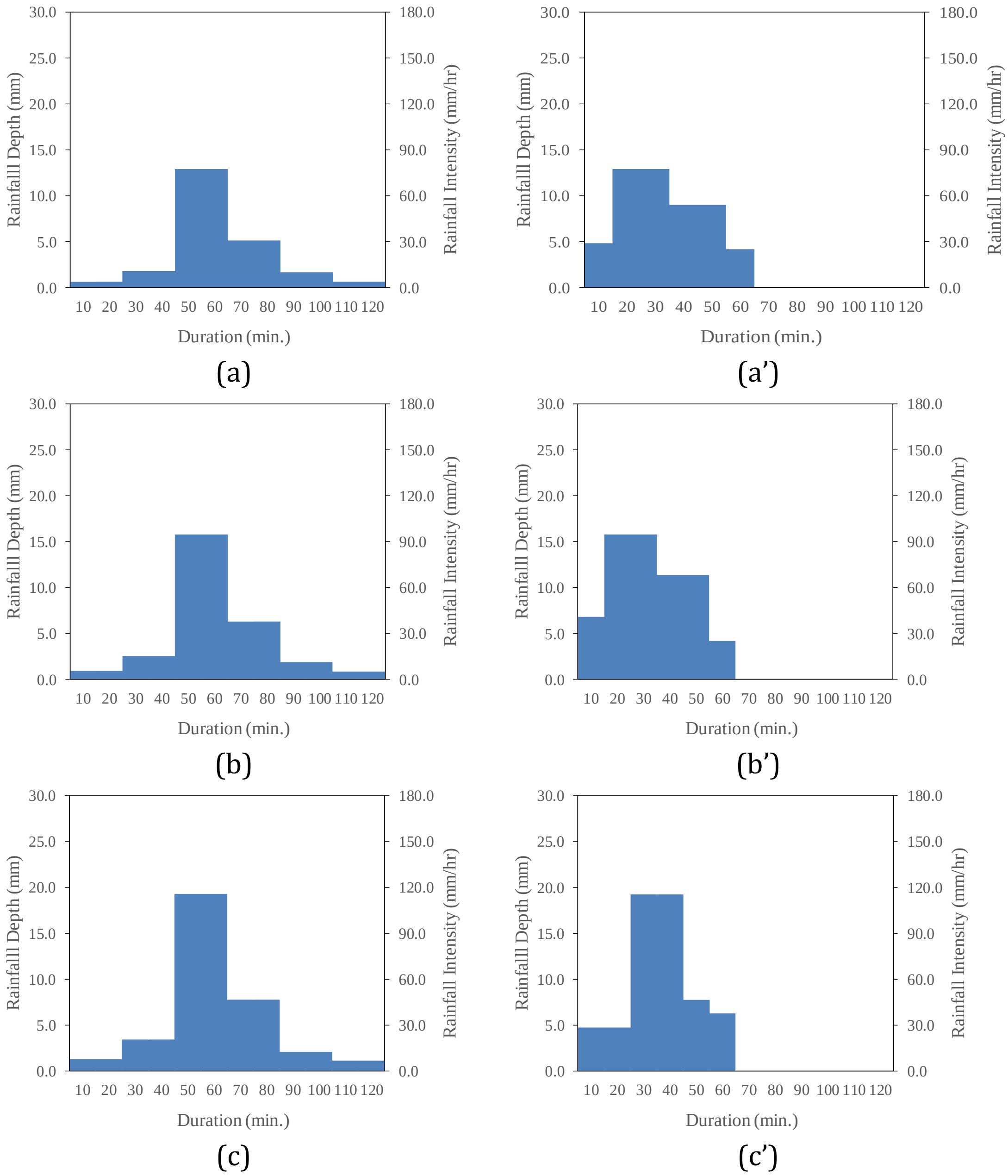

Figure 5.18 The Hyetographs with 20 Minute Time Interval for Different Return Periods; A) 25 Year Original, A’) 25-Year EAEH (Set-1) B) 50 Year Original, B’) 50-Year EAEH (Set-2) C) 100 Year Original, C’) 100-Year EAEH (Set-3)

Moreover, Figure 5.19 showed the original hyetographs and the EAEHs for the 30-minute time interval. While Figure 5.19a and 5.19a’ demonstrated the original hyetograph and the EAEH for 25 year return period, Figure 5.19b and 5.19b’ indicated the hyetographs for the return period of 50 years, respectively. Finally, the hyetographs for 100 year return period were also given in Figure 5.19c and 5.19c’, respectively.

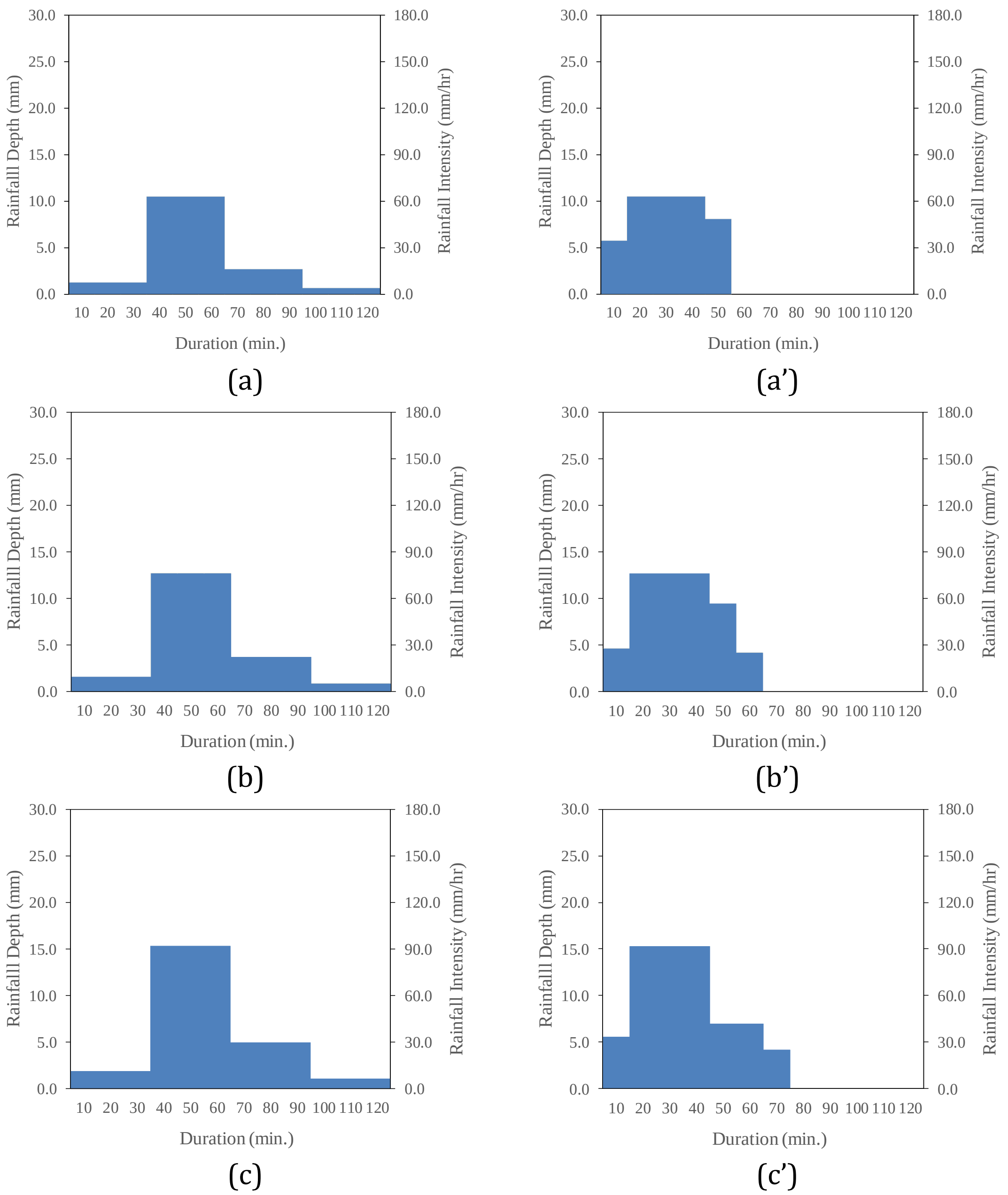

Figure 5.19 The Hyetographs with 30 Minute Time Interval for Different Return Periods; A) 25 Year Original, A’) 25-Year EAEH (Set 10), B) 50 Year Original, B’) 50-Year EAEH (Set-4) C) 100 Year Original, C’) 100-Year EAEH (Set-5)

Similarly, considering 40 minute time intervals, Figure 5.20a and 5.20a’ the original hyetograph and the EAEH for 25 year return period, Figure 5.20b and 5.20b’ indicated the hyetographs for the return period of 50 years, respectively. The hyetographs for 100 year return period were also given in Figure 5.20c and 5.20c’ for 40 minute time intervals, respectively.

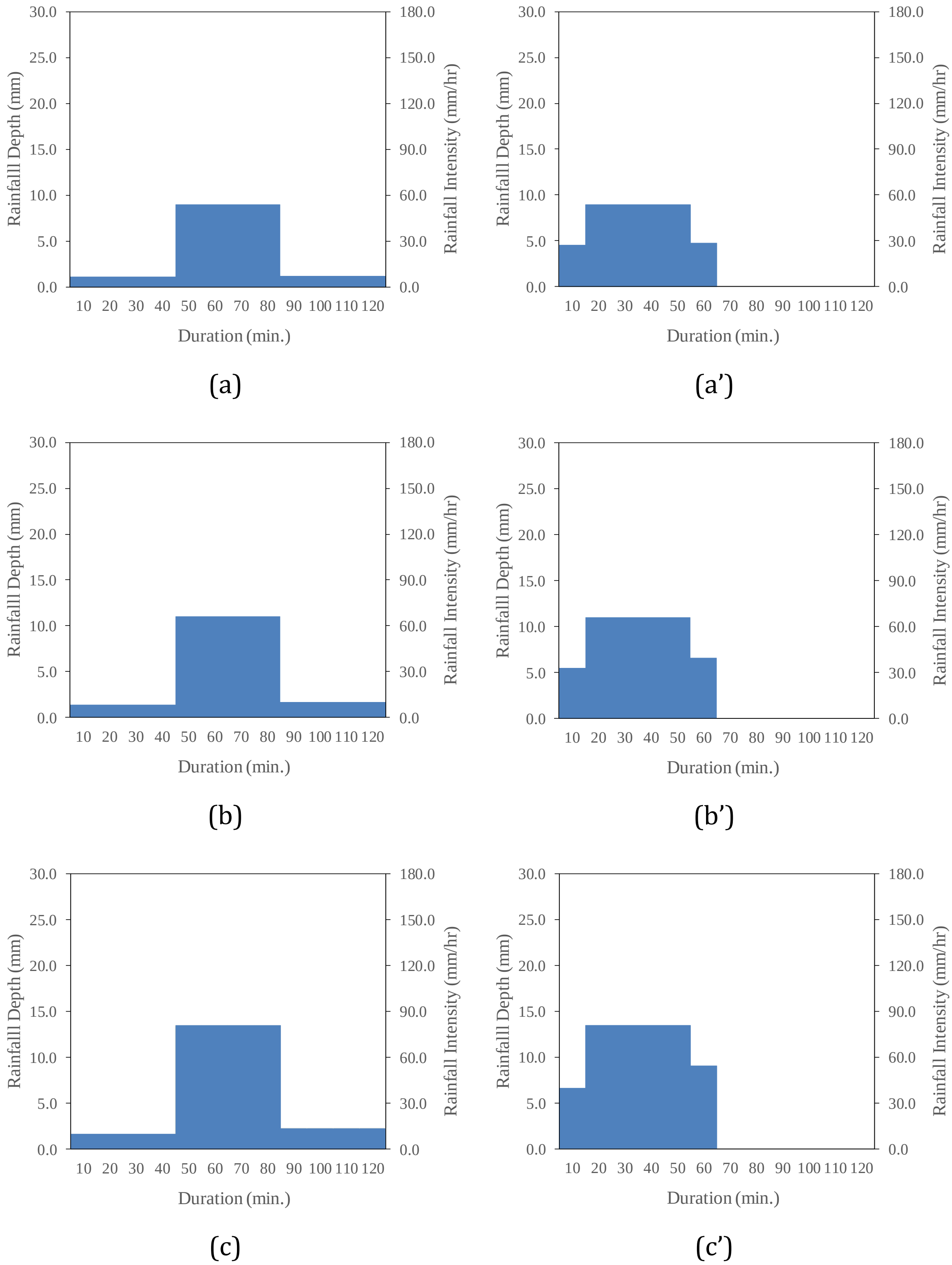

Figure 5.20 The Hyetographs with 40 Minute Time Interval for Different Return Periods; A) 25 Year Original, A') 25-Year EAEH (Set-6) B) 50 Year Original, B') 50-Year EAEH (Set-7) C) 100 Year Original, C') 100-Year EAEH (Set-8)

These hyetographs were exposed to different drainage layers used in the sports field with the notations given in Table 5.4. That was classified according to different return periods and time intervals. For instance, the EAEH with 25 year return period and 20 min. the time interval was named with the experimental hyetograph notation of Set-1.

Table 5.4 Experimental notation for experimental applicable equivalent hyetographs (EAEH) for different return periods and time intervals

Return Period (year)	Time Interval (min.)	Notation
25	20	Set-1
50	20	Set-2
100	20	Set-3
50	30	Set-4
100	30	Set-5
25	40	Set-6
50	40	Set-7
100	40	Set-8
100	10	Set-9
25	30	Set-10

5.3.2 Hyetographs for Nozzle System

For the second part of the drainage experiments, the experimental hyetographs for the nozzle system (two nozzles) were only developed based on 100 year-return periods (*T*) rainfall intensities for 10, 20, 30, and 40 minutes time intervals and 120 minutes of the total duration of storms. They were given in Figure 5.21 below, respectively. The reason for choosing only 100 year return period was that these hyetographs were more effective on the drainage layers. Applying these hyetographs was sufficient enough for the design of the sports field drainage systems.

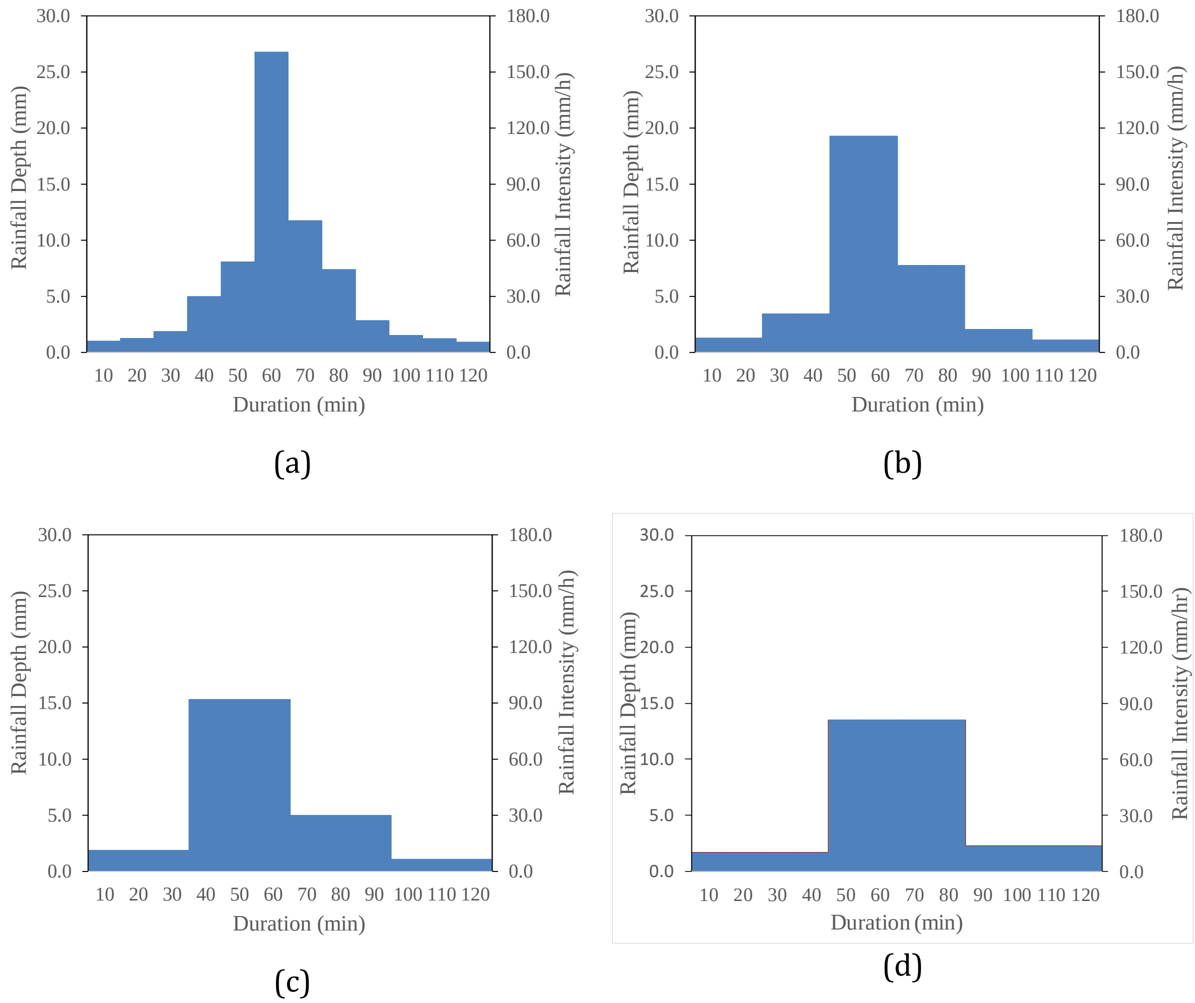

Figure 5.21 100-Year Hyetographs With Different Time Intervals; A) 10 Min., B) 20 Min., C) 30 Min, D) 40 Min.

Therefore, there were not any limitations regarding rainfall intensity that a wider range of intensities was simulated and the hyetographs were originally created. The nozzle system was produced the rainfall intensities with the range of 2 mmh^{-1} and 266.6 mmh^{-1} and the hyetographs were obtained considering this intensity gap. These hyetographs were applied to different drainage layers as two consecutive hyetographs for ensuring initial conditions at field capacity. The total duration of each experiment was determined as 240 minutes for the evaluation of drain outflows.

5.4 Measurement Devices for Soil-Water Interaction

In this study, some measurement devices were used to determine the soil moisture, temperature, metric (capillary) potential. 10-HS soil moisture sensor given in Figure 5.22 measures the dielectric constant of the soil in order to find its volumetric water content (VWC). Its applications include irrigation scheduling, vadose zone monitoring, and plant-soil-water interaction studies. The details of technical specifications for 10-HS was given in Table 5.5. Therefore, MPS-6 is a matrix water potential sensor that provides long-term, maintenance-free soil water potential and temperature readings at any depth without sensitivity to salts (Figure 5.23). The details of technical specifications for MPS-6 was also shown in Table 5.6. The EM50, the data logger is a 5-channel, self-contained data recorder designed for use with any sensor. The sensors are plugged into the 5 channels and measured as directed by the user. The schematic view of the EM-50 was illustrated in Figure 5.24.

Figure 5.22 10-HS Soil Moisture Sensor (Decagon Devices)

Table 5.5 Technical specifications for 10-HS, soil moisture sensor

	Measurement
Range:	Apparent dielectric permittivity (?$_a$) : 1 (air) to 50 Soil volumetric water content : 0 – 0.57 m^3/m^3 (0 -57% VWC)
Accuracy:	Apparent Dielectric Permittivity (?$_a$) : ± 0.5 from (?$_a$) of 2 to 10, ±2.5 from (?$_a$) of 10 to 50 (VWC) VWC: Using standard calibration equation: ± 0.05 m^3/m^3 (± 5% VWC) typical in mineral soils. Using soil site specific calibration, ± 0.02 m^3/m^3 (± 2% VWC)
Resolution:	(?$_a$): 0.1 from ?$_a$ of 1 to 30, 0.2 from (?$_a$) of 30 to 50 VWC: 0.0008 m^3/m^3 (0.08% VWC) in mineral soils from 0 to 0.50 m^3/m^3 (0-50% VWC)
Time	10 ms (milliseconds)
	Power
Power requirements:	3VDC @ 12mA to 15 VDC @ 15 mA On board voltage regulator allows 10HS sensor to be used with any excitation voltage above 3V
	Operating Conditions
Operating Temperature:	0 – 50°C
	Interface
Frequency:	70 MHz
Output:	300 (dry soil) – 1250 (saturated) mV, independent of excitation voltage
	Mechanical
Connector Types	3.5 mm "stereo" plug or stripped and tinned lead wires
Cable Length	5 m standard
Dimensions	Dimensions 14.5 x 3.3 x 0.7 cm

Figure 5.23 MPS-6 Soil-Water Potential Sensor (Decagon Devices)

Table 5.6 Technical specifications for MPS–6, soil-water potential sensor

Accuracy	Soil Water Potential: ±(10% + 2 kPa) from -9 to -100 kPa (see manual for additional accuracy specifications past -100 kPa) Soil Temperature: ± 1°C
Resolution	Soil Water Potential: 0.1 kPa Soil Temperature: 0.1°C
Range	Soil Water Potential: -9 to -100,000 kPa Soil Temperature: -40° to 60°C – Sensors can be used at higher temperatures under some conditions. Contact us for more details.
Measurement Speed	150 ms (milliseconds)
Equilibration time	10 min to 1 hr depending on soil water potential
Sensor Type	Frequency domain with calibrated ceramic discs, thermistor
Output	RS232 (TTL) with 3.6 volt levels or SDI-12 communication protocol
Operating Environment	-40° to 60°C – Sensors can be used at higher temperatures under some conditions. Contact us for more details. Water potential measurements will not be accurate below 0°C.
Power	3.6 – 15 VDC, 0.03 mA quiescent, 10 mA max during 150 ms measurement
Cable Length	5m, custom cable lengths available
Cable Connector Types	3.5 mm "stereo" plug or stripped and tinned lead wires (3)
Sensor Dimensions	9.6 cm (l) x 3.5 cm (w) x 1.5 cm (d)
Data Logger Compatibility (not exclusive)	Meter/Decagon Em50 Series (rev 2.13+), ProCheck (rev 1.53+), any SDI-12-capable data logger

Figure 5.24 EM-50 Data Logger (Decagon Devices)

5.5 Experimental Methodology

In the present study, a new methodology was developed that includes creating rainfall patterns with design hyetographs and investigating different drainage layers for both removing excessive rainfall from the field surface and storing sufficient water for the rootzone at the same time.

First, calibration experiments for the RS were conducted to simulate natural rainfall with a wider range of rainfall intensities in the laboratory. Second, different stratified layers that consisted of sand and gravel materials without rootzone were prepared to investigate flow mechanisms under different rainfalls by measuring hydrographs. They were named with coarse material (sand and gravel) experiments for the drainage of the sports field. The aim of this part was to determine the distinctive effects of material diameters, the length of sand and gravel layers for the drainage of the sports field. Therefore, these experiments were carried out to observe any internal piping and filtering conditions through these layers. After these steps, considering the results for the experiments of coarse materials and examples of football fields as suggested in the FIFA quality concept for football turf (FIFA (2004) and FIFA (2012), different drainage layers of sports fields were created.

For preparing drainage layers, five different materials (M1, M2, M3, M4, and M5) with changing mean diameters between 0.5 and 6 mm were used and the DT was packed with considering the different thickness and mean diameter of each layer. Based on literature and traditional experience, the thickness of the rootzone can be selected between 15 cm and 30 cm, according to USGA (United States Golf Association) green section specifications (USGA Green Section Staff, 1993). In the literature, blinding or sandwich layer thickness also takes values between 5 and 10 cm, for instance, Adams (1986) recommended a 5 cm blinding layer in his research. The gravel layer is the most uncertain part. In addition, according to traditional experience, 15 cm gravel can be prepared for the drainage experiments by means of evaluating the results of the coarse material experiments. Within the scope of this study that was supported by the Turkish Scientific and Technological Research Council (TUBITAK), different combinations of drainage layers were determined as 4 cm turf grass, which was specially grown for football fields, 15 cm rootzone, 15 cm blinding layer, and 15 cm gravel layer over the drainage pipes as seen in Figure 5.25 schematically (Dogan et al., 2018). Although the preparing drainage layers are definitely laborious on the 1.5m x 1.3m DT, these layers were exposed to different design hyetographs. Therefore, the selected rootzone consisted of 90% sand and 10% silt, clay, and organic matter mixture. Numerous experiments were conducted and analyzed by considering the relationship between hyetographs and drain outflow hydrographs. These hydrographs were obtained by measuring drain outflows at 5-minute intervals. Experiments were conducted with the RS and DT in the Hydraulic laboratory of Yıldız Technical University.

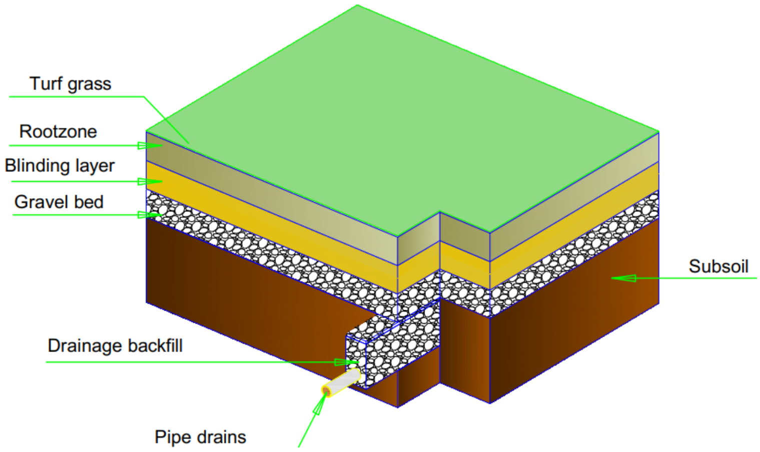

Figure 5.25 The Schematic View of the Three-Layer Drainage Construction (Sport England, 2011)

Design hyetographs were prepared for different return periods and time intervals using AB Method suggested by Chow et al. (1988). These hyetographs were applied to drainage layers as a single nozzle and nozzle system. According to materials, some drainage layers were created with rootzone, blinding layer, and gravel layer similar to the practices for sports field drainage. These drainage layers included some layers that were created for representing the drainage conditions for Galatasaray and Beşiktaş stadiums which are significantly two of the most modern and used football fields in Istanbul, Turkey. After these drainage experiments, the results were analyzed by considering hyetograph and hydrograph parameters such as maximum discharge, concentration-time, and lag time. According to the results, one of them was determined as an optimum drainage layer. That was considered one of the most optimum layers with a 15 cm rootzone (90% 0.5 mm sand and 10% silt, clay, and organic matter mixture), 15 cm blinding layer with a mean diameter of 1 mm, 15 cm gravel layer with a mean diameter of 6 mm was determined. For the next step, this layer was exposed to numerous drainage experiments. In this final experiment, the thickness of the gravel layer was not altered while different thicknesses of the rootzone and blinding layer were tested. All drainage layers were exposed to two identical hyetographs consecutively due to ensuring similar experimental conditions. The experimental results showed that turfgrass was damaged after a few experiments due to the lack of healthy root growing conditions of sports turf in the laboratory even artificial sunlight was used. Therefore, turfgrass was not used because it blocked the infiltration and drainage process. MPS-6 and 10-HS sensors were used to determine the suction pressure and soil water content through the drainage profile, respectively.

Three sets of experiments were carried out using a newly developed experimental setup. In the first set, 12 experiments were conducted with the same total thickness of the drainage layer (L =45 cm). Therefore, three experiments were also made with L=40 cm, and three experiments were conducted with L=35 cm. The thickness of the gravel bed (15 cm) was not changed in the experiments. For the experimental notation, E25 L=45 cm showed that the thickness of the rootzone and blinding layers were 25 cm and 5 cm through the 45 cm drainage layer, respectively. Therefore, all experiments were also conducted considering a change of water content with respect to depth and time.

6
RESULTS AND DISCUSSION

6.1 Performance of the Experimental Setup

6.1.1 Rainfall Simulator

6.1.1.1 Rainfall Intensity

Rainfall intensities were obtained from two different nozzles in the present study. Kesgin et al. (2018) produced rainfall intensities between 26 mmh^{-1} and 266.6 mmh^{-1} using a single GG-W nozzle. In addition, the LNN nozzle was used to create smaller rainfall intensities. Figure 6.1 shows the relationship between discharge and rainfall intensity for each nozzle. Table 1 summarizes the details of boundary conditions for discharge and rainfall intensity relations. By employing two different nozzle systems, a wide range of rainfall intensities and their relationships between discharges were determined. Eq. (6.1) was obtained for the range of discharges of $0.29 \leq Q \leq 1.81\ (L\min^{-1})$ and the range of rainfall intensities of $2.0 \leq R \leq 25.7\ (mmh^{-1})$ for the LNN nozzle. Similarly, for the GG-W nozzle, Eq. (6.2) was obtained as a power function within the discharge range of $1.98 \leq Q \leq 13.48\ (L\min^{-1})$ and the range of rainfall intensities of $26.0 \leq R \leq 266.6\ (mmh^{-1})$ as given by Kesgin et al. (2018), as follows.

$$R = 13.93Q \tag{6.1}$$

$$R = 19.554e^{0.1975Q} \tag{6.2}$$

where Q is discharge in liters per minute $(L\min^{-1})$, and R is rainfall intensity in mmh^{-1}

Observing trends for Eqs. (6.1) and (6.2) were fitted in good agreement with determination coefficients of 0.9853 and 0.9953, respectively. As mentioned by Kesgin et al. (2018), pressures were measured at the inlet and outlet of the orifice meter and named “system pressure” and “orifice pressure,” respectively. In addition, nozzle pressure was also measured with a simple manometer at the inlet of the nozzle system. The measurement of pressure values for different rainfall intensities is shown in Figure 6.2 for each nozzle. The increasing values of pressure for the LNN nozzle remarkably changed when compared with the pressures for the GG-W nozzle. Moreover, as expected, pressure values diminished from the inlet of the orifice meter to the inlet of the nozzle system. Maximum rainfall was measured at the LNN nozzle as 25.7 mmh^{-1} when the system, orifice, and nozzle pressures became 41.46, 40.87, and 39.5 bar, respectively. Likewise, 266.6 mmh^{-1} of maximum rainfall was obtained when the pressures were measured as 38.22, 25.31, and 15.2 bar for the GG-W nozzle, respectively

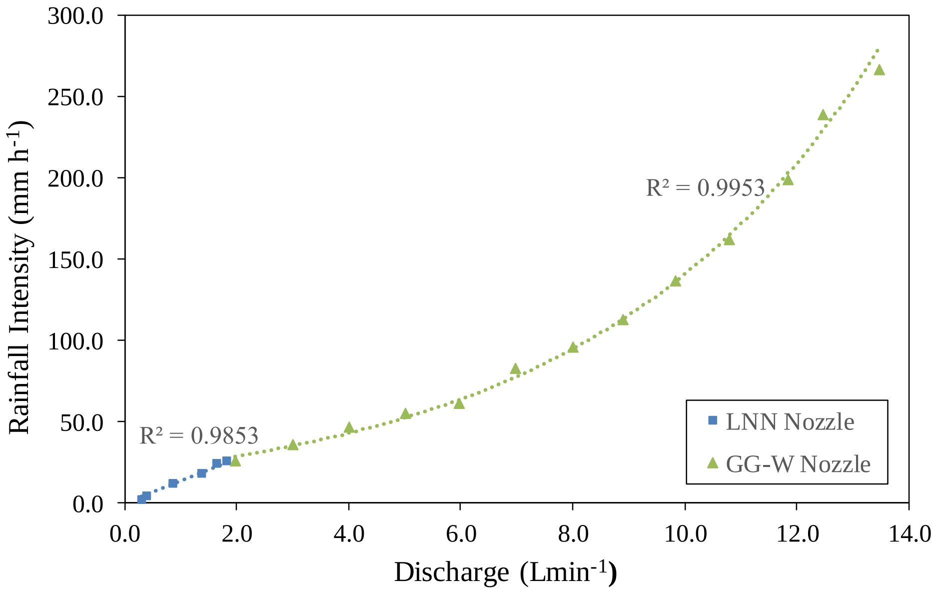

Figure 6.1 The Discharge-Rainfall Intensity Relationship for Two Different Nozzles

Table 6.1 The Rainfall-discharge equations for different nozzles

Nozzle	Minimum Discharge, $L\min^{-1}$	Maximum Discharge, $L\min^{-1}$	Rainfall-Discharge Relation	R^2
LNN	0.29	1.81	R=13.931Q	0.98
GG-W	1.98	13.48	$R=19.554e^{0.1975Q}$	0.99

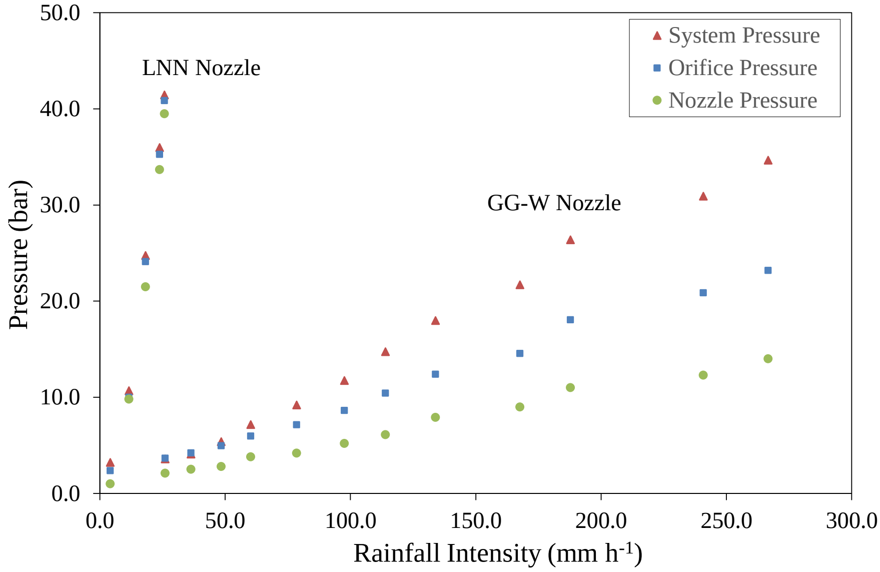

Figure 6.2 Measured Pressures Corresponding to Rainfall Intensities

Linearized plots of Eqs. (6.1) and (6.2) for the prediction of rainfall intensities (R) versus measured values R are in good agreement with the determination coefficients of 0.982 and 0.9956, respectively (Figure 6.3).

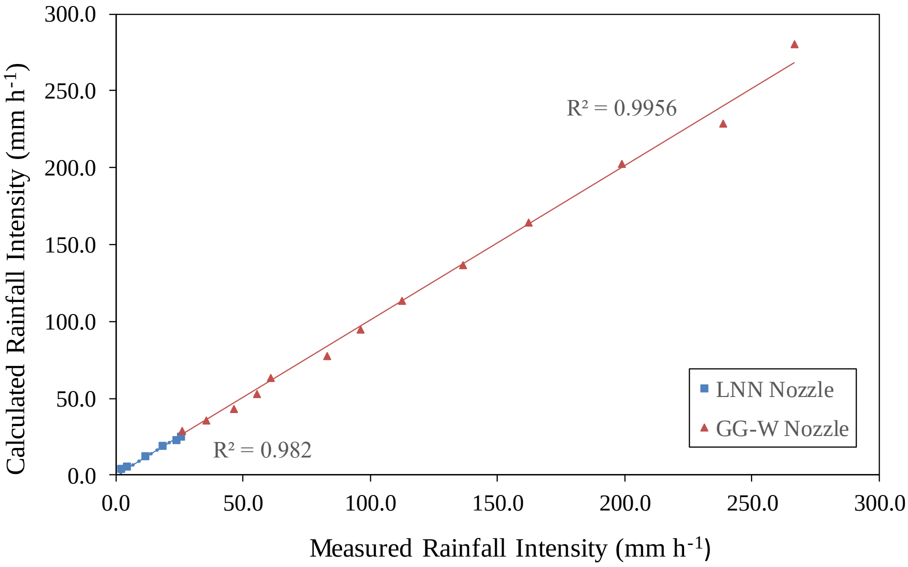

Figure 6.3 Comparison Between Measured and Calculated Rainfall Intensities

6.1.1.2 Raindrop Diameter

In this study, raindrop size was determined using the flour pellet method. The experimental details of this method can be found in Kesgin et al. (2018). The distribution of the pellet diameters produced by the LNN nozzle is shown in Figure 6.4 for four different rainfall intensities of 5, 11.9, 17.8, and 25.7 mmh^{-1}. The pellet diameters were similar to the results of Kesgin et al. (2018), and they took very close values when this nozzle was used. Likewise, Figure 6.5 shows the distributions of pellet diameters created by the GG-W nozzle for different rainfall intensities. Following the same experimental methodology as Kesgin et al. (2018), raindrop diameters were determined, and the distributions are plotted in Figure 6.6. The intervals of the raindrop diameters suggested by van Dijk et al. (2002) are also shown in Figure 6.6 together with the results of the present study. They showed that raindrop diameters were determined within the range of van Dijk et al. (2002). The raindrop size distribution was sufficient for producing simulated rainfall. The presented results were closer to the lower boundary than to the upper boundary. The maximum raindrop diameter produced by the LNN nozzle (smaller rainfall intensities) was greater than the minimum raindrop diameter created by the GG-W nozzle (larger rainfall intensities). Although the rainfall intensities of the GG-W nozzle were always larger than the LNN's, the difference between raindrop diameters could be explained with the presence of the mesh that was located 1 m beneath the nozzle system. Because of higher pressures in larger rainfall intensities of the LNN nozzle, the larger diameter of simulated raindrops (smaller drops grew after they hit the mesh) were created, as mentioned in Carvalho et al. (2014).

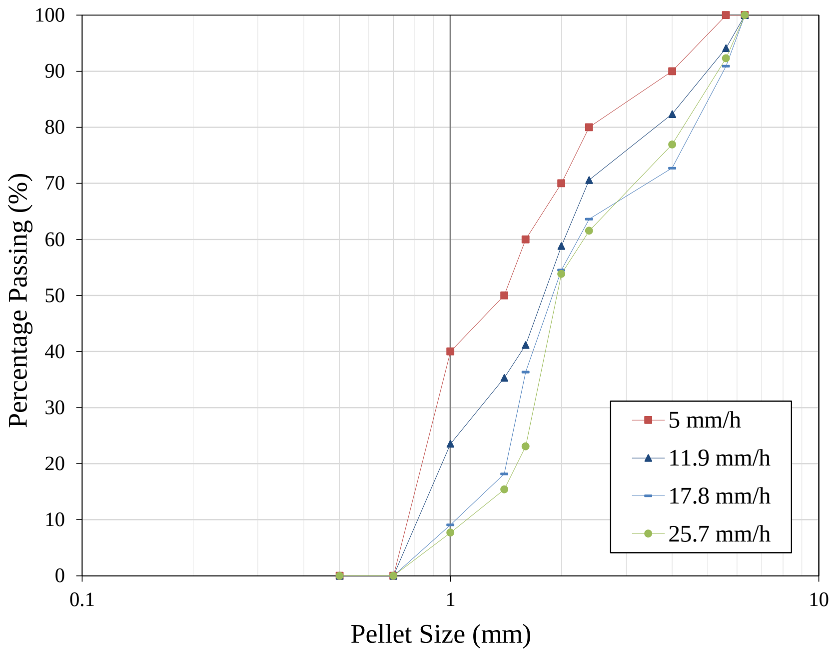

Figure 6.4 Pellet Size Distribution for Different Rainfall Intensities Produced by LNN Nozzle

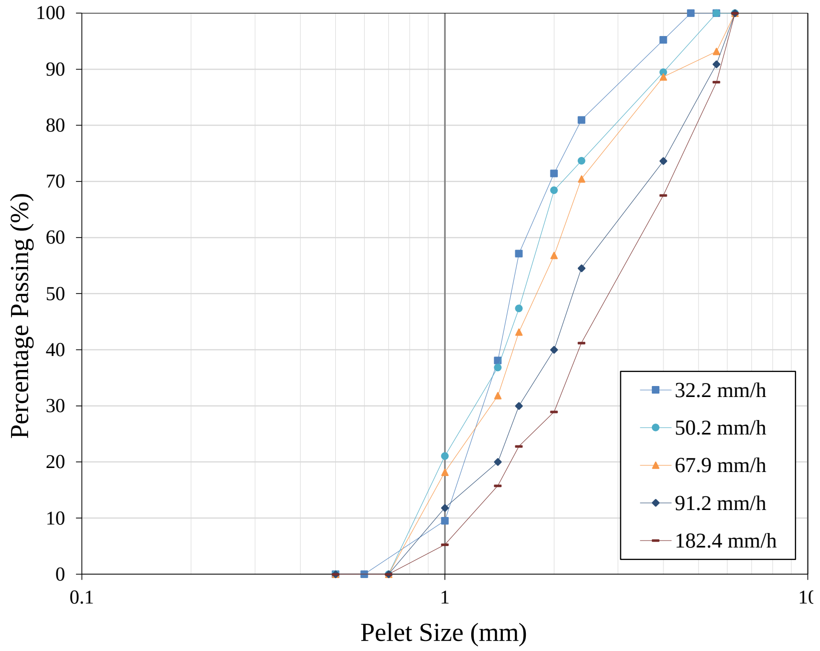

Figure 6.5 Pellet Size Distribution for Different Rainfall Intensities Produced by GG-W Nozzle

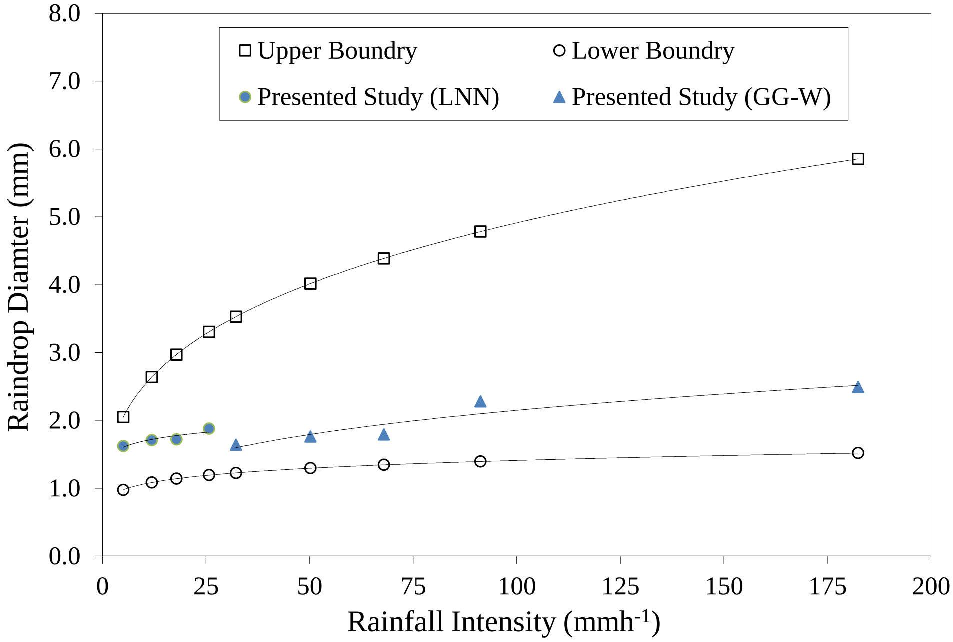

Figure 6.6 Comparisons of Raindrop Diameters for Different Nozzles

6.1.1.3 Uniformity of the simulated rainfall

The coefficient of uniformity ($CU,\%$) defined by Christiansen (1942) was calculated using Eq. (2) over the 1.5- × 1.3-m surface area of the DT. According to the results for the LNN nozzle, the coefficients of uniformity took values between 80% and 85% in the range of 10 and 25.7 mmh^{-1}, although they were determined to be between 70% and 80% for rainfall intensities less than 10 mmh^{-1} (Figure 6.7). However, for the greater rainfall intensities produced by the GG-W nozzle, they were always greater than 80% and reached a maximum uniformity of 90.76% for the rainfall intensities between 45 and 90 mmh^{-1}. Therefore, the maximum rainfall intensities for both nozzles, CU was determined to be approximately 82%.

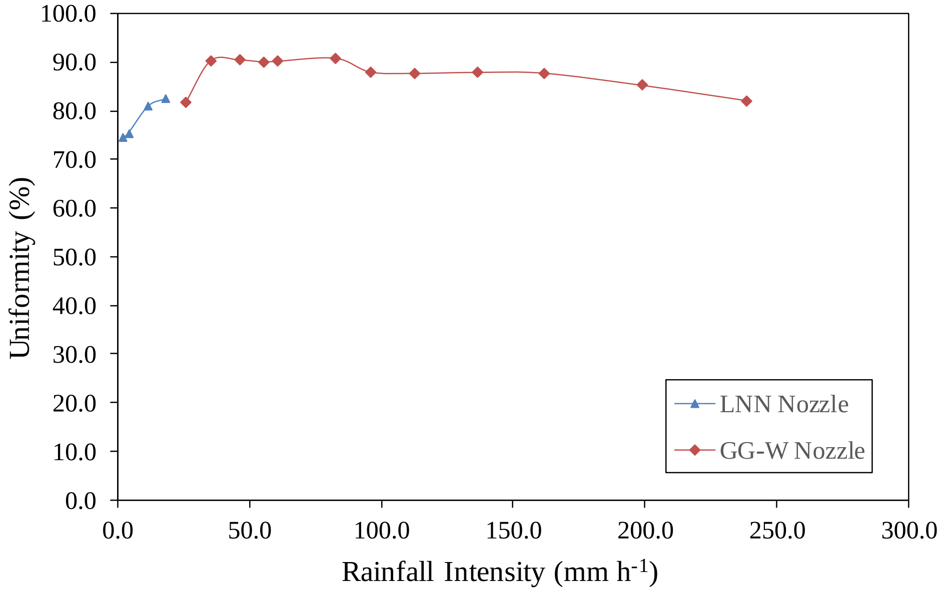

Figure 6.7 Comparison of the Average Spatial Uniformities for Different Rainfall Intensities

Moazed et al. (2010) stated that when CU is greater than 80%, the rainfall can be accepted as a uniform rainfall. Similarly, Luk et al. (1993) expressed that, for larger plots, rainfall can be accepted as uniform if CU is greater than 70%. Except for the smaller rainfall intensities of less than 10 mmh^{-1} produced by the LNN nozzle, the coefficient of uniformity was sufficient for the simulation of the natural rainfall, and the results were compatible with those in the literature. However, the coefficients of uniformity for smaller rainfall intensities were also acceptable, as suggested by Luk et al. (1993).

Raindrop velocities and kinetic energies of simulated rainfall were examined in a similar way as in the work of Kesgin et al. (2018). The range of the rainfall intensity became wider, while the minimum rainfall intensity was 26 mmh^{-1} in the previous RS. The LNN nozzle produced rainfall in the range of 2 to 25.7 mmh^{-1}, although the spatial uniformity of simulated rainfall for this nozzle had values between 70% and 80% within the rainfall intensities between 2 and 10 mmh^{-1}.

6.1.2 Soil-Water Retention Curves of Materials

SWRC was also obtained from calibration tests for each material separately. These data were optimized using HYDRUS-3D and Figure 6.8 shows the comparisons of measured and optimized values. The comparisons of results for the gravel bed and the blinding layer were more compatible. On the other hand, the SWRC of the rootzone was not sufficiently fitted although many calibration experiments were conducted. Therefore, the best-fit and closest relation was used as given in Figure 6.8.

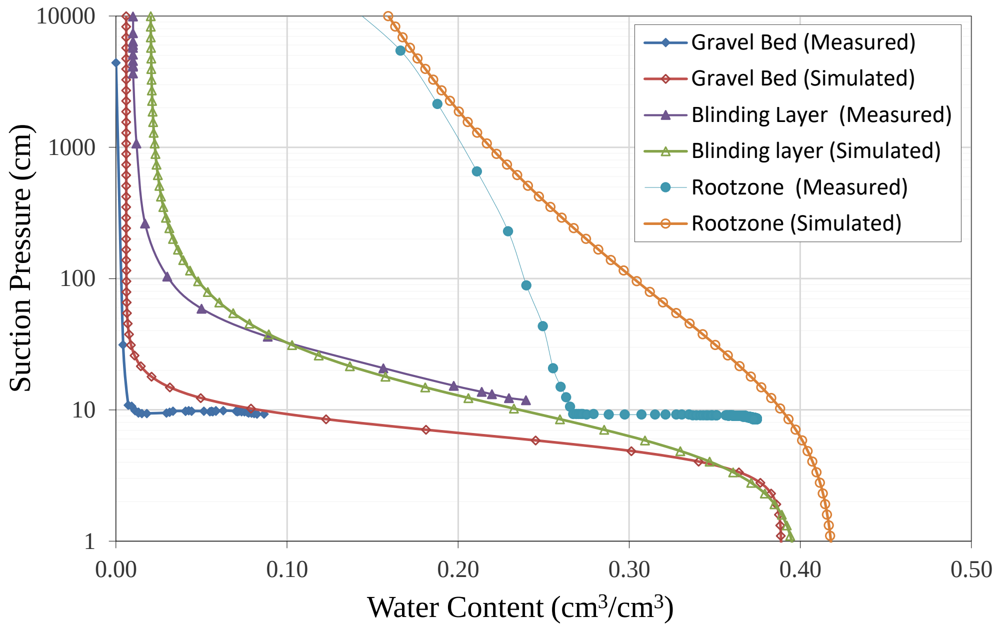

Figure 6.8 Comparisons of SWRCs for Drainage Layers

6.2 Drain Outflow Hydrographs

In this study, 18 drainage experiments were conducted as three different sets by changing the thicknesses of the drainage layers (Table 6.2). The first set of experiments was performed on a 45-cm-thick total drainage layer (L = 45 cm), and the others were performed on 40- and 35-cm-thick drainage layers. All sets were exposed to three different rainfall hyetographs with time intervals of 10 (R10), 20 (R20), and 30 (R30) min. The experimental results were classified according to different hyetographs and drainage layers. Figure 6.9, Figure 6.10, and Figure 6.11 show the drain outflow observations of L = 45 cm for R10, R20, and R30, respectively. Similarly, Figure 6.12, Figure 6.13, and Figure 6.14demonstrate drain outflow hydrographs for the experiments of L = 40 cm and L = 35 cm for R10, R20, and R30, respectively.

When all of the hydrographs were analyzed, the type of rainfall hyetograph was more dominant on the drain outflow hydrograph than the type of drainage layer. Therefore, the shape of the drain outflow hydrograph did not prominently alter according to the type of drainage layer. As expected, the shape of the hydrographs for R10 was sharper because of a shorter time interval of 10 min (Figure 6.9).

Figs. 6.9a and 6.9c show the hydrographs for E15 and E25 for L = 45 cm, which were different from the other group of hydrographs resulting from R10 rainfall. That was because of the initial conditions of water content through different layers. When the consecutive hyetographs were applied to drainage layers, the first peak discharge (FPD) was much smaller than the second peak discharge (SPD) because of the dry initial condition of the drainage layer, as seen in Fig. 6.9a. This result was also supported by the simulation result. It also demonstrated the behavior of the drainage layer for both the dry condition and the condition at its field capacity. Although the initial condition for the experiment of E25 L = 45 cm given in Fig. 16c was not dry but was very close to the field capacity condition, the difference between the first and second discharges was distinctive, and FPD was smaller than SPD. Considering the drain outflow hydrographs for E20 and E30 for L = 45 cm that are shown in Figs. 6.9b and 6.9d, the shape of the hydrographs was very compatible with simulation results, and FPD was sufficiently close to SPD.

To evaluate the effect of the blinding layer, maximum discharges (FPD and SPD) were observed in the experiment of E30 L = 45 cm (without blinding layer) for all rainfall hyetographs. When the thickness of the blinding layer increased for the L = 45-cm experiments, FPD and SPD generally decreased or took almost the same discharges. This was also confirmed with the simulation results. When the peak rainfall intensity for the different hyetographs diminished from R10 to R30, the differences between maximum discharges for different drainage layers were getting closer, and the shape of the drain outflow hydrographs became almost similar. These results are given in detail in Table 6.3. Similarly, as anticipated, FPD and SPD decreased from R10 to R30 when compared to the same drainage layer. Moreover, because of the 20- and 30-min time intervals, there were almost constant values (as a horizontal line) for the drain outflow hydrographs for both experiment and simulation after peak discharges came. After 500 min, the observed and simulated discharges became less than 0.1 $L\,\mathrm{min}^{-1}$ for all experiments.

Table 6.2 Experimental notation details of the different drainage layers

The Thickness of Drainage Layers			Experimental Notation
Rootzone (cm)	Blinding Layer (cm)	Gravel Bed (cm)	
30	0	15	E30 L=45 cm
25	5	15	E25 L=45 cm
20	10	15	E20 L=45 cm
15	15	15	E15 L=45 cm
15	10	15	E15 L=40 cm
15	5	15	E15 L=35 cm

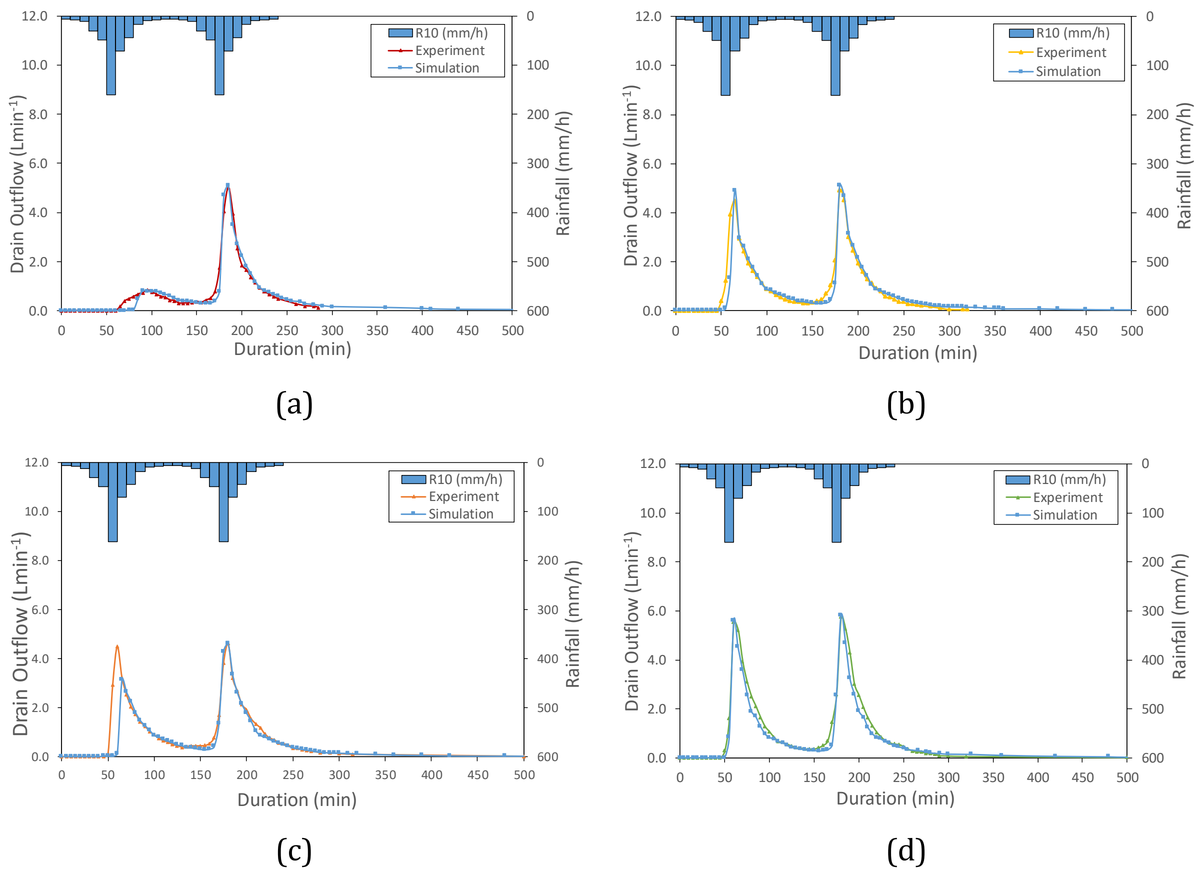

Figure 6.9 Comparisons of Drain Outflows for Different Drainage Layers under R10 Rainfall: A) E15 for L=45 Cm, B) E20 for L=45 Cm, C) E25 for L=45 Cm, D) E30 for L=45 Cm

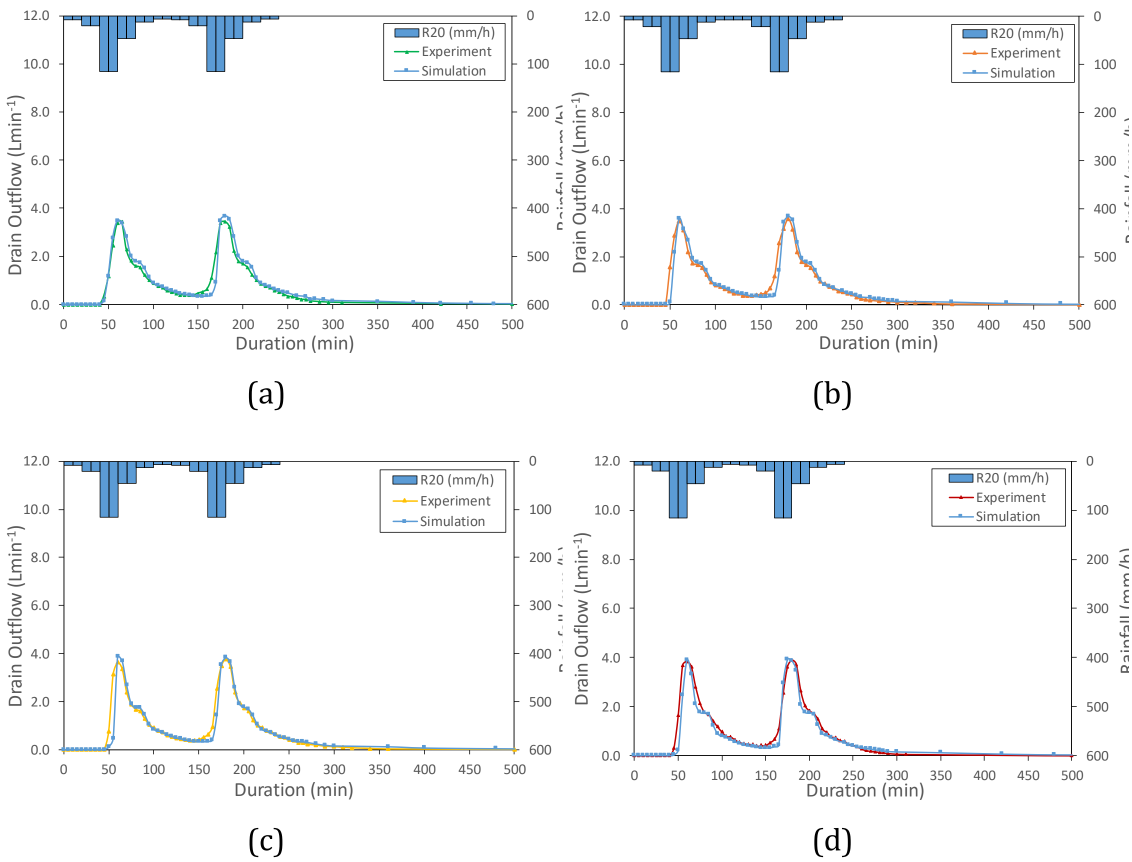

Figure 6.10 Comparisons of Drain Outflows for Different Drainage Layers under R20 Rainfall: a) E15 for L=45 cm, b) E20 for L=45 cm, c) E25 for L=45 cm, d) E30 for L=45 cm

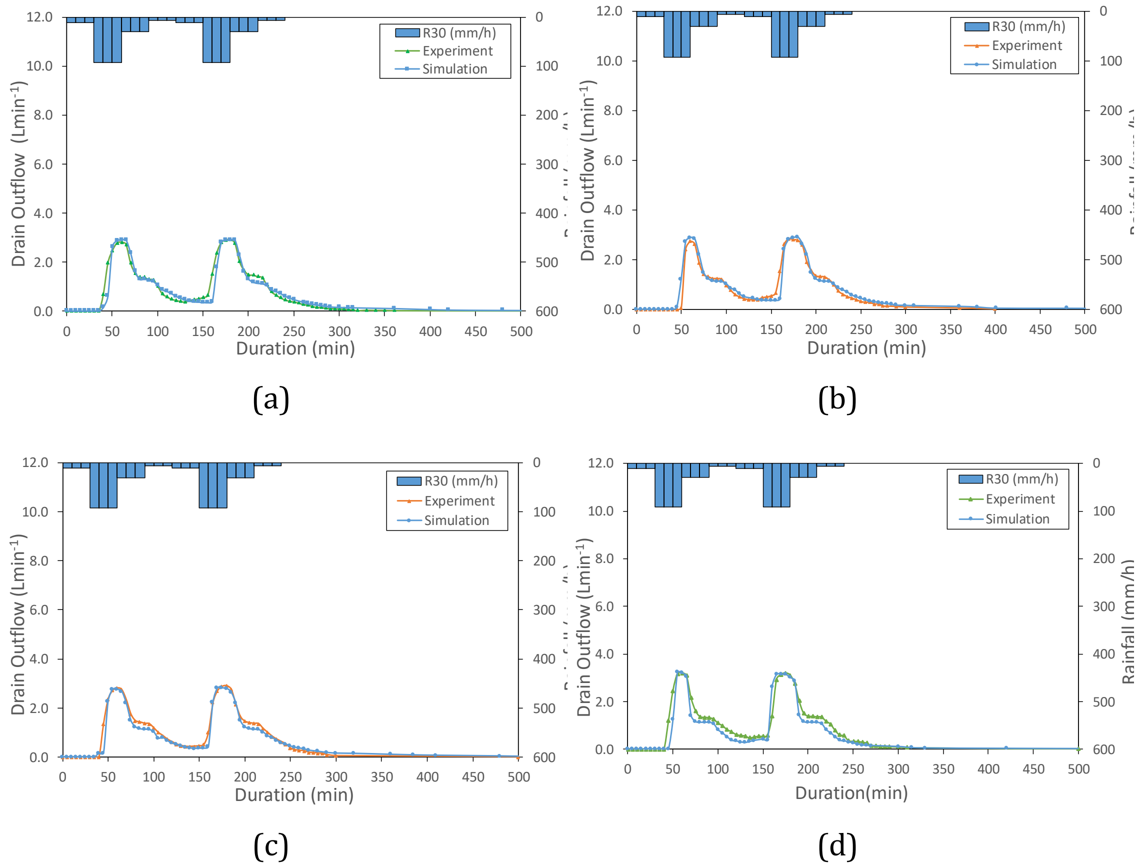

Figure 6.11 Comparisons of Drain Outflows for Different Drainage Layers under R30 Rainfall: a) E15 for L=45 cm, b) E20 for L=45 cm, c) E25 for L=45 cm, d) E30 for L=45 cm

When the thickness of the drainage layers was changed from L = 45 cm to L = 40 and L = 35 cm, compatible results were obtained from experiments and simulations. However, there were not predictable and reasonable results in terms of maximum discharges (FPD and SPD). Although maximum discharges for E15 L = 40 cm were greater than for E15 L = 35 cm for R10, there were no similar relationships for R20 and R30. The results obtained from R20 for E15 L = 35 cm had a bigger peak discharge, and it took almost the same values for R30 when the two drainage layers were compared. When the experiment of E15 L = 45 was compared with the experiments for L = 40 and L=35 cm under R20 and R30 rainfalls, the results for R20 showed that the compatibility for observations and simulations was acceptable and the shape of the hydrographs was sufficiently fitted. However, peak discharges for L = 45 and L = 35 cm became closer, while the others were apparently smaller.

Considering the R30 results, all the discharges were almost similar with good fitting. However, the compatibility of E15 L = 35 cm for both experiment and simulation was weaker when compared with the results of the experiments for L = 45 and L = 40 cm.

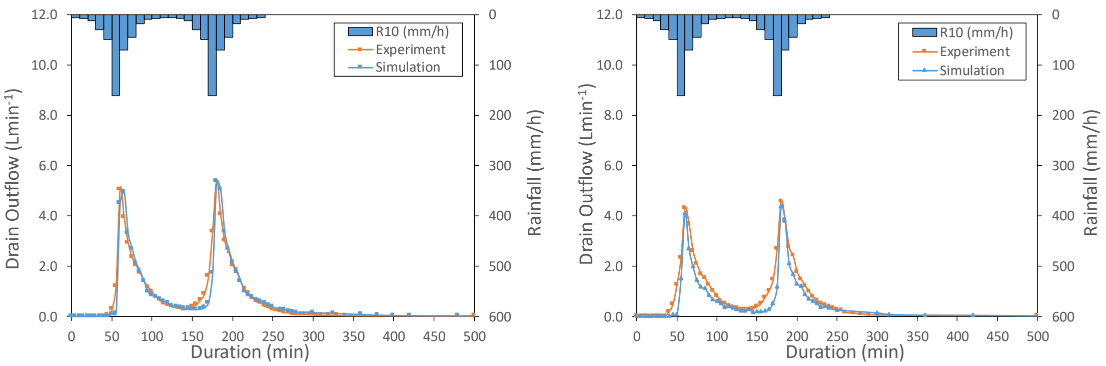

(a) (b)

Figure 6.12 Comparisons of Drain Outflows for Different Layer thickness under R10: a) E15 for L=40 cm b) E15 for L=35 cm

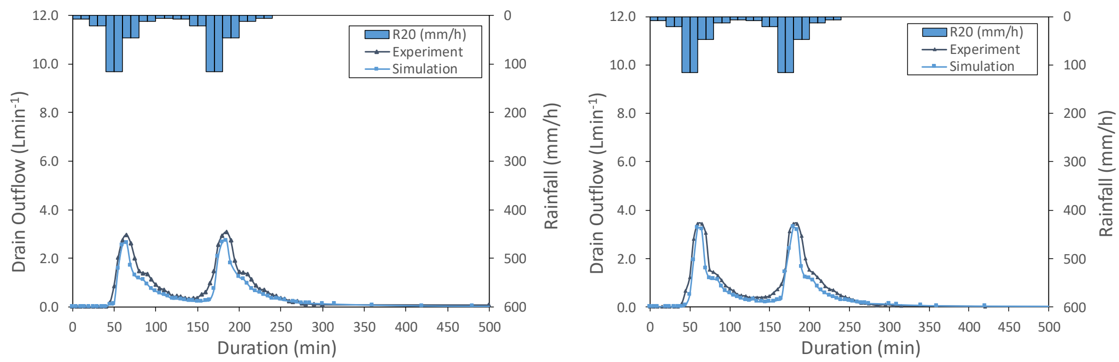

(a) (b)

Figure 6.13 Comparisons of Drain Outflows for Different Layer Thickness under R20: a) E15 for L=40 cm b) E15 for L=35 cm

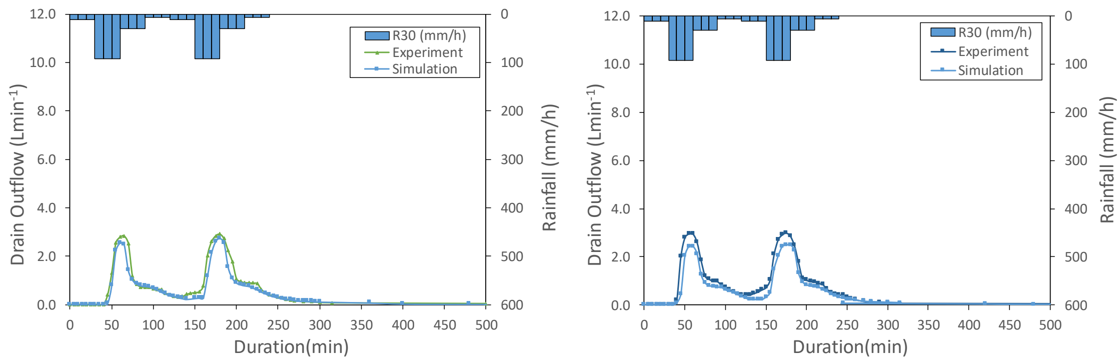

(a) (b)

Figure 6.14 Comparisons of Drain Outflows for Different Layer Thickness under R30: a) E15 for L=40 cm b) E15 for L=35 cm

Table 6.3 was obtained from the drain outflow hydrographs. The table summarizes the results of FPD, SPD, time of concentration (TOC), and lag time (LT) for each consecutive hyetograph. When the values of TOC were analyzed, simulation results were greater than experimental results, although the experimental and simulated results were slightly different from each other for R10. The results for R20 and R30 were almost similar, while a few simulation values of TOC were bigger. It is clear that the experimental results of drain outflow started to come earlier when compared with simulations. The values of TOC also demonstrated that there was no significant change for different drainage layers, especially for L = 45 cm. After the thickness of the drainage layer was altered, TOC slightly decreased, particularly for L = 35 cm.

Considering the lag times (LT1 and LT2) of two consecutive hyetographs, the results were compatible with experiments and simulations for each drainage layer. LT1 and LT2 were almost the same in most of the experiments. LT1 and LT2 generally had values of 5, 10, and 15 min for R10, R20, and R30, respectively. LT1 was also identical to or greater than LT2 for all the rainfalls and drainage layers. While considering the lag times results for the R30 rainfall, the lag times for E15 L = 35 cm were smaller and the lag times of E15 L = 40 cm were bigger for the results of the R20 rainfall.

The results obtained from the lag time showed that there were no differences in terms of drainage layers, and there was also no significant effect of the blinding layer on the hydrograph parameters for 45-cm-thick drainage layers in the case of reaching or exceeding the field capacity. In addition, small differences between experiments and simulations originated from discrepancies between observed and simulated water content results. Therefore, the reason for applying two consecutive hyetographs was to make it possible to reach or exceed the field capacity condition. This was successfully applied to different drainage layers and always found to be *LT2* < *LT1*.

Table 6.3 Hydrograph parameters for different drainage layers under R10, R20, and R30 rainfalls

Type of Rainfall	Results	Hydrograph Parameters	Type of Drainage Layer					
			E30 L=45 cm	E25 L=45 cm	E20 L=45 cm	E15 L=45 cm	E15 L=40 cm	E15 L=35 cm
R10	Experiment	FPD	5.54	4.51	4.48	0.84	5.04	4.30
		SPD	5.75	4.63	4.89	5.03	5.39	4.57
		TOC	45.00	45.00	45.00	60.00	45.00	35.00
		LT1	5.00	5.00	10.00	40.00	5.00	5.00
		LT2	5.00	5.00	5.00	10.00	5.00	5.00
	Simulation	FPD	5.59	3.14	4.89	0.80	4.96	4.09
		SPD	5.81	4.63	5.09	5.10	5.38	4.37
		TOC	50.00	55.00	45.00	70.00	45.00	40.00
		LT1	5.00	10.00	10.00	45.00	10.00	5.00
		LT2	5.00	5.00	5.00	10.00	5.00	5.00
R20	Experiment	FPD	3.84	3.63	3.49	3.45	2.96	3.42
		SPD	3.89	3.76	3.56	3.46	3.07	3.42
		TOC	40.00	45.00	45.00	40.00	40.00	35.00
		LT1	10.00	10.00	10.00	15.00	15.00	10.00
		LT2	10.00	10.00	10.00	10.00	15.00	10.00
	Simulation	FPD	3.89	3.87	3.87	3.47	2.64	3.26
		SPD	3.92	3.83	3.83	3.67	2.73	3.29
		TOC	40.00	45.00	45.00	40.00	40.00	40.00
		LT1	10.00	10.00	5.00	10.00	15.00	10.00
		LT2	10.00	10.00	5.00	10.00	15.00	10.00
R30	Experiment	FPD	3.19	2.82	2.74	2.82	2.83	2.96
		SPD	3.20	2.91	2.82	2.93	2.90	2.99
		TOC	40.00	40.00	45.00	40.00	40.00	35.00
		LT1	15.00	15.00	15.00	15.00	20.00	10.00
		LT2	10.00	15.00	15.00	15.00	15.00	10.00
	Simulation	FPD	3.23	2.76	2.87	2.90	2.55	2.43
		SPD	3.16	2.82	2.90	2.91	2.74	2.48
		TOC	40.00	35.00	40.00	35.00	40.00	35.00
		LT1	15.00	15.00	15.00	15.00	15.00	10.00
		LT2	15.00	15.00	15.00	15.00	15.00	10.00

FPD: First Peak Discharge ($Lmin^{-1}$)
SPD: Second Peak Discharge ($Lmin^{-1}$)
TOC: Time of Concentration (min)
LT1: Lag Time for First Hyetograph (min)
LT2: Lag Time for Second Hyetograph (min)

For better understanding, the first observed and simulated peak discharges (FPD and SPD) were compared, as shown in Figure 6.15. They were in good agreement with the determination coefficient (R^2) of 0.9108 and had a linear relationship (y = 0.9811x). HYDRUS-3D slightly underestimated the drain outflow results as approximately 2% less than observations when compared with the peak discharges. Figure 6.16, Figure 6.17, and Figure 6.18 also show the detailed comparisons of all measurements and simulations marked on the drain outflow hydrographs for R10, R20, and R30, respectively. These relationships were given according to the types of drainage layer by considering the reference line (y = x) indicated with a bold black line. The results showed that most of the measurements were underestimated by HYDRUS-3D, similar to the peak discharges. The distribution of the results for each drainage layer was well established around the reference line. Moreover, there were no discharges larger than 6 $L\,\mathrm{min}^{-1}$ for R10. Similarly, discharges greater than 4 $L\,\mathrm{min}^{-1}$ and 3 $L\,\mathrm{min}^{-1}$ were not observed for R20 and R30, respectively. This resulted from decreasing maximum rainfall intensity for the corresponding hyetograph. There were also scattered values caused by the small differences for the time of concentrations. The drain outflow hydrographs showed that larger discharges were observed for the case without the blinding layer (E30 L = 45 cm) under different rainfall intensities. Therefore, the results for E15 L = 40 cm were close enough to the result of E30 L = 45 cm. If the peak rainfall intensity decreased, the distinctive difference for different drainage layers also diminished. In other words, the hydrograph parameters significantly changed when greater rainfall intensities were exposed to the drainage layers. The effects of the thickness of the blinding layer and rootzone were not obvious for smaller rainfall intensities.

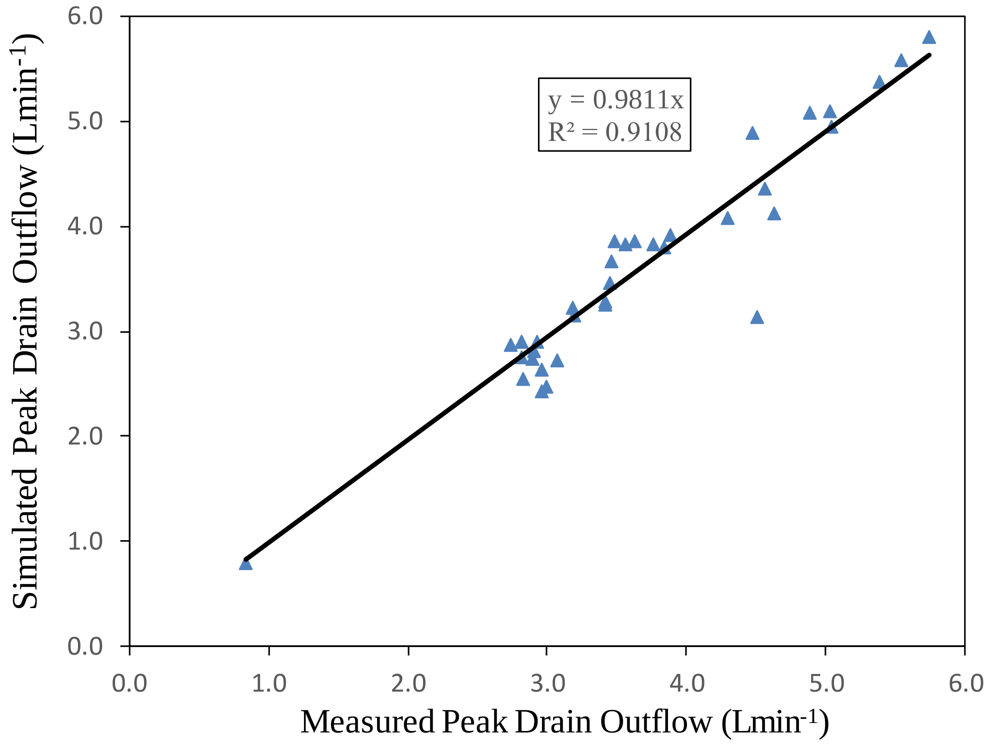

Figure 6.15 Comparison of the Peak Measured and Simulated Drain Outflows

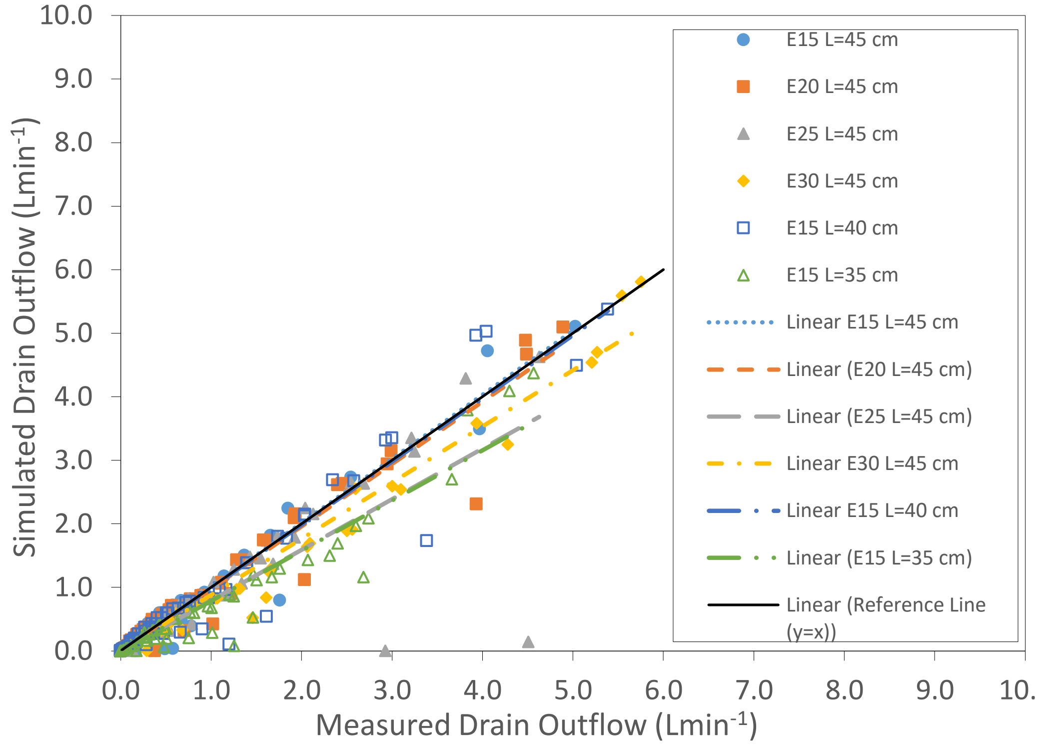

Figure 6.16 Comparison of Measured and Simulated Outflows for Different Layers under R10

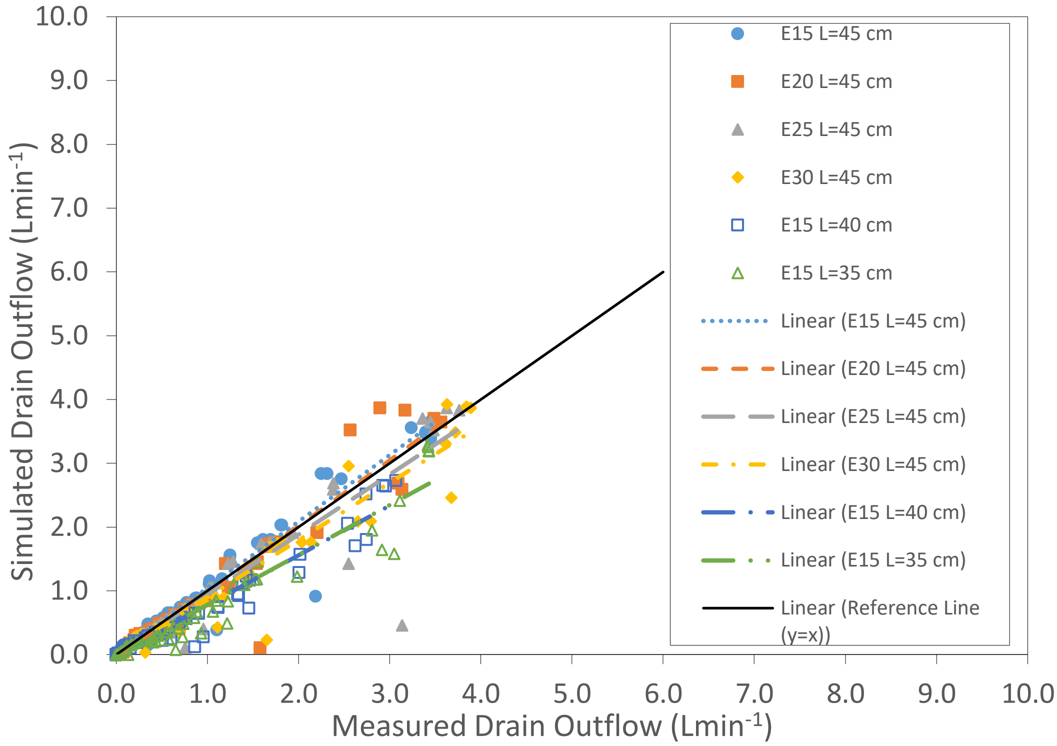

Figure 6.17 Comparison of Measured and Simulated Outflow for Different Layers under R20

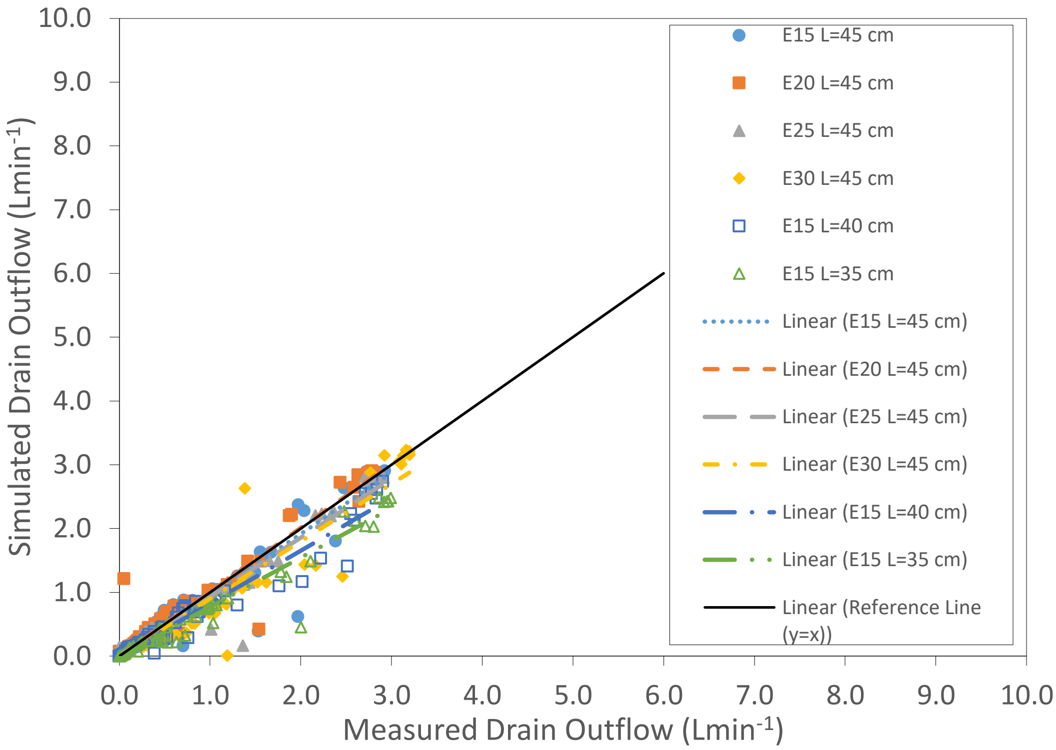

Figure 6.18 Comparison of Measured and Simulated Outflow for Different Layers under R30

Table 6.4 indicates the results of three widely used statistical indices that were used to evaluate hydrological model accuracy in terms of the type of drainage layer and each hyetograph. According to Eqs. (6.1) and (6.2), the goodness of fit values of the simulated experimental data in accordance with the adjusted determination coefficient (R^2) took values between 0.868-0.975 except for the experiment of E25 L = 45 cm. Therefore, the accurate performance of the simulation was confirmed with the NSE index varied between 0.865 and 0.958. However, the KGE index varied a wider range of values between 0.594 and 0.954. For the experiments that used a 45-cm-thick drainage layer, it was larger than 0.741. NSE and R^2 were good for validation, whereas the wide dispersion of KGE was not accurate enough for the experiments of L = 40 and L = 35 cm thick. The comprehensive results demonstrated that measurements and simulations were in good agreement with statistical indices with R^2, NSE, and KGE. Also, simulation results indicated that the HYDRUS-3D model is reliable.

Table 6.4 Statistical parameters for measured and simulated drain outflow hydrographs under R10, R20, and R30 rainfalls

Type of Rainfall	Statistical Parameters	Type of Drainage Layer					
		E30 L=45 cm	E25 L=45 cm	E20 L=45 cm	E15 L=45 cm	E15 L=40 cm	E15 L=35 cm
R10	NSE	0.958	0.663	0.947	0.951	0.917	0.859
	KGE	0.797	0.741	0.972	0.954	0.931	0.594
	R^2	0.975	0.671	0.947	0.955	0.924	0.915
R20	NSE	0.928	0.860	0.912	0.941	0.875	0.865
	KGE	0.843	0.909	0.918	0.919	0.600	0.597
	R^2	0.939	0.868	0.923	0.951	0.948	0.927
R30	NSE	0.874	0.951	0.930	0.916	0.910	0.865
	KGE	0.799	0.890	0.950	0.941	0.722	0.604
	R^2	0.897	0.958	0.932	0.918	0.948	0.944

6.3 Water Content

Water contents were measured using 10-HS sensors in the drainage experiments. These sensors were located at depths of 5, 10, 15, 20, 25, and 30 cm. In this study, time-dependent water contents through the corresponding depths were measured and simulated by HYDRUS-3D. The comparisons between observed and simulated water content for R10 rainfall and various thicknesses of drainage layers are given in Figure 6.19 and Figure 6.20. The results for R20 and R30 are given in Figure 6.21 and Figure 6.22. The water contents were measured for 1440 min (a day) after each experiment started. The distribution of the water content through the drainage layer was drawn by splicing the measurements of water contents at corresponding depths linearly. For instance, while Figure 6.19a shows observed water content for E30 L = 45 cm under R10, Fig. 24b shows simulated water content for identical conditions. Except for E15 L = 45 cm, all experiments started with an initial condition that was not less than field capacity. For experiment E15 L = 45 cm, the initial condition was dry, as seen in Fig. 6.19g.

The general results indicated that, if the initial water content was greater than the field capacity, for both observed and simulated water content, the distribution of time-dependent water content was almost identical for each drainage layer under different rainfall hyetographs. When compared with the observation, the HYDRUS-3D model underestimated the change of the water content due to the wetting front. Moreover, in the stratified layers, the hydraulic barrier at the interface of the rootzone and the blinding layer control the wetting front. Gerke and van Genuchen (1993) stated that simulations based on the Richards equation, as given in Eq. (5), are not reliable and accurate enough for the consideration of a change of the water content in the wetting zone. Huang et al. (2011) confirmed this result in their field observations. They also stated that the infiltration and drainage were nonuniform because of different hydraulic conductivities in the drainage layer, and this influenced the simulation in HYDRUS-3D. The observation of the water content change was apparent through the drainage layer when compared with the simulation results. In addition, greater TOC values and smaller peak discharges resulted from the lack of water content change in the simulation. Similarly, the effect of the blinding layer on the water content distribution was more distinctive for observation in the drainage experiments. The water content at the interface of the rootzone and the blinding layer or the gravel bed was measured as the almost maximum value for without the blinding layer condition. Therefore, water content results obtained from the drainage layers with 5- and 10-cm blinding layers were almost similar, and a slight effect of the blinding layer was observed. However, a 15-cm blinding layer was more effective for the distribution of the water content. For the simulation results, there was no clear difference for comprehending the effect of the blinding layer. In most of the experiments, the HYDRUS-3D model simulated the water content without showing the effects of the presence of the blinding layer. In addition, there was no significant change according to the type of rainfall; in other words, the type of drainage layer was dominant.

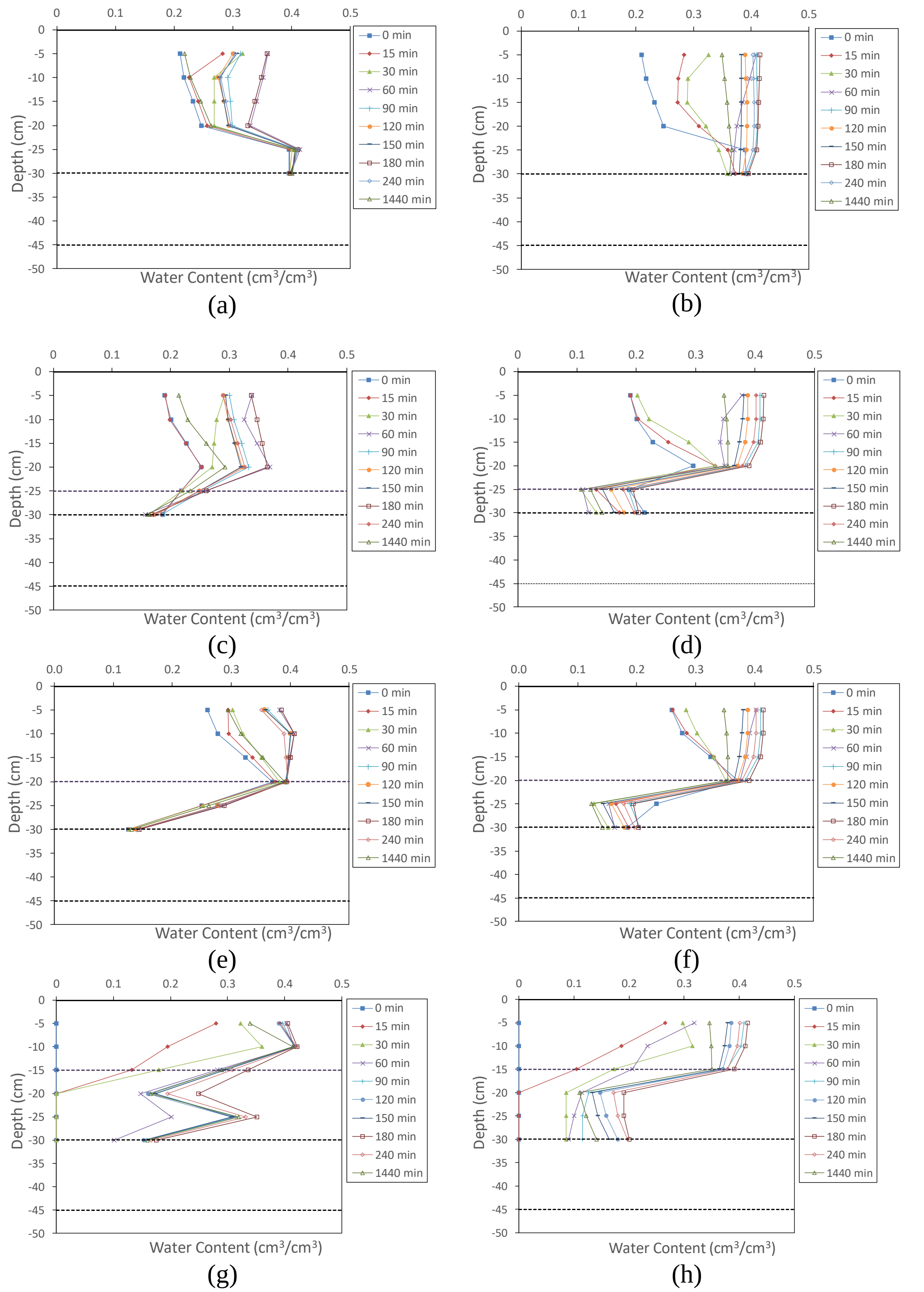

Figure 6.19 Comparisons of the Measured and Simulated Time Dependent Water Content Through Different Drainage Layer Depths under R10 Rainfall: A) E30 L=45 Cm (Measured) B) (Simulated) C) E25 L=45 Cm (Measured) D) (Simulated) E) E20 L=45 Cm (Measured) F) (Simulated) G) E15 L=45 Cm (Measured) H) (Simulated)

Figure 6.20 also shows the water content results for drainage layer thicknesses of 40 and 35 cm (L = 40 and L = 35 cm) for R10 rainfall. The other results are given in Figure 6.23 and Figure 6.24 according to corresponding rainfalls, respectively. Although there was a similar discrepancy between observations and simulations, the results were sufficiently compatible for the experiments of L = 40 and L = 35 cm. When the experiments for E15 L = 40 cm were compared with those for E20 L = 45 cm and E15 L = 45 cm, water content results were similar to the experiments that had the same thickness of the blinding layer of 10 cm. However, the drain outflow hydrographs were more similar for the same thickness of the rootzone. When the maximum rainfall intensity increased, these differences and discrepancies became more distinctive by considering identical experimental conditions. For the same thickness of rootzones (E15 L = 45 cm, L = 40 L = 35 cm), maximum peak discharges were generally similar, and the peak discharge of E15 L = 40 cm was slightly smaller. However, at the interface of the rootzone and blinding layer, water content was comparatively less in the experiment with a 15-cm-thick blinding layer. Considering simulations for the same experiments, the distributions of the water content were almost the same, and the differences were not obvious, as obtained from the observations.

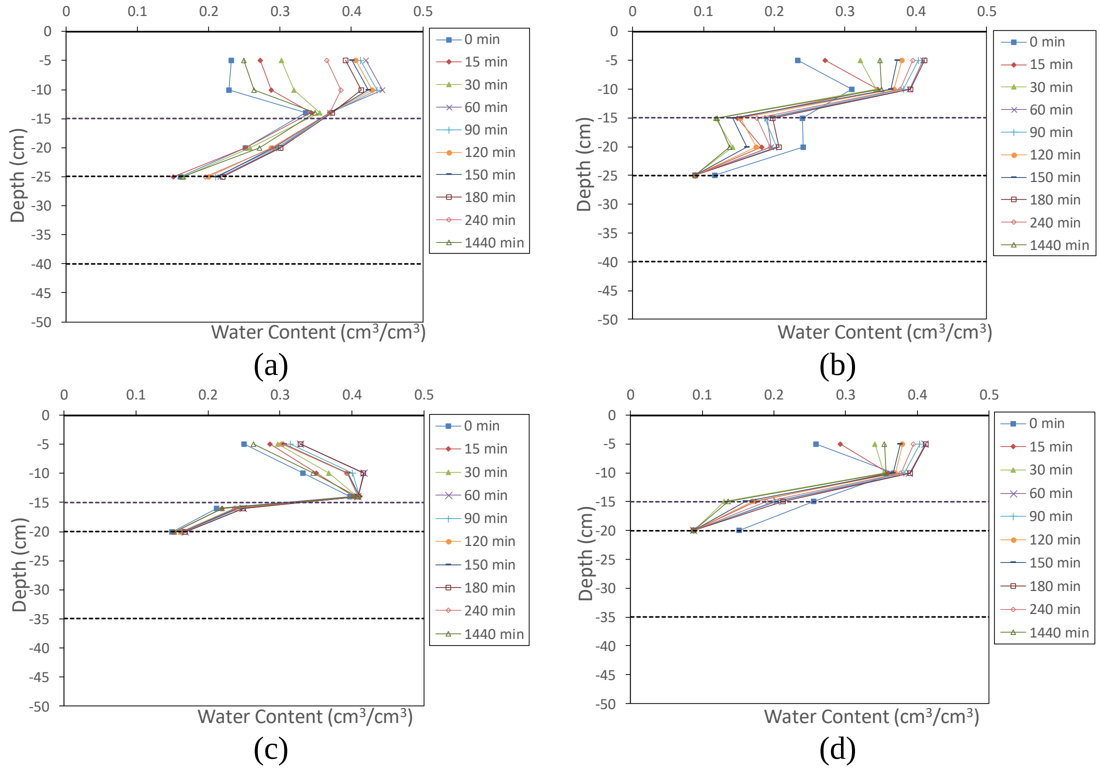

Figure 6.20 Comparisons of the Measured and Simulated Time Dependent Water Content Through L=40 And 35 Cm: A) E15 for L=40 Cm for R10 (Measured) B) (Simulated) C) E15 L=35 Cm for R10 (Measured) D) (Simulated)

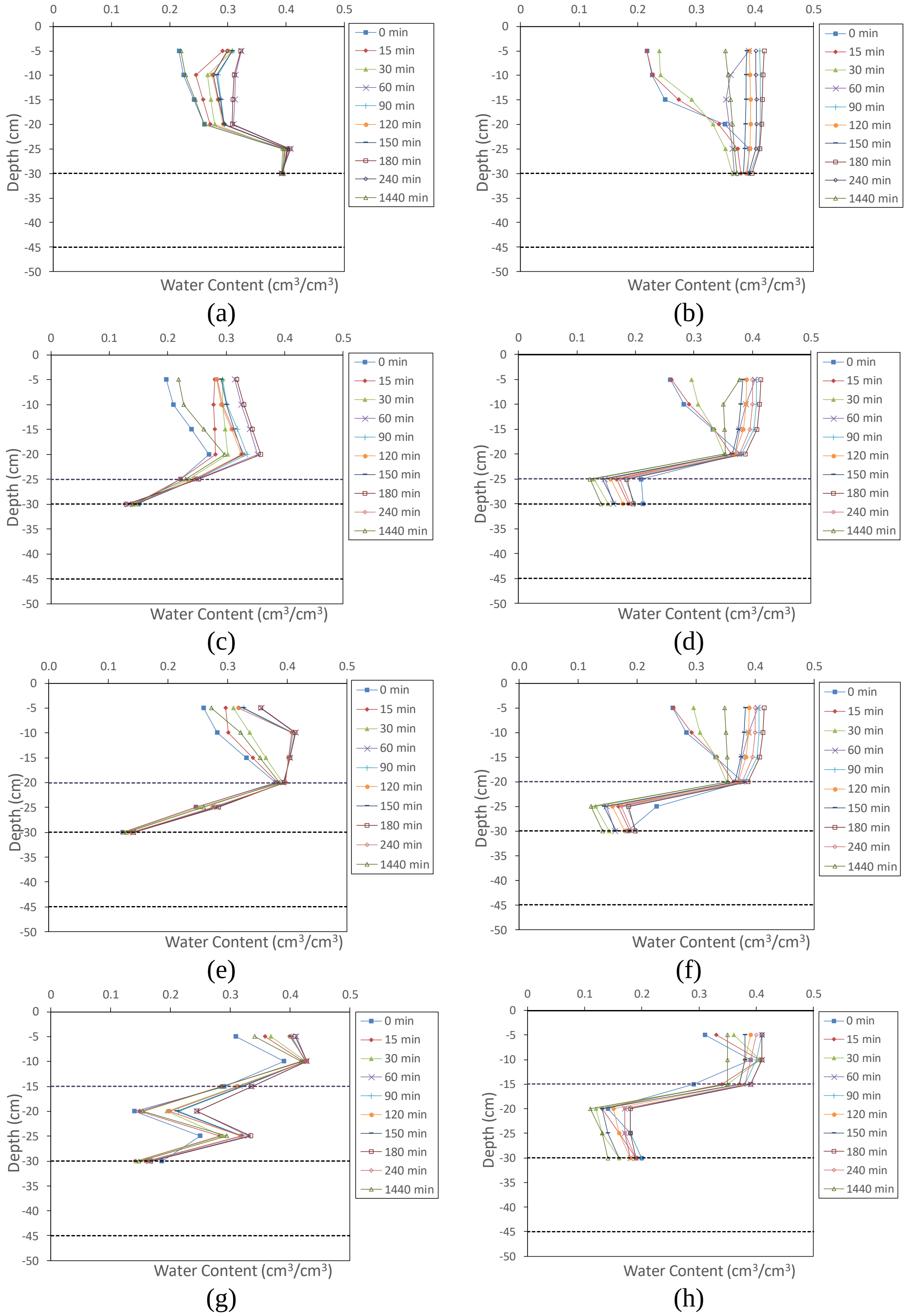

Figure 6.21 Comparisons of the Measured and Simulated Time Dependent Water Content Through Different Drainage Layer Depths under R20 Rainfall: A) E30 L=45 Cm (Measured) B) (Simulated) C) E25 L=45 Cm (Measured) D) (Simulated) E) E20 L=45 Cm (Measured) F) (Simulated) G) E15 L=45 Cm (Measured) H) (Simulated)

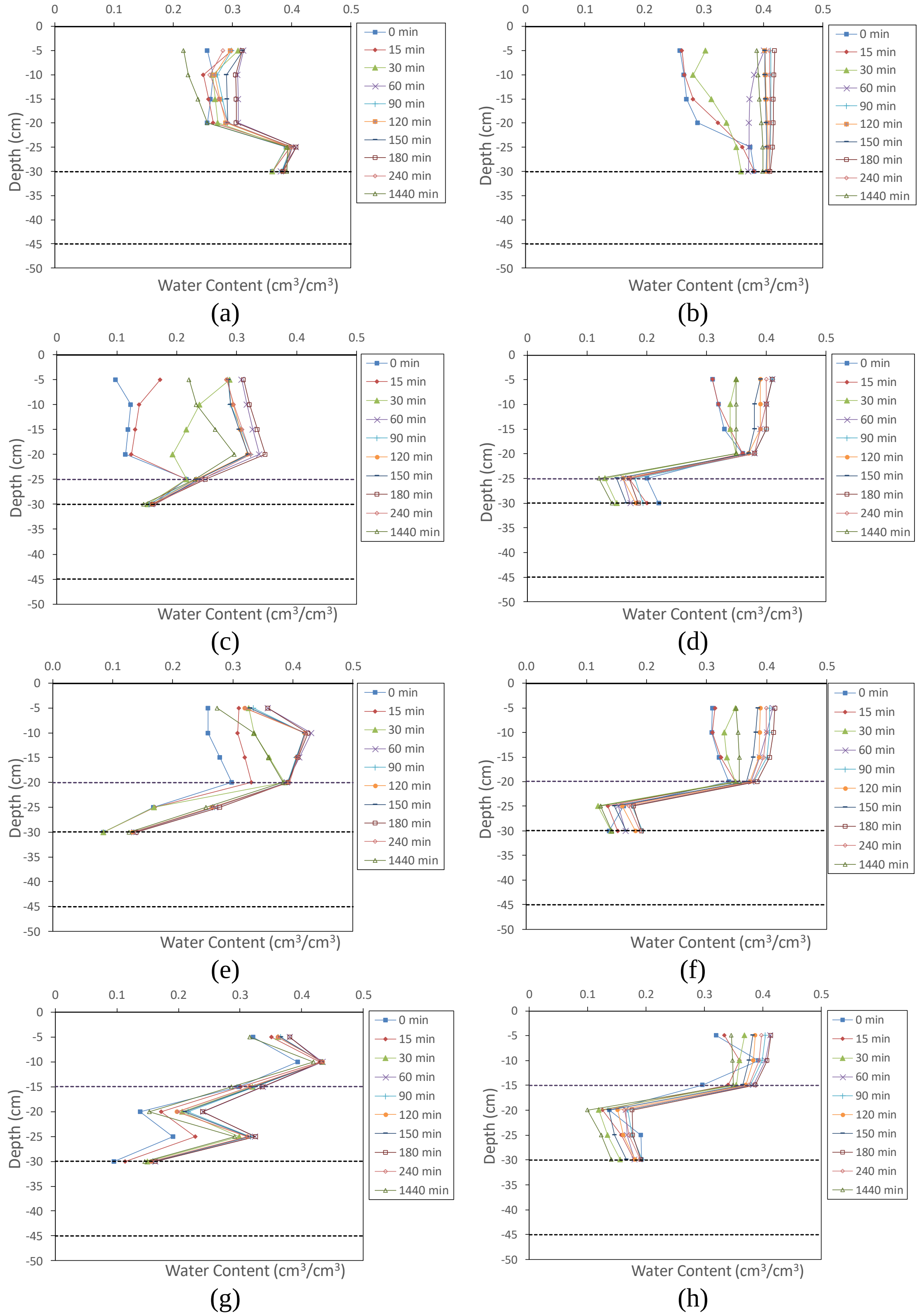

Figure 6.22 Comparisons of the Measured and Simulated Time Dependent Water Content Through Different Drainage Layer Depths under R30 Rainfall: A) E30 L=45 Cm (Measured) B) (Simulated) C) E25 L=45 Cm (Measured) D) (Simulated) E) E20 L=45 Cm (Measured) F) (Simulated) G) E15 L=45 Cm (Measured) H) (Simulated)

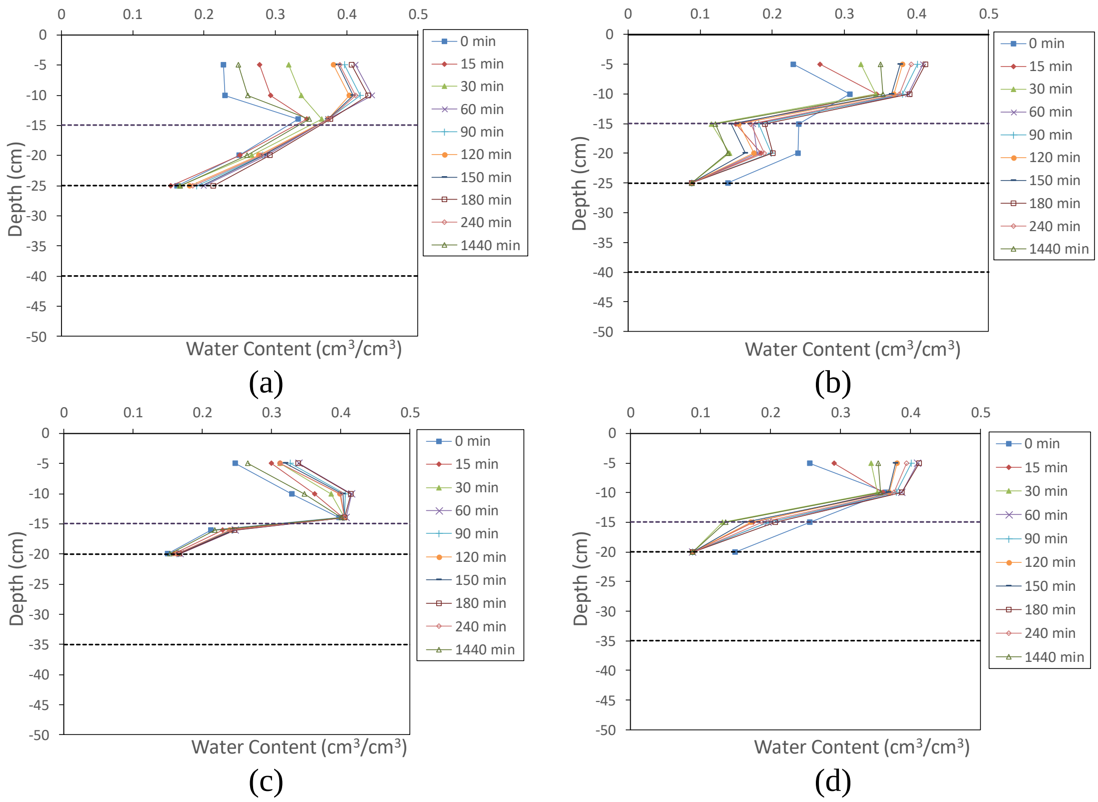

Figure 6.23 Comparisons of the Measured and Simulated Time-Dependent Water Content Through L=40 And 35 Cm: A) E15 L=40 Cm for R20 (Measured) B) E15 L=40 Cm for R20 (Simulated) C) E15 L=35 Cm for R20 (Measured) D) E15 L=35 Cm for R20 (Simulated)

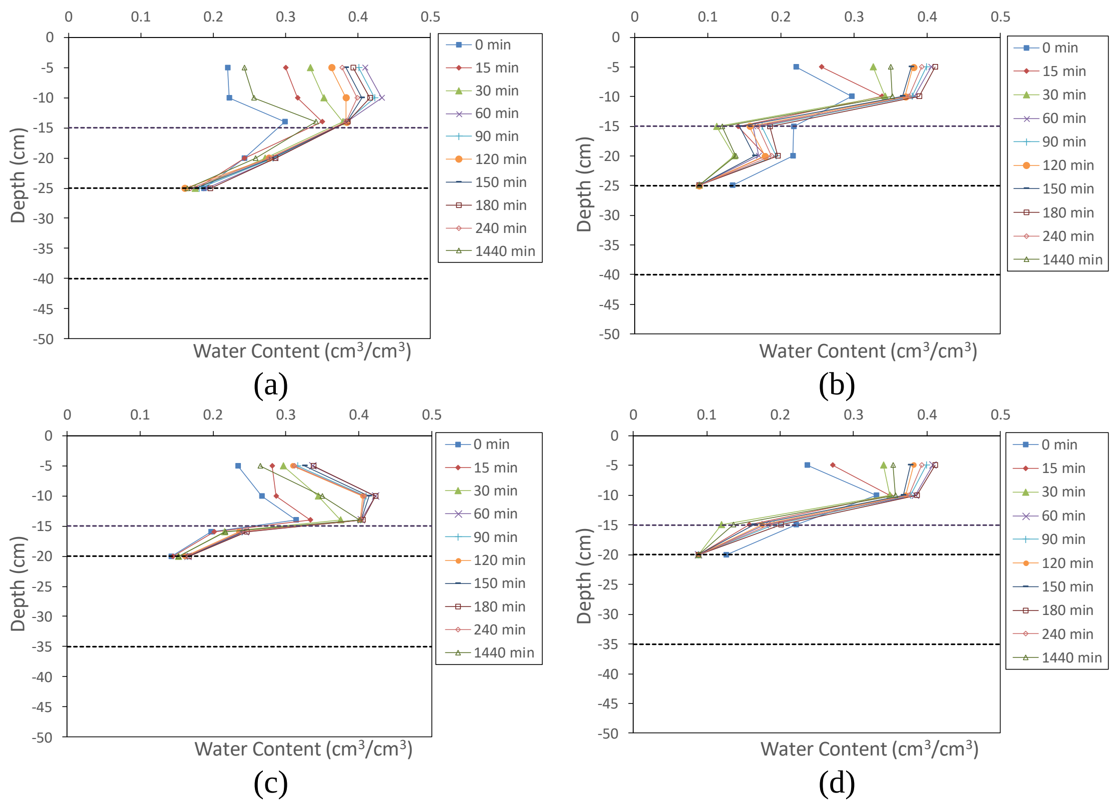

Figure 6.24 Comparisons of the Measured and Simulated Time-Dependent Water Content Through L=40 And 35 Cm under R30 Rainfall: A) E15 L=40 Cm (Measured) B) E15 L=40 Cm (Simulated) C) E15 L=35 Cm (Measured) D) E15 L=35 Cm (Simulated)

6.4 Results for Different Drainage Methods

Within the scope of the experimental study, numerous experiments were carried out for each section on 4 different drainage sections and a total of 40 experiments were conducted. Each drainage technique was subjected to 4 different design hyetographs with 10 (R10), 20 (R20), 30 (R30), and 40 (R40) minute intervals and 6 different constant rainfall of 40, 55, 70, 90, 110, and 130 mmh^{-1}. As seen in Figure 3, all experiments were conducted with 120 minutes hyetograph and the experiments were carried out until the hydrograph's drain outflow reached to under 0.1 Lmin^{-1} at last. In order to better evaluate the results of the experiments, they were divided into two main groups: Figure 6.25 shows the drain outflow hydrographs that were classified according to different drainage techniques. Likely, the effects of different rainfalls were also demonstrated considering relevant drainage techniques. According to the results, while there were significant differences between maximum drain outflows in R10; the results for R40 have become closer to each other and took almost the same value. Thus, it has been observed that the rainfall pattern was more determinant on the drain outflow hydrographs. Therefore, R10 caused a sharper hydrograph due to the shorter time interval as expected. As the rainfall pattern becomes uniform from R10 to R40, the shape of the drain outflow hydrograph became rounder. Similarly, it can be stated that the rainfall pattern is a more effective parameter than the drainage section for the drainage system designs of sports fields (Kesgin et al., 2020). The SWT and PD had higher drain outflows compared to the other two methods for R10 and R20, which have relatively shorter time intervals. However, during the R30 and R40, higher values of drain outflows were observed for the SG and SD. The response of the drain outflow hydrographs for slit systems (SG, SD) with the increase of the rainfall intensities also showed similar relationships in the results of experiments for constant rainfall (Figure 6.26).

The PD is known as an ineffective drainage technique due to the low infiltration rate in local soil conditions with high clay content. However (Sport England, 2015) stated that replacing the local soil with a rootzone with a high sand content (90% sand) could prevent negativities (ponding, surface wearing, etc.). The experimental results supported this distinctive sight, no experiments caused ponding at the surface. Another important point to note for Figure 6.25 is that the SD and SG showed significant similarities considering the maximum drainage outflow, rising limb, and recession curves, except for R30 rainfall. For R30, the maximum drain outflows for SD had a higher value than SG. According to the results of the experiment obtained in Figure 6.25, the time to start to drain for these two drainage techniques occurred noticeably earlier, regardless of the rainfall order. Simpson (2016) and Dixon et al. (2015) stated that as the common point of these two techniques, it is aimed to create a high-permeability path that will ensure the rapid passage of water between the field surface and the drainage bed. Therefore, the quicker the rainfall is delivered to the drainage bed, the earlier the drain start time will occur, and this was observed in Figure 6.25 in the experimental results.

The second group results were the S hydrographs that were obtained from the application of constant rainfall to different drainage techniques. It was clearly observed that the drain outflow took place first in the SD and then started to flow for the SG a very short time later unless the first drain outflows started to drain 15 minutes later in the other drainage techniques. In addition, the concentration-time, which refers to the time that the first drain outflow starts to drain after rainfall exposed to drainage techniques, took smaller values for the SG and SD (Table 6.5).

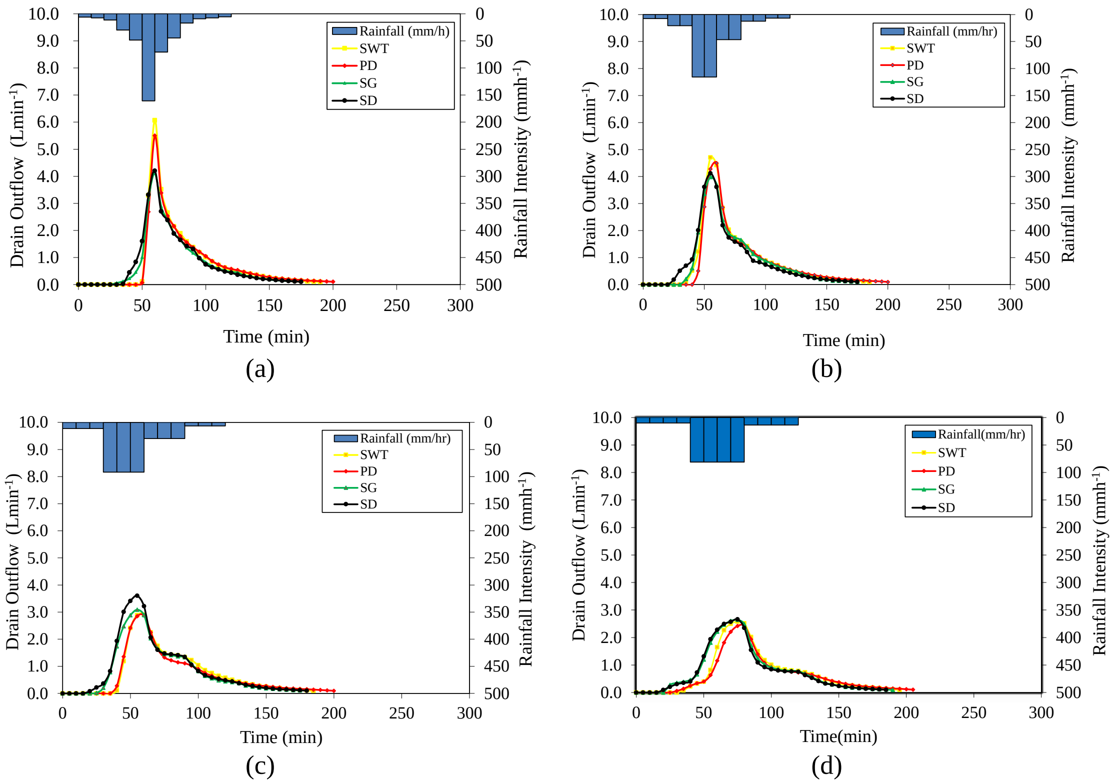

Figure 6.25 Drain Outflow Hydrographs of SWT, SD, SG, and PD: A) R10, B) R20, C) R30, D) R40

However, SG and SD formed by slits had different behaviors. Regardless of rainfall patterns, drainage outflows were close to each other and the impact of rainfall on drainage has decreased. The drain outflows obtained for different rainfall patterns were also close to each other. Considering R10 and R20 rainfall conditions for the SD, it can be clearly seen that the drain outflows were 4.20 Lmin^{-1} and 4.12 Lmin^{-1}, respectively, and there was almost no difference. Among all rainfall patterns and drainage techniques, the greatest drain outflow for R10 was observed from the SWT method. Sport England (2011) claims that a comprehensive feeding and irrigation system should exist in sports fields for the SWT structure is supported by the results of these experiments. An additional and comprehensive irrigation system for this system, which provides large outflow flows, will ensure that the necessary water content on the ground is maintained, as the outflow of large amounts of water poses a danger to the growth and health of the grass on the sports field surface. Unlike the drainage technique which caused the bigger drain outflows seems the most preferable, it is the most successful drainage system because the turf grass in the sports field will provide the water needed to stay healthy from the rootzone. Furthermore, the design diameter of the drain pipe is directly related to the maximum drain outflow. According to the results of the experiments, when the drain outflow reached the desired 0.1 $Lmin^{-1}$, similar recession curves were observed for all rainfalls (Figure 6.25). The longest time for the recession curves was observed for the PD (Table 6.5). In brief, it can be seen in Figure 6.25 and Table 6.5, the PD had the longest drain outflow duration and time to base flow regardless of the rainfall pattern. Adams (1986) stated that the drainage problems do not occur due to the fact that the sports fields are built from large-scale permeable filling material. However, problems such as the decrease in infiltration rate, plasticization of the surface, and loss of strength of the surface may occur as a result of wear and deterioration of the field surface. This is the main cause of the drainage problem. Therefore, it can be said that the PD, consisting of a rootzone with a high sand percentage (90%), is also a successful system, and experiments also support this result.

Moreover, this study aimed to investigate the behavior of the drainage methods under constant rainfall (40, 55, 70, 90, 100, and 130 mmh^{-1}). Thus, S hydrographs, which consist of continuous rainfall with constant intensities, were drawn in Figure 6.26. As expected, after a while, the drain outflow reached to a fixed value for each rainfall and drainage method with the continuation of the constant rainfall. Furthermore, examining the relationship between constant drain flows/infiltration rates and constant rainfall intensities for each drainage method made a significant contribution to the hydrological evaluation of the sports field drainage design.

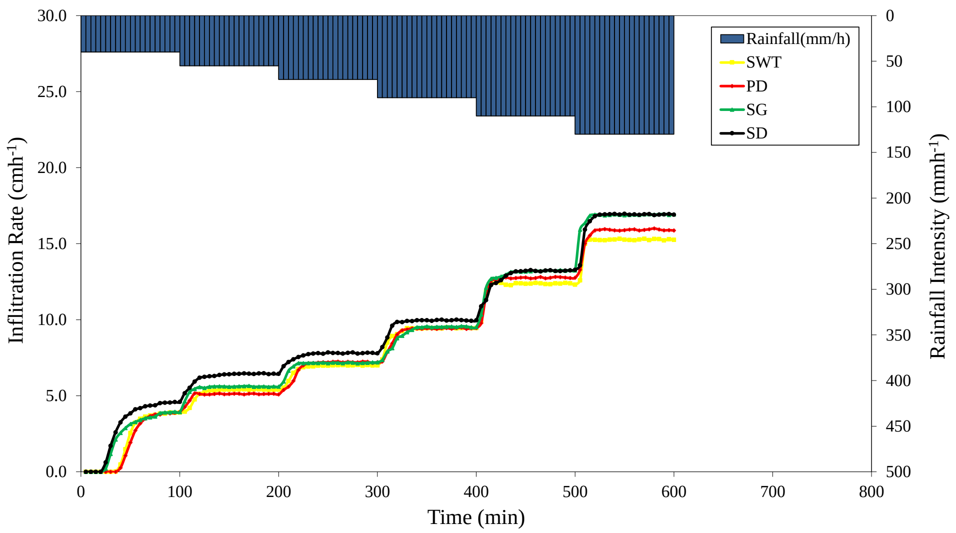

Figure 6.26 S Hydrographs Obtained under Constant Rainfall Conditions

Table 6.5 Hydrograph parameters for different drainage techniques and rainfalls

Rainfall	Drainage Technique	Time of Concentration (min)	Lag Time (min)	Total duration (min)	Time to base flow (min)
R10	PD	50	5	150	140
	SWT	50	5	140	130
	SD	35	5	140	115
	SG	30	5	145	115
R20	PD	45	10	155	140
	SWT	35	5	150	130
	SD	25	5	150	120
	SG	35	5	140	120
R30	PD	40	15	160	140
	SWT	40	15	145	125
	SD	20	10	160	125
	SG	25	10	150	120
R40	PD	30	15	175	125
	SWT	35	15	160	120
	SD	20	15	165	110
	SG	25	15	165	115

As seen in Figure 6.26, constant intensity rainfalls were applied in 4 drainage methods until the drain outflows reached to a continuous value. The first noticeable result was that the time to start to drain for SG and SD was significantly earlier. In addition, the SD was determined as the drainage technique with the highest maximum drain outflow in all constant rainfalls. Particularly, for constant rainfall up to 90 mmh^{-1}, distinctive similarities were observed for, PD, SWT, and SG. While the drainage methods started to behave disparately in the case of 90 mmh^{-1} rainfall was exposed (Figure 6.26). According to S hydrographs derived from constant and continuous intensity rainfall exceeding 90 mmh^{-1}, the mean of the maximum drain outflows was also separately measured for SD, SG, PD, and SWT. However, as demonstrated in Figure 6.26, it can be clearly stated that there was no significant difference in terms of hydrological aspects when the constant and continuous rainfalls applied to different drainage techniques in identical conditions due to the fact that the highest of average infiltration rates at all constant rainfall were observed for SD. This result showed that the SD is appropriate for use in areas where field conditions are problematic due to low permeability soils. In addition, the drain outflows were higher when compared with PD, SWT, and SG that has a significant effect on drain pipe diameter in the design of the collector pipe system. In other words, SD has a maximum of average drain outflows for the identical circumstances with PD, SWT, and SG. Therefore, the economic impact of this result should be examined by comparing the economic value of removing the existing local ground on the field surface and replacing it with a sand-dominated content.

The infiltration rates were obtained by dividing the drain outflows obtained under the experiments of constant rainfall intensities to 1.5m x 1.3m surface area of the experimental system. For rainfall of 130 mmh^{-1}, which is the most intense rainfall, the infiltration rate was observed at 16.92 cmh^{-1} for SD, while they were measured 16.89, 15.90, and 15.26 cmh^{-1} for SG, PD, and SWT, respectively (Figure 6.27). It can be also inferred that during low-intensity rainfall, infiltration rates took almost similar and close values. However, when the rainfall increased, differences in infiltration rates started to be observed. Table 6.6 summarized the relationship between the rainfall intensity and the infiltration rate for all drainage techniques. It was shown that the determination coefficient (R^2) varied between 0.94-0.97 with linear relationships. When the minimum slope of the trend lines was determined for the SWT, a maximum one was observed for SD (Table 6.6). In other words, lesser infiltration rates were observed in SWT for the same rainfall conditions.

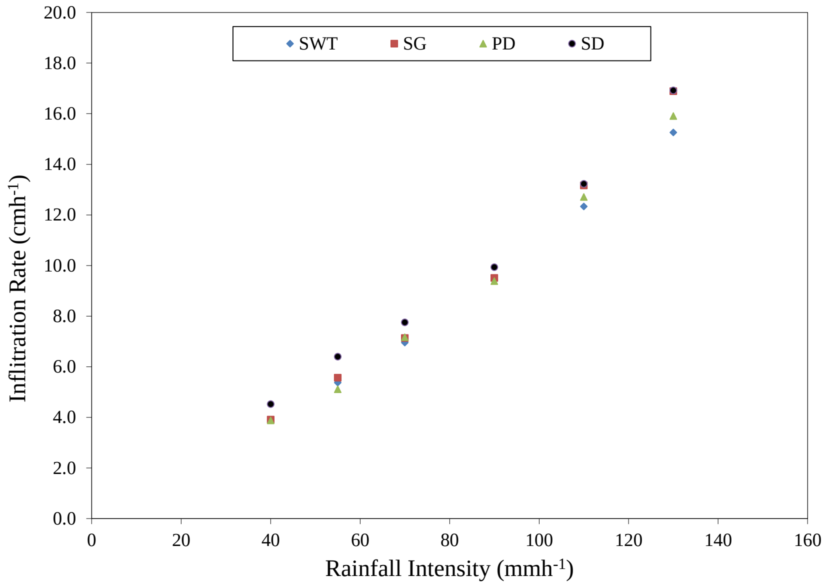

Figure 6.27 Comparison of Rainfall Intensity and Infiltration Rate

Table 6.6 The statistical results of rainfall intensity-infiltration rate relation

Drainage Technique	Rainfall Intensity-Infiltration Rate Relation	Determination Coefficient (R^2)
SD	y = 1.2062x	0.97
SG	y = 1.1713x	0.94
SWT	y = 1.0997x	0.97
PD	y = 1.1253x	0.95

6.5 Conclusion

An experimental and numerical investigation was conducted to determine the drainage mechanisms of sports fields. New and more accurate insights into the drainage mechanism of sports fields were presented. A rainfall simulator developed by Kesgin et al. (2018) was improved by increasing the capability to simulate a wider range of natural rainfall intensities. Therefore, for the two-nozzle system, a new methodology based on nozzle discharge and rainfall intensity relationships was determined with $R = 13.93Q$ for smaller rainfall intensities produced by the LNN nozzle and $R = 19.554e^{0.1975Q}$ for larger rainfall intensities produced by the GG-W nozzle. According to these relationships, the predicted and measured rainfall intensities at the LNN and GG-W nozzles were also in good agreement with R^2 values of 0.982 and 0.9956, respectively.

Considering the drain outflow hydrographs, the type and shape of the hyetograph were found to have more influence on the shape of the hydrograph than the type of drainage layer did. The shape of the hydrograph did not significantly change with the type of drainage layer. It was sharper for intense rainfalls that had shorter time intervals. Therefore, the initial water content had a significant effect on the drain outflow hydrograph.

The effect of the thickness of the blinding layer and the rootzone was not clearly seen for smaller rainfall intensities. Especially, the results obtained in the experiments under the most intense rainfall (R10) were distinctive. Larger peak discharges were observed without the blinding layer (E30 L = 45 cm) for different rainfalls. In other words, the blinding layer had a considerable effect on the amount of peak rainfall. That was more obvious for the experiment with a 15-cm blinding layer. The results also showed that there was no distinct effect of the blinding layer on the hydrograph parameters in the case of reaching or exceeding the field capacity. Slight differences between the experiment and simulation originated from discrepancies between observed and simulated water content results. Determining optimal drainage layers (thickness of layers and type of material) depends highly on long-term rainfall records for a relevant region. The results of the unsaturated flow model (HYDRUS-3D) showed satisfactorily that the description of the drainage flow for sports fields is the steady-state flow, and this was also confirmed by the proposed soil hydraulic parameters for the definition of the drainage processes of sports fields.

PD, SWT, SG, and SD drainage techniques that are commonly used in the drainage application in the sports fields were experimentally examined for the hydrological evaluation of the drainage mechanism in sports fields. The experimental results were classified according to the drain outflow hydrograph obtained from 4 different design hyetographs with various time intervals and the S hydrograph obtained from 6 different constant intensities and infinite duration rainfall. To sum up, briefly, the following insightful findings were particularly determined for future works that are highly open to new perspectives regarding the drainage of sports fields.

The shape of the design hyetograph was a very effective parameter on the drain outflow and shape of its hydrograph.

Higher drain outflows were obtained for R10 as expected. Therefore, it was observed that during longer time intervals of rainfall, the drain outflow decreases, and the shape of the hydrograph became rounder.

In all rainfall conditions, the time of concentration in the SD and SG were significantly earlier. Thus, it can be thought that these are more advantageous in preventing ponding on the sports field surface during sudden and heavy rainfall.

It can be also argued that there were no ponding conditions on the surface when all rootzones at the top selected as sand-dominated content (90%) with the appropriate amount of material and granulometry for all different drainage techniques.

When comparing the S hydrographs obtained as a result of continuous constant intensity (40, 55, 70, 90, 110, and 130 mmh^{-1}) rainfall, no significant difference was observed between the average of the maximum outflows and infiltration rates in the case that rainfall was 90 mmh^{-1} or less. For the SD, higher drain outflows were obtained although a minimum of them was measured for SWT.

Considering sand-dominated rootzone and proper drainage installation in low rainfall conditions (<90 mmh^{-1}), it was clearly observed that the drainage of sports fields does not demonstrate distinctive differences in terms of a hydrological point of view

REFERENCES

Adams, W. A., (1986). Practical aspects of sports fields drainage. *Soil Use and Management*, *2*(2), 51–54.

Alfnes, E., Kinzelbach, W., and Aagaard, P., (2004). Investigation of hydrogeologic processes in a dipping layer structure: 1. The flow barrier effect. *Journal of Contaminant Hydrology*, *69* (3–4), 157–172.

Alway, F. J., & McDole, G. R. (1917). Relation of the water-retaining capacity of a soil to its hygroscopic coefficient. J. Agr. Res, 9, 27-71.

Baker, S. W. (1989). Soil physical conditions of the rootzone layer and the performance of winter games' pitches. Soil use and management, 5(3), 116-122.

Bentley, W.A., (1904). Studies of raindrops and raindrop phenomena. *Mon. Weather Rev., 32,* 450–456.

Bubenzer, G.D., 1979. Inventory of rainfall simulators. Proc. rainfall Simulator Workshop, Tucson, Az. USDA-SEA ARM-W-10, pp. 120–131

Canaway, P. M. (1994). Maximizing the performance of sports turf (Doctoral dissertation, University of Liverpool).

Carvalho, C. P. S., de Lima, J. L. M. P, de Lima, M. I. P., (2014). Using meshes to change the characteristics of simulated rainfall produced by spray nozzles. *International Soil and Water Conservation Research. Vol. 2, No. 2,* 67-78.

Cereti, C. F., Rossini, F., & Romoli, F. (2003, June). Improvement of the drainage capacity in sports turf. In I International Conference on Turfgrass Management and Science for Sports Fields 661 (pp. 315-318).

Chou, C., & Lan, C. W. (2012). Changes in the annual range of precipitation under global warming. Journal of Climate, 25(1), 222-235.

Chow, V. Te, Maidment, D. R., Mays, L. W., (1988). Applied Hydrology, McGraw – Hill Book Company, United States, pp 465-470.

Christiansen, J.E., (1942). The uniformity of application of water by the sprinkler system. *Agricultural Engineering, 22*, 89–92.

Dixon, S., Fleming, P., James, I., & Carre, M. (Eds.). (2015). The science and engineering of sport surfaces. Routledge.

Dogan, A., Agaccioglu, H., Basayigit, L., (2018) 'Investigation of techniques to provide rapid and effective drainage of sports fields under various hydrologic conditions', (Report Number: 214M616), Ankara, TUBITAK.

Ebrahimian, H., and Noory, H., (2015). Modeling paddy field subsurface drainage using HYDRUS-3D. *Paddy and Water Environment*, *13* (4), 477–485.

Fédération Internationale de Football Association. FIFA: Financial Report 2014 (Zurich: FIFA, 2015).

FIFA, (2004). FIFA Quality Concept for Football Turf, 103.

FIFA, (2012). FIFA Quality Concept for Football Turf: Handbook of Requirements.

Fleming, P.R., Frost, M.W. and Simpson, M.R., (2016). Drainage behavior of sports pitches. Findings from a research study, Loughborough, Loughborough University, 25.

Gerke, H. H., and van Genuchten, M. Th., (1993). A dual-porosity model for simulating the referential movement of water and solutes in structured porous media. *Water Resources. Research. 29*, 305-319

Gupta, H.V., Kling, H., Yilmaz, K.K., Martinez, and G.F., (2009). Decomposition of the mean squared error and NSE performance criteria: Implications for improving hydrological modeling. *Journal of Hydrology, 377*, 80–91.

James, I. T., Blackburn, D. W. K., & Godwin, R. J. (2007a). Mole drainage as an alternative to sand slitting in natural turf sports surfaces on clays. Soil use and management, 23(1), 28-35.

James, I. T., Hann, M. J., & Godwin, R. J. (2007b). Design and operational considerations for the use of mole ploughing in the drainage of sports pitches. Biosystems Engineering, 97(1), 99-107.

J.J. Henderson, J.R. Crum, T.F. Wolff, and J.N. Rogers III., (2001). Athletic Field Rootzone Mixes: What is the Best Mix for Your Field? *Athletic Field Session Papers*, 96–99.

Hilten, R. N., Lawrence, T. M., and Tollner, E. W., (2008). Modeling stormwater runoff from green roofs with HYDRUS-1D. *Journal of Hydrology*, *358* (3–4), 288–293.

Huang, M., Lee Barbour, Elshorbagy, A., S., and Zettl, J. D., Cheng Si, B., (2011). Infiltration and drainage processes in multi-layered coarse soils. *Canadian Journal of Soil Science*, *91* (2), 169–183.

Kearney, A. T. (2011). The sports market. Major trends and challenges in an industry full of passion. AT Kearney.

Kesgin, E., Dogan, A., and Agaccioglu, H., (2018). Rainfall simulator for investigating sports fields drainage processes. *Measurement: Journal of the International Measurement Confederation*, *125* (May), 360–370.

Kesgin, E., Agaccioglu, H., & Dogan, A. (2020). Experimental and numerical investigation of drainage mechanisms at sports fields under simulated rainfall. Journal of Hydrology, 580, 124251.

Kowalik, T., & Rajda, W. (2014). Physical properties, permeability, and retentiveness of silt loam and its composites with sand for constructing carrying a layer of a football field. Journal of Ecological Engineering, 15(4), 37-45.

Laws, J.O., Parson, D.A., 1943. The relationship of raindrop size to intensity. Trans. Am. Geophys. Uni. 24, 452–460.

Liu, S. C., Fu, C., Shiu, C. J., Chen, J. P., & Wu, F. (2009). Temperature dependence of global precipitation extremes. Geophysical Research Letters, 36(17).

Luk, S. hung, Abrahams, A. D., and Parsons, A. J., (1993). Sediment sources and sediment transport by rill flow and interrill flow on a semi-arid piedmont slope, southern Arizona. *Catena*, *20* (1–2), 93–111.

Magni, S., Volterrani, M., & Miele, S. (2003, June). Soccer pitches performances as affected by construction method, sand type, and turfgrass mixture. In I International Conference on Turfgrass Management and Science for Sports Fields 661 (pp. 281-285).

Miller, D. E. (1973). Water retention and flow in layered soil profiles. Field soil water regime, 5, 107-117.

Moazed, H., Bavi, A., Boroomand-Nasab, S., Naseri, A., and Albaji, M., (2010). Effects of climatic and hydraulic parameters on water uniformity coefficient in solid set systems. *Journal of Applied Sciences*.

Moore, I.D., Hirschi, M.C., Barfield, B.J., 1983. Kentucky rainfall simulator. Transactions of ASAE 26, 1085–1089.

Mualem, Y., (1976). A new model for predicting the hydraulic conductivity of unsaturated porous media. *Water Resources Research*, *12* (3), 513–522.

Nash, J. E., and Sutcliffe, J. V., (1970). River flow forecasting through conceptual models part I - A discussion of principles. *Journal of Hydrology*, *10* (3), 282–290.

Pachauri, R. K., & Reisinger, A. (2008). Climate change 2007. Synthesis report. Contribution of Working Groups I, II, and III to the fourth assessment report. Cambridge University Press, Cambridge.

Pifer, N. D., Wang, Y., Scremin, G., Pitts, B., & Zhang, J. J. (2018). Contemporary global football industry: an introduction. The Global Football Industry-Marketing Perspectives, 1-33.

Sakellariou-Makrantonaki, M., (1997). Water Drainage in Layered Soils. Laboratory Experiments and Numerical Simulation. *Water Resources Management*, *11 (6),* 437–444.

SAPCA, 2010. The SAPCA Code of Practice for the Design, Construction, and Improvement of Natural Sports Turf. s.l.: SAPCA.

Sejna, M., J. Šimůnek, and van Genuchen, M. Th., (2012). The HYDRUS Software Package for Simulating Two and Three Dimensional Movement of Water, Heat, and Multiple Solutes in Variably Saturated Media, User Manual, Version 2.0, PC Progress.

Simpson, M. R., Fleming, P. R., & Frost, M. W. (2013, December). Briefing: Sustainable drainage for sports pitch developments. In Proceedings of the Institution of Civil Engineers-Municipal Engineer (Vol. 166, No. 4, pp. 211-215). Thomas Telford Ltd.

Simpson, M. R. (2016). Sustainable drainage of sports pitches (Doctoral dissertation, Loughborough University).

Šimůnek, J., van Genuchten, M. Th., and Sejna, M., (2006). The HYDRUS Software Package for Simulating the Two- and Three-Dimensional Movement of Water, Heat, and Multiple Solutes in Variably-Saturated Porous Media, User Manual, Version 1.0, PC Progress.

Šimůnek, J., van Genuchten, M. T., and Šejna, M., (2016). Recent Developments and Applications of the HYDRUS Computer Software Packages. *Vadose Zone Journal*, *15*(7), 0. https://doi.org/10.2136/vzj2016.04.0033

Sport England, (2011). Natural Turf for Sport: Design Guidance Note.

Stiles, V. H., James, I. T., Dixon, S. J., & Guisasola, I. N. (2009). Natural turf surfaces. Sports Medicine, 39(1), 65-84.

Still, C., Sarwer, D. B., & Blankenship, J. (2014). The ASMBS Textbook of Bariatric Surgery. New York, NY: Springer Science+ Media.

Taylor, D. H., & Blake, G. R. (1979). Sand content of sand-soil-peat mixtures for turfgrass. Soil Science Society of America Journal, 43(2), 394-398.

Taylor, D.H., Williams, C.F., and Nelson, S.D., (1997). Water retention in root-zone soil mixtures of layered profiles used for sports turf. *Hortscience 32 (1),* 82-85.

Taylor, D. H., Nelson, S. D., Williams, C. F., (1993). Sub-Rootzone Layering: Effects on Water Retention in Sports Turf Soil Profiles. *Agronomy Journal*, *85* (3), 626-630.

Turco, M., Kodešová, R., Brunetti, G., Nikodem, A., Fér, M., and Piro, P., (2017). Unsaturated hydraulic behavior of a permeable pavement: Laboratory investigation and numerical analysis by using the HYDRUS-3D model. *Journal of Hydrology*, *554*, 780–791.

USGA Green Section Staff, (1993). USGA Recommendations for a Method of Putting Green Construction.

US Golf Association. (2004). USGA recommendations for a method of putting green construction. USGA: Far Hills, NJ, USA.

Todd, D.K., Mays, L. W. (2005). Groundwater Hydrology. John Wiley & Sons. New Jersey, USA.

United States Geological Survey (USGS) (2013). Unsaturated Flow Basics. https://wwwrcamnl.wr.usgs.gov/uzf/unsatflow/unsatflow.html

Van Dijk, A. I. J. M., Bruijnzeel, L. A., and Rosewell, C. J., (2002). Rainfall intensity-kinetic energy relationships: A critical literature appraisal. *Journal of Hydrology*, *261* (1–4), 1–23.

Van Genuchten, M.Th. (1980). A Closed-Form Equation for Predicting the Hydraulic Conductivity of Unsaturated Soils. *Soil Sci. Soc. Am. J. 44,* 892-898.

Van Genuchten, M. T., Leij, F. J., and Yates, S. R., (1991). The RETC Code for Quantifying the Hydraulic Functions of Unsaturated Soils. EPA Report 600/2-91/065. *U.S. Salinity Laboratory, USDA, ARS*, (December), 93.

Woods Ballard, B., Wilson, S., Udale-Clarke, Illman, S., Scott, T., Ashley, R., and Kellagher, R., (2015). The SUDS manual. Ciria.

Zhao, N., Yu, F., Li, C., Wang, H., Liu, J., and Mu, W., (2014). Investigation of Rainfall-Runoff Processes and Soil Moisture Dynamics in Grassland Plots under Simulated Rainfall Conditions'. *Water (Switzerland), 6 (9),* 2671-2689.

PUBLICATIONS FROM THE THESIS

Conference Papers

1. Kesgin E, Dogan A, and Agaccioglu H (2017). A New Laboratory Scale Apparatus for Evaluation of Sports Field Drainage Process. International Conference on Civil and Architectural Engineering (ICCAE) San Francisco, USA 20th-21st October 2017.

2. Dogan, A., Rukundo, E., Agaccioglu, H., Kesgin, E. (2017). Simulation of Drainage Process in Sport Fields Subject To Various Rainfall Intensities and Various Drainage Layer Orientations. The 3rd International Conference on Engineering and Natural Sciences (ICENS), Budapest, Hungary

Papers

1. Kesgin E, Dogan A, and Agaccioglu H (2018). Rainfall simulator for investigating sports field drainage processes. Measurement, 125, pp. 360-370, doi: 10.1016/j.measurement.2018.05.001

2. Kesgin E, Agaccioglu H, and Dogan A (2020). Experimental and numerical investigation of drainage mechanisms at sports fields under simulated rainfall. J. of Hydrology, 580:124251. Doi: 10.1016/j.jhydrol.2019.124251

3. Gezici K, Kesgin E, and Agaccioglu H. (2021). Hydrological Assessment of Experimental Behaviors for Different Drainage Methods in Sports Fields. J. Irrig. Drain. Eng. (ASCE), vol. 147, no. 9, p. 04021034, 2021, doi: 10.1061/(ASCE)ir.1943-4774.0001597.

Projects

1. Investigation of Techniques to Provide Rapid and Effective Drainage of Sports Fields under Various Hydrologic Conditions (2015). TUBITAK-1001 (214M616).